Aus dem Zentrum für Medizinische Forschung

der Medizinischen Fakultät Mannheim

Direktor: Prof. Dr. med. Norbert Gretz

The Role of Podocytes in

Diabetic and Hypertensive Renal Diseases

and Their Nanoscale Evaluation by Expansion Microscopy

Inauguraldissertation

zur Erlangung des akademischen Grades

Doctor scientiarum humanarum (Dr. sc. hum.) der

Medizinischen Fakultät Mannheim

der Ruprecht-Karls-Universität

zu

Heidelberg

vorgelegt von
Yalçın KUZAY

aus
Istanbul, Turkey
2020

Dekan: Prof. Dr. med. Sergij Goerdt…….
Referent(in): Frau Prof. Dr. Sigrid Hoffmann. ……………….

TABLE OF CONTENTS

ABBREVIATIONS

ACE: Angiotensin-converting enzyme
AGE: Advanced glycation end products
AHS: Amplification hydrogel solution
Ang II: Angiotensin II
AT1R: Angiotensin type 1 receptor
AT2R: Angiotensin type 2 receptor
AZAN: Heidenhain's AZAN trichrome staining
BSA: Bovine serum albumin
CD2AP: CD2-associated protein
CTRL: Control
D: diabetes
DBP: Diastolic blood pressure
D-HBP: Diabetic high blood pressure
DN: Diabetic nephropathy
DSS: Dextran Sulfate Sodium
EM: Electron microscopy
ExFISH: Expansion fluorescent in-situ hybridization
ExM: Expansion Microscopy
FF: Filtration flow
FHH: Fawn Hooded Hypertensive
FITC-Sinistrin: fluorescein-isothiocyanate labeled sinistrin
FPE: Foot Process Enfacement
FPs: Foot process
FSD: Filtration slit density
FSGS: Focal segmental glomerulosclerosis
GDA: Glutaraldehyde
GFB: Glomerular filtration barrier
GFR: Glomerular filtration rate
GLUT-2: Glucose transporter 2
GMB: Glomerular basement membrane
HBP: High blood pressure
H&E: Hematoxylin and Eosin staining
I3C: Indole-3-Carbinol
IHC: Immunohistochemistry
iExM: Iterative expansion Microscopy
MAP: Magnified analysis of the proteome
MCs: Megangial cells
PAS: Periodic acid-Schiff
PBS: Phosphate buffered saline
PBST: Phosphate buffered saline triton
PFA: Paraformaldehyde
PTA: Phosphotungstic acid
RAAS: Renin-angiotensin-aldosterone system
Rac1: Ras-related C3 botulinum toxin substrate 1
RAGE: Receptor for advanced glycation end products
RAS: Renin-Angiotensin System
RI: Refractive index

ROS: Reactive oxygen species
SD: Slit diaphragm
SDS: Sodium Dodecyl Sulfate
SHHF: Spontaneously hypertensive heart failure
SHR: spontaneously hypertensive rats
SIM: Structured Illumination microscopy
STZ: Streptozotocin or streptozocin
TFPC6: Transient receptor potential cation channel
TGR: Transgenic rat
TRPC5: Short transient receptor potential channel 5
ZSF-1: ZSF1-Lepr-fa-Lepr-cp/Crl Hybrid rats

1 INTRODUCTION

1.1 Structure and function of the glomerular filtration barrier in the kidney

The kidneys are two bean-shaped organs that receive blood from the paired renal arteries, while blood exits through the paired renal veins. Each kidney is connected to a ureter, which transports excreted urine to the bladder, a hollow muscular organ **[Figure-1A].** Kidneys are involved in several vital functions in the human body, such as the formation of urine, hormone secretion, blood pressure regulation, acid-base balance, and the regulation of osmolarity. Urine formation is a result of filtration, reabsorption, secretion and excretion processes in the nephron, which is the smallest functional unit of the kidney. Each nephron consists of glomeruli, proximal tubules, a loop of Henle and distal tubules [**Figure-1B**].
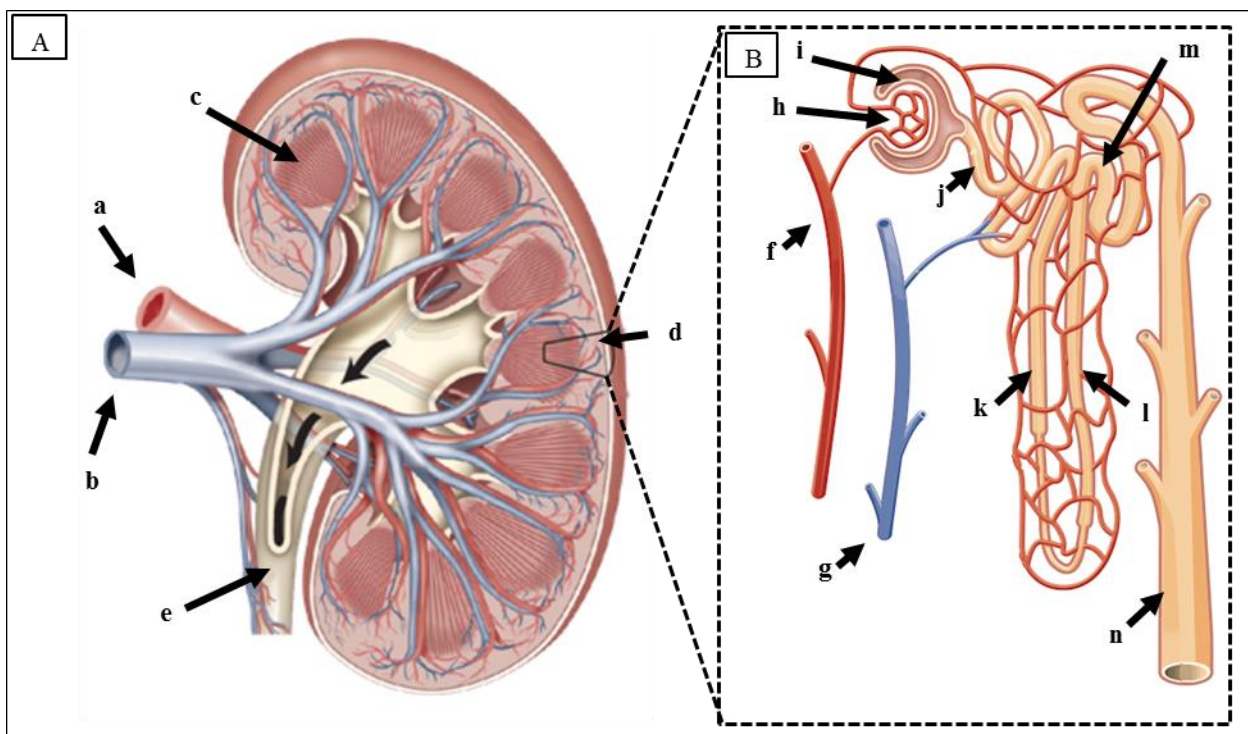
Figure-1: *Representation of kidney anatomy.* A- Kidney crossection; a- Renal artery, b- Renal vein, c- Renal pyramid, d- Renal cortex and e- Renal pelvis and Ureter. B- Anatomic representation of a nephron; f- Intertubular artery, g- Intertubular vein, h- Glomerular capillaries, i- Glomerular capsule, j- Proximal convoluted tubule, k- Descending part of loop of Henle, l- Ascending part of loop of Henle, m- Distal convoluted tubule and n- Collecting duct.

The glomeruli are composed of a tuft of capillaries and a surrounding structure called the Bowman's capsule, which is connected to the proximal convoluted tubule. The glomerular tuft architecture is supported by the mesangium, which consists of

mesangial cells that fill the space between capillaries and are the main force for folding the capillaries[1] [**Figure-2A**]. The glomerular filtration barrier (GFB) is formed in three layers: the fenestrated capillary endothelium (fenestrae) at the inner wall of the capillaries, the glomerular basement membrane (GBM) and the podocytes, highly sophisticated, terminally differentiated epithelial cells with a complex structure [**Figure-2B**]. Each podocyte consists of a large cell body, freely floating above the capillaries on the urinary side, and large primary foot processes extending into numerous secondary foot processes (FPs) that are linked to the GBM by integrins and wrap around the capillaries. Secondary FPs of different podocytes interdigitate with each other and are connected by the slit diaphragm (SD), where nephrin is one of the main constituents [**Figure-2C**]. The internal nephrin domain binds to podocin and CD2AP at the insertion site of the SD. The external domain of one nephrin is connected to another nephrin's external domain, extending from the FP of another podocyte[2] [**Figure-2C**]. The SD has signaling functions but also represents a major molecular filter with a slit size of 5x 14 nm[3]. The filtration barrier filters the urine from the blood and does not allow blood-derived proteins to leak into urine[4]. FP morphology is highly dependent on the architecture of the actin cytoskeleton.

The three layers of the GFB depend on and closely communicate with each other[5]. Damage to any of the layers can cause leakage of the GFB that could result in the presence of protein and albumin, a blood serum protein, in the urine. Detection of protein or albumin in the urine is called proteinuria and albuminuria, respectively. Proteinuria and albuminuria are vital clinical signs for the evaluation of the kidney's function. The degree of filtration is determined by a calculation called glomerular filtration rate (GFR)[6].
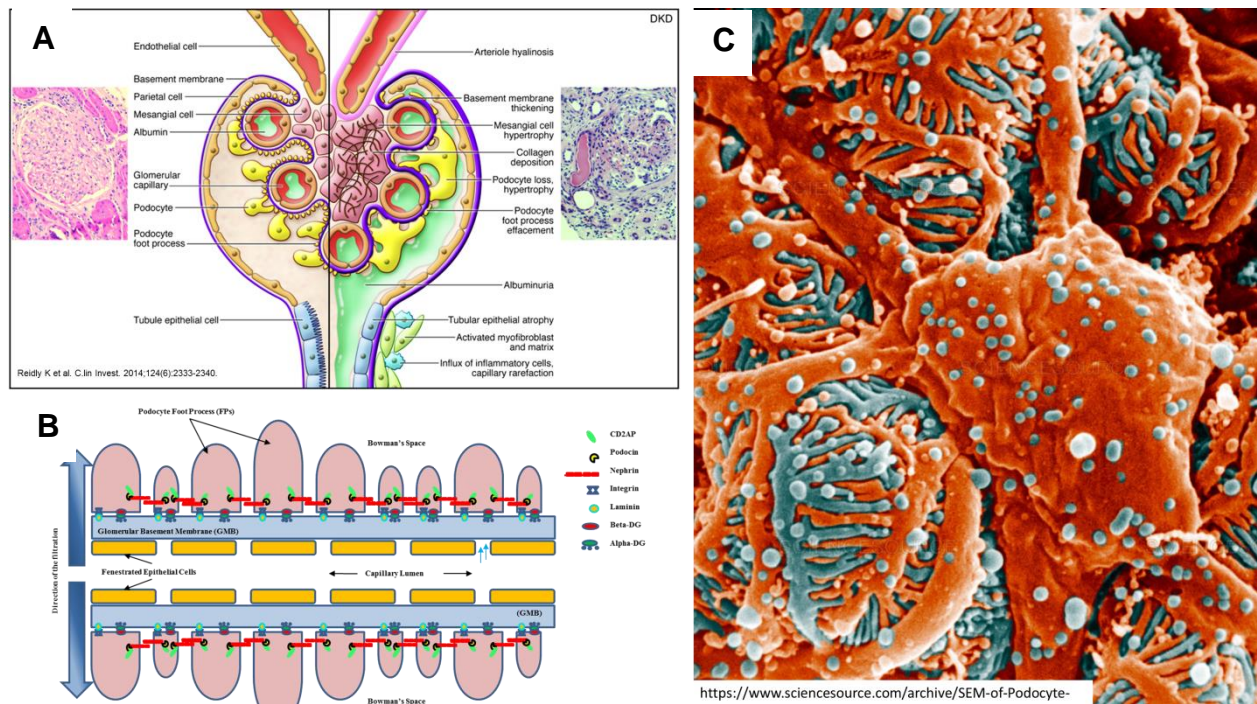
Figure-2: *Graphic illustration of the glomerulus and the filtration barrier.* A- Scheme illustrates the pathological changes in glomeruli during diabetic nephropathy. B- 3 layers of the glomerular filtration barrier: fenestrated epithelial cells with pores enabling filtration, the glomerular basement membrane (GBM) and the podocyte foot processes (FP) fixed to the GBM by laminin and integrin. Nephrin is the main constituent of the slit diaphragm (SD) and attaches at its internal domain to podocin and CD2AP at the insertion site of SD. The direction of filtration is from the capillary lumen to the Bowman's space. Fenestrated epithelial cells, the GMB, the slit membrane and FPs are involved in the filtration process. C- Podocyte morphology with a large cell body, primary foot processes and interdigitating secondary foot processes.

1.2 Glomerular lesions in diabetic nephropathy and hypertension

Many diseases affect kidney function by attacking the glomeruli resulting in glomerular disease. It may be the direct consequence of an infection or a drug with renal toxicity or can result from a condition which affects the entire body, like diabetes or hypertension. Many different kinds of diseases can lead to swelling or scarring of the nephron or glomerulus[7]. However, sometimes the glomerular disease is idiopathic, meaning that it occurs without an apparent associated disease.

1.2.1 Diabetic nephropathy

Discoveries of a metabolic disease related to renal failure are ancient. Ancient Indian and Chinese physicians mentioned the diagnosis of sweet urine disease (sugar cane urine) as early as 300 BC and 600 AD[8]. In Europe, the sweet taste of urine due to diabetes was first mentioned by Thomas Willis in 1674[9]. Sugar was then discovered to be the sweet compound in urine by Matthew Dobson in 1776[9]. In 1880, Etienne

Lancereaux improved the understanding of diabetic nephropathy (DN) by suggesting that diabetes may result in proteinuria in obese individuals. Today, DN is at the center stage of research, since increased wealth worldwide has dramatically increased the frequency of Type-2 diabetic patients. DN is one of the most serious complications in diabetic patients[10], and 30 – 40 % of Type-1 and Type-2 diabetic patients develop DN[11-13]. The first clinical signs of DN are hyperfiltration and albuminuria which indicate leakage of the filtration barrier. Hyperfiltration is closely linked with glomerular hypertrophy. DN typically includes glomerulopathy and tubulopathy. Although the disease progression more closely correlates with the degree of tubulopathy than with glomerular lesions, it is still unclear whether it is molecular and functional alterations in the glomeruli or tubules that initiates the disease. Histopathological changes include thickening of the glomerular and tubular basement membranes and mesangial expansion, which is partially caused by the depositing of worn-out GBM in the mesangium[14]. Nodular Kimmelstiel-Wilson-lesions in glomeruli are an advanced feature of human DN and consist of hyaline, fibrosis and vascular alterations, which results in a decline in the GFR. Albuminuria is often associated with tremendous changes in podocyte shape due to foot process effacement (FPE). FPE is characterized by the retraction, widening and shortening of the FPs, and is regarded as a protective response to prevent podocyte detachment from the GBM[3, 15]. The early stages of FPE are reversible. However, once FPE is complete, podocytes are mainly attached to the GBM by their cell bodies, having lost all of their FPs. Shear stress, produced by filtrate flow through the GBM during hyperfiltration, is a significant challenge specifically for podocytes and can cause them to disconnect from the GBM[15]. Podocyte loss into the urine is characteristic of DN and correlates with albuminuria and the progression of DN[16].

1.2.2 Hypertensive renal diseases

In the 20th century, Franz Volhard suggested that kidney diseases are not only due to diabetes but can be strongly influenced by accompanying diseases (cardiac disease, tuberculosis, etc.)[17-19]. The first critical study showing that high blood pressure (HBP) promotes albuminuria, was completed by Mogensen. He revealed that HBP increases albuminuria and decreases the GFR[20]. Later, they have clearly shown that antihypertensive treatment inhibits the progression of DN[21]. A key determinant in HBP is Angiotensin II (Ang II), initially termed hypertensin, which was first described

in 1940 by Page. This opened a new era for the discovery of novel drugs targeting the renin-angiotensin system (RAS) for renal disease [19, 22, 23]. Hypertension is one of the most common diseases worldwide. Although the exact reason for hypertension often cannot be explained, it produces progressive health problems since it can cause stroke, heart disease, eye problems and kidney failure if untreated[24, 25]. The risk factors double if hypertension occurs alongside with other diseases such as obesity[25, 26] and diabetes [27, 28].

HBP causes arteries around the kidneys to narrow, weaken or harden. These damaged arteries are no longer able to deliver enough blood to the kidney tissue. Long term glomerular ischemia can damage the endothelium, commonly known as the blood vessel lining. This may lead to a build-up of plaques that may be accumulated in the renal arteries causing stenosis and ischemic kidney disease[29, 30]. In this situation, the kidney suffers from inadequate blood flow due to being supplied by the narrowed renal artery, which in turn causes the size of the kidneys to decrease. Other consequences include arterial stiffening, due to the gradual breakdown of elastic fibers, and thickening of the intima (the innermost layer of a blood vessel). An alternative mechanism of hypertensive nephropathy is prolonged glomerular hypertension[30]. These can occur simultaneously or alone. The current hypothesis is that hypertension results in the sclerosis of the glomeruli that ultimately leads to reduced kidney function. Within the unaffected nephrons, the preglomerular arterioles vasodilate as a compensatory mechanism to increase blood flow to the kidney and increase glomerular filtration across undamaged glomeruli[7].

In benign nephrosclerosis, the alterations are gradual and progressive; however, there can be sufficient reserve kidney capacity to maintain sufficient kidney function for many years. The large renal arteries exhibit intimal thickening, medial hypertrophy and duplication of the elastic layer. The alterations in small arterioles include hyaline arteriolosclerosis (accumulation of hyaline, collagenous material) [29, 31], which leads to glomerular collapse (wrinkling and thickening of capillary basement membranes and the collapse of the capillary lumen) and hardening (glomeruli exhibit sclerosis and increases in the mesangial matrix). The degree of damage correlates with the degree of glomerular filtration deficits. Malignant nephrosclerosis occurs in the presence of malignant hypertension (when diastolic BP > 130mmHg). Vessels feature intimal thickening, fibrinoid necrosis, red blood cell fragmentation, extravasation and

thrombosis. These changes create an exaggerated, layered appearance (onion skinning) [7, 29].

1.3 The Renin Angiotensin System in diabetic nephropathy and hypertension

The RAS has been well known for more than a hundred years as a hormonal cascade, regulating fluid and electrolyte balance, as well as blood pressure. The angiotensin peptides are produced in a cascade initiated by renin, which is generated as preprorenin in juxtaglomerular cells of the kidney. Renin cleaves liver-derived angiotensinogen into Ang I, a decapeptide, which is then processed by angiotensin-converting enzyme (ACE) into Ang II[32]. Ang II is the crucial component of this system and binds to two G-protein coupled receptors, the AT1R and AT2R [**Figure-3A**].. Most of the well-known effects of Ang II are transmitted via the AT1R, which is the primary Ang II receptor in the adult kidney. The AT1R utilizes various signaling cascades, which functionally crosstalk with other signaling pathways[33] [**Figure-3B**]. It is now well established that, besides the classic systemic RAS, an independently regulated tissue RAS acting paracrine exist. Recently there are evidence for intracrine acting RAS, which are able to produce Ang II within cells and express Ang II receptors on intracellular organelles[34, 35]. In addition, new components of the system were found including ACE2, Angiotensin (1-7) and the mas receptor which, together with the AT2R, belong to the protective arm of the RAS and often counter-regulate AT1R transmitted Ang II effects [**Figure-3A**].
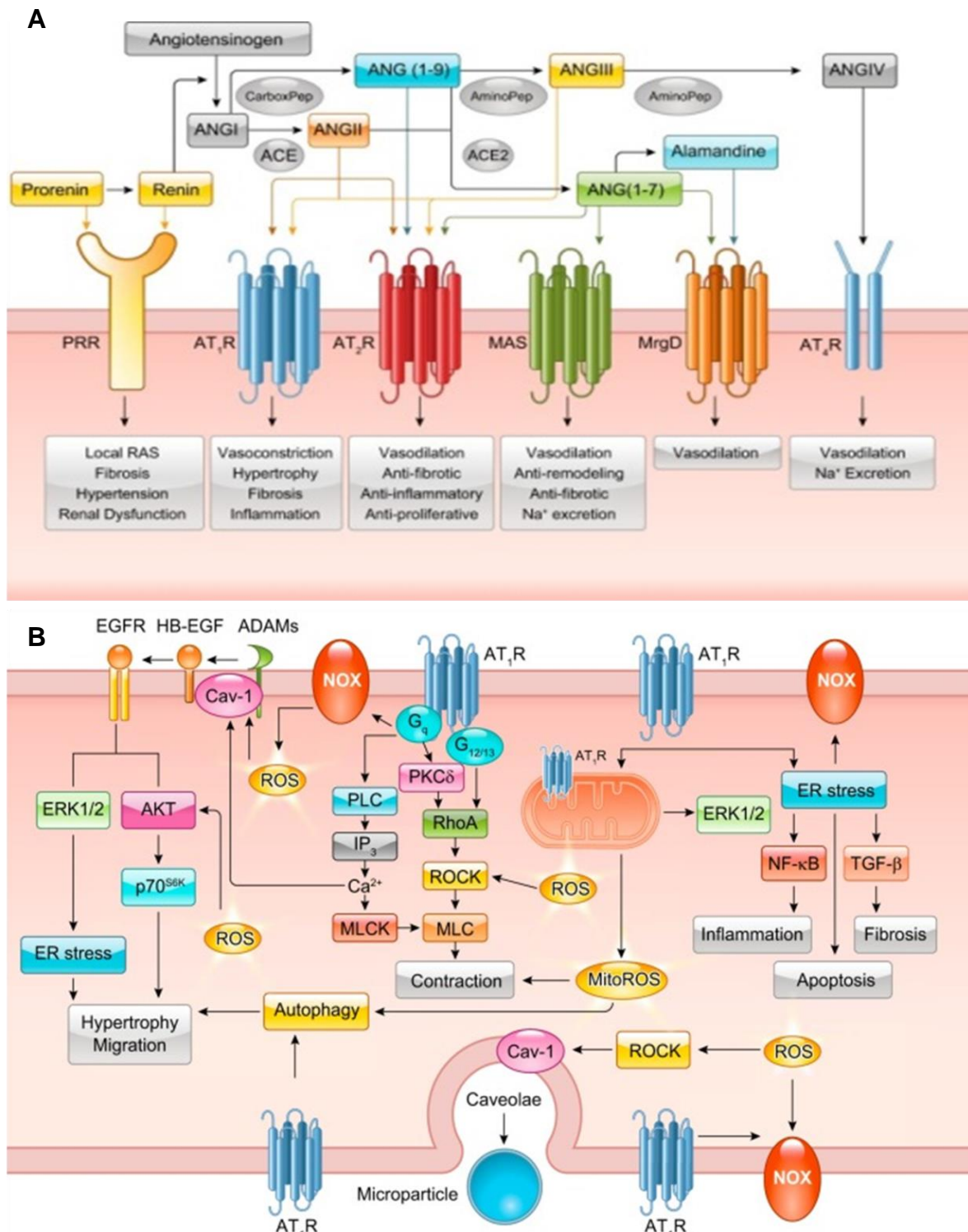
Figure-3: *Renin-Angiotensin System (RAS).* A- Peptides, enzymes and receptors of the RAS and transmitted effects. B- Classical AT1R signaling pathways and their interaction with other pathways *(Forrester et al. 2018).*

The kidney is one of the most critical targets of the RAS. Ang II not only regulates renal function indirectly via its hemodynamic actions, but also by direct actions on renal cells independent of hemodynamic effects. Thus, inhibiting Ang II production or blocking AT1Rs is currently the first-line therapy in DN and hypertension. However, the complex underlying mechanisms have not yet been resolved. Within the

14

glomerulus, AT1Rs are found on mesangial cells and stimulate hypertrophic and proliferative growth[36]. Podocytes express all components of the RAS, allowing independent intracrine and paracrine Ang II action[37]. Local renal Ang II production results in Ang II levels in the nanomolar range within the Bowman's space and the proximal tubules which is roughly 1000-times higher than in the plasma, where Ang II levels are in the femtomolar range[38]. It has previously been shown that AT1R overexpression in podocytes causes slowly progressing FSGS and renal failure[39]. The underlying mechanisms of AT1R action in the podocytes have been intensively studies. It has been shown that AT1Rs in podocytes mediate the Ang II-induced stimulation of the TRPC5/rac1/ROS pathway. Rac1 also leads to a reduction of 4α-actinin and ezrin/radixin/moesin phosphorylation[40-42]. 4α-actinin and the ezrin/radixin/moesin complex regulate the attachment of membrane proteins to the actin cytoskeleton. Therefore, the AT1R induced pathway leads to a reorganization of the actin cytoskeleton and SD protein redistribution. In parallel, ROS decreases RhoA activity resulting in a phenotypic switch in podocytes from a stable to a migratory phenotype that, in vivo, might promote the detachment of podocytes in stress situations[39, 40, 43] [**Figure-4**]. The depletion of podocytes is an important feature in the progression of DN. DN amplifies AT1R signaling in podocytes by specifically stimulating the renal and the intra-podocyte RAS[37, 41].
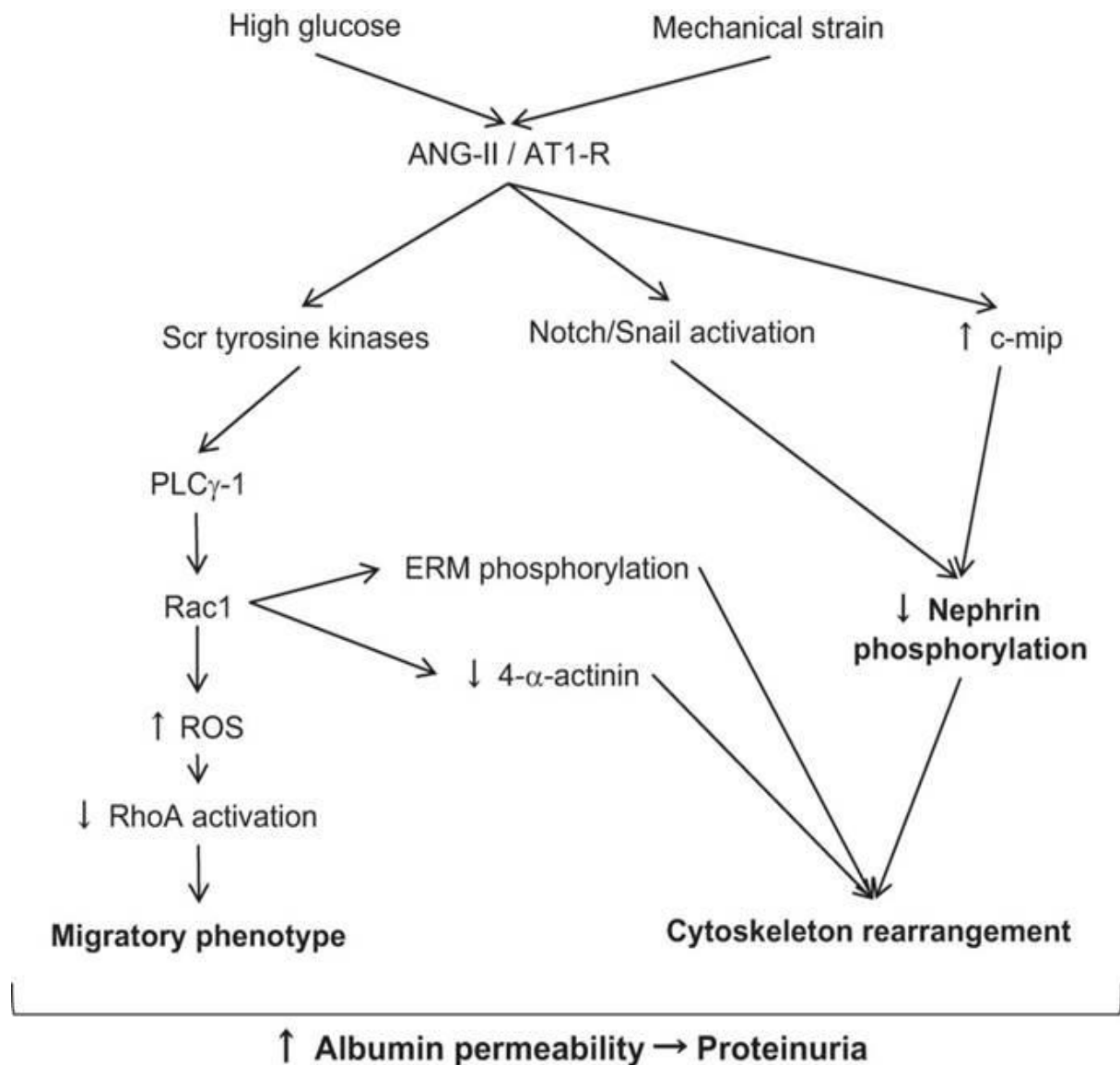
Figure-4: A*T1R mediated signaling in podocytes.* High glucose and mechanical strain stimulate AT1R mediated Angiotensin II (Ang II) signaling in podocytes affecting migratory phenotype and cytoskeleton rearrangement. * *This figure originally published by Marquez, E. et al. 2015*

1.4   Rodent models for diabetic nephropathy and hypertension

Developments and increases in drug discovery studies opened up new questions in the field, as the safety novel drugs are never guaranteed. To be able to surpass this lack of clarity, as well as ethical issues, animal experiments became a gold standard for drug testing in Europe and other countries. Initially, the main problem was finding the right animals to use in research. Since rodents do not usually develop kidney impairments, they were not the best model to study the kidney[44]. Subsequently, scientists have found different ways to induce renal disease in rodents by inbreeding, chemical inducements and genetic manipulations.

1.4.1 Diabetic nephropathy

There are now many animal models used in diabetic research (both Type 1 and Type 2 Diabetes Mellitus), which can be categorized into two main classes as genetically modified animals and chemically induced animals.

Genetically modified rodent models can be subcategorized according to which type of diabetes they are meant to model. BB rats [45-47], LEW 1AR1/ -iddm rats[48, 49], Monobase Diabetic mice[50] and Akita mice[51, 52] are the genetically modified rodent models developed to study Type-1 diabetes mellitus. ZDF rats[53] and Goto-Kakizaki rats[54, 55] are the genetically modified rats developed to study Type-2 diabetes mellitus. A major limitation of these models was their resistance to developing DN. Thus, these rats were subsequently cross-bred with other disease models. In rats, it has been shown that the AT1R is responsible for post-glomerular vasoconstriction and is increased in the renal cortex of obese Zucker rats [56]. Overall, increases in circulating RAS elements, due to excess amount of adipose tissue in obesity, stimulates renal AT1R expression and leads to efferent arteriolar vasoconstriction and elevated glomerular pressure which increases filtration flow (FF)[57]. Another widely applied method is the chemical induction of diabetes type 1 by injection of streptozotocin (or alloxan) (STZ) into healthy animals [58]. Importantly, this model is still the most widely used one. STZ is a chemical compound that is an analog of N-acetylglucosamine. It is transported into insulin-producing B-cells by GLUT-2, where it leads to apoptosis by inhibiting the activity of O-acetlyglucosaminese[59]. STZ was first described as an antibiotic[60], and was marketed as an antibacterial compound. Afterward, it was used for the treatment of malignant islet-cell tumors[61] until a study showed that STZ is toxic to insulin-producing cells specifically[62].

Today, STZ is the most commonly used chemical to induce diabetes for research purposes. Hundreds of experiments have made use of STZ. Some scientists prefer the injection of multiple small doses of STZ to induce diabetes while others prefer to inject a single large dose[63-68]. The route of administration also varies among scientists. Generally, the preferred way is either intravenous (i.v) or intraperitoneal (i.p) injection of the compound. In spite of these variations in application, in practice, there is no proven difference in the degree of diabetes.

STZ-diabetic rodent models only develop the earliest features of DN. Some lines, like the Sprague Dawley rat, are almost entirely resistant to renal damage from STZ diabetes.

1.4.2   The ZSF1 rat

The ZSF-1 rat (ZSF1-Lepr-fa-Lepr-cp/Crl Hybrid) is based on the hypertensive SHR rat, into which both the fa mutant allele, from the sugar diabetic rat ZDF with a leptin receptor defect fa/fa[69], and the cp mutant allele, from the JCR:LA cp/cp rat with the leptin receptor defect cp/cp, were crossed in[70]. Due to the combination of all three defects, the ZSF1 rat spontaneously develops Type 2 diabetes, hypertension, cardiac dysfunction, obesity and severe renal damage. Disease progression is associated with oxidative stress and increased AGE and RAGE[71]. Thus, in addition to hyperglycemia these rats suffer from a metabolic syndrome, which reflect the situation in human DN patients. Obese patients exhibit increased kidney and glomerular size, even in the absence of detectable changes in renal function [72]. Increased GFR is also detectable in obese patients (with or without diabetes mellitus) due to hemodynamic changes [73]. Hemodynamic changes in obesity increase the risk of increased salt sensitivity, which activates the RAS[74, 75]. Furthermore, adipose tissue can activate RAS and induce hypertension, which may result in proteinuria [76].

1.4.3   Hypertension

The spontaneously hypertensive rat (SHR) was the first rat model of hypertension. It was developed by Okamoto and colleagues in the 1960s and was widely used for cardiovascular research[77]. The SHR starts to develop hypertension from around 5–6 weeks of age, and systolic pressure reaches between 180 and 200 mmHg[78, 79]. In this model, scientists have shown that hypertension accelerates microalbuminuria[80, 81]. Leonarda B. Sablay and his colleagues in 1986 in the USA investigated the effect of hypertension on proteinuria, creatinine clearance and renal histology in hypertensive diabetic rats. In the same year, A.E. Doyle and the colleagues in Australia used the same experimental setup to evaluate the effect of hypertension on diabetes. Both experiments showed that hypertension accelerates proteinuria and albuminuria [82, 83]. Thereafter, many hypertensive models have been developed. Among the genetic models the SHR[77], Sabra hypertensive[84, 85], DSS[86], FHH[87], Lyon hypertensive[88, 89] and the Milan hypertensive rats[90] are the most commonly used

ones. Another approach is the chemical induction of hypertension by the chronic infusion of Ang II via osmotic pumps[91-93].

1.4.4   The TGR Cyp1a1Ren2 rat

The development of gene manipulation techniques opened the possibility of developing more sophisticated hypertensive models. The first transgenic rat model was developed by Mullins' group in 1990, in which overexpression of the mouse renin 2 gene caused malignant hypertension[94]. This rat line was often used as a model for DN after induction of STZ-diabetes. However, they developed a malignant phase of hypertension, which limited the usefulness for the study of DN[95, 96]. The Mullins group later developed a more sophisticated transgenic rat carrying the renin 2 gene under the control of the inducible Cytochrome P4501a1 promoter whose activity is tightly controllable through dietary indole-3-carbinol (I3C) supplementation[96, 97].

Using this rat model, J.J. Mullins' group identified severe albuminuria and renal pathohistological changes mimicking DN in human patients when hypertension was induced together with STZ-diabetes. However, it took 7 months of diabetic conditions to develop these alterations. Importantly, they have also shown that none of the genes that were upregulated in human DN were induced through diabetes alone in rats whereas 21% were upregulated in the hypertensive rats and 42% in the diabetic and hypertensive rats[98].

Rats suffering from diabetes and hypertension for 28 weeks generally have high mortality and morbidity, and show aging-related symptoms, which complicate studies on these rats. A similar problem also persists in obese murine models. Although they develop significant renal failure and glomerular impairments, either disease progression takes too much time (28 weeks to 40 weeks) or it is difficult to understand the real reason of the disease since obesity models have both hypertension and hyperglycemia. Due to these problems, a novel rat model to study diabetic nephropathy is urgently needed.

1.4.5   The TGR Neph-hAT1R rat

Another model targeting elements of the RAAS is a transgenic rat which specifically overexpresses the AT1R in podocytes, which was developed in 2004 by our research group[39]. As a result, these rats develop albuminuria and FSGS in the absence of

HBP. The disease starts to develop when rats are more than 16 weeks old and progress slowly.

1.5 Expansion microscopy

Biopsy samples obtained from patient kidneys are mostly stained with hematoxylin and eosin (H&E), Periodic acid–Schiff (PAS) and Heidenhain's AZAN trichrome stain (AZAN) depending on the suspected disease. These samples are then examined under a light microscope to identify the disease or to evaluate the disease progression. Pathologists can detect fibrosis, FSGS[99], glomerular hyalinosis[99], mesangial expansion[99], glomerular adhesion[100], tubulopathy[101] and more using conventional light microscopy. However, the resolution of light microscopy is limited by the diffraction limit of light which varies between 180 – 250 nm, depending on the wavelength of the light used, the refractive index of the immersion media and the focusing angle of the objective. However, important markers for the diagnosis of glomerular diseases such as GBM thickening and FPE are separated by less than 100 nm, making them impossible to resolve using traditional light microscopy. This is why electron microscopy (EM), which provides a resolution 10- to 100-fold better, was required[102, 103]. The recently developed method of super-resolution microscopy[104] achieves a resolution beyond the diffraction limit of light and overcomes some of the drawbacks of EM, like the limited ability to study the distribution of specific proteins using antibody labelling[105, 106] and the super-thin <100nm sections that limit high-resolution volumetric information[105, 106]. Despite of this, super-resolution microscopy is still limited by a working distance of between 10-20µm. Moreover, both techniques, EM and super-resolution microscopy, require sophisticated instruments and are technically demanding. The necessity for expensive and highly specific fluorophore-conjugated antibodies limits the use of super-resolution microscopy.

In 2015, the Boyden group established a method called expansion microscopy (ExM)[107], which allows large-volume-super-resolution imaging using confocal microscopy. Unlike other super-resolution imaging techniques, ExM achieves super-resolution beyond the diffraction limit by physically expanding the tissue sample in a swellable hydrogel, which is placed into water to expand 4 to 4.5 fold isotropically, and thereby increasing the effective resolution by the same factor.

Today, multiple variants and applications of the ExM technique exist, such as Protein-retention ExM, Magnified analysis of the proteome (MAP), Expansion fluorescent in-situ hybridization (ExFISH), iterative expansion Microscopy (iExM). The main difference among the methods is how the target protein or structure is labeled[108-113].

Altogether, the main advantages of ExM are;

1. Conventional antibodies can be used to label a protein of interest[110], whereas labeling is still an issue in electron microscopy, and specific antibodies are very expensive for super-resolution microscopy.

2. Conventional microscopes such as confocal and fluorescent microscopes can be used with no modification

3. ExM does not have any limitations on free working distance allowing super-resolution imaging in 3D of large-volume samples, while electron microscopy is restricted by super-thin samples with a maximum of 100nm and super-resolution microscopy limits the working distance to between 10 and 20µm.

The principal of ExM is similar to the optical clearing technique CLARITY[114], originally developed by the Deisseroth group in 2013, which renders tissue transparent. Thus, the light scattering properties of biological tissues are avoided, and by using confocal microscopy, the imaging depth can be increased to study large three-dimensional structures. Scattering of light in biological samples occurs due to non-homogenous refraction indexes in tissues. The basic method for ExM is the immersion of the tissue in a solution containing paraformaldehyde (PFA) for fixation of amino groups, and acrylamide monomers, which will in turn bind to the PFA molecules and form the gel. In addition, sodium acrylate is added, which absorbs water when polymerized and swells. The acrylamide is then polymerized, anchoring the proteins in a firm gel that keeps the integrity of the sample. The lipids are removed by SDS, and the proteins are denatured by heating. By removing lipids, the RI differences between proteins and lipids disappear.

1.6   The aim of the study

There is a lack of animal models mimicking the structural alterations typically seen in human glomerular diseases. The resistance to diabetic nephropathy in rodent models might partly be explained by the lack of hypertension as a contributing factor or second hit.

In humans, DN affects only 30% of diabetic patients and is often associated with hypertension or obesity as contributing co-factors[115, 116]. A hallmark of chronic kidney diseases caused by diabetes and hypertension is the leakage of the GFB leading to albuminuria and glomerulosclerosis. A key component of the GFB is the podocyte, which is directly regulated by Ang II via its AT1R. Nanoscale evaluation of podocyte FPs required electron microscopy since the physical diffraction limit of optical microscopes prevents high-resolution imaging.

Thus, this study had the following aims:

1. Develop a rat model, which mimics glomerular lesions in human DN.
2. Compare the effects of HBP, DN and synergistic action of HBP and DN on the kidney.
3. Study the role of AT1R signaling in podocytes in these diseases
4. Develop an ExM method for nanoscale evaluation of the podocyte FPs to quantify the degree of FPE in these diseases

2 MATERIAL AND METHODS

2.1 Materials

Materials are the machine, device, software, chemicals, solutions and other consumables used during the experiment.

2.1.1 Equipment

Table 1: *Devices and equipment used to complete this research.*

Name of product	Company	Catolog Number
Multi-Functional Precision Balances	A&D Medical	APOLLO GF-A
Accu-Chek Compact Plus	Roche Inc.	Accu-Chek Compact Plus
Sphygmomanometer S-2	Hugo Sachs Elektronik, Germany	Ser. No. 9003
USB-Device	Mannheim Pharma & Diagnostics GmbH	NIC USB device (UDxxx)
Semi-enclosed Benchtop Tissue Processor	Leica	TP1020
HistoCore Arcadia H - Heated Paraffin Embedding Station	Leica	14039357258
Autostainer XL	Leica	ST5010
HistoCore MULTICUT - Semi-Automated Rotary Microtome	Leica	149MULTI0C1
Cryostat	Leica	CM3050 S
Vibrating blade microtome	Leica	VT1200 S
Sp8 Confocal Microscope	Leica	Leica TCS SP8
Axio Scan.Z1 Slide Scanner	ZEISS	Axio Scan.Z1
Dyad Peltier Thermal Cycler	Bio-Rad	PTC-220
Gel Electrophoresis System	Thermo Scientific	OW-D2BP
Gel Imager	Intas	GEL iX20 Imager Windows Version
Cobas c 311 analyzer	Roche Diagnostics International Ltd.	RS-232C
Infinite® 200 PRO Plate Reader	Tecan Trading AG	Infinite M200

2.1.2 Software for analysis

Transcutaneous GFR Measurement:

• MPD Studio Ver. RC14 (MediBeacon Inc.)

• MPD Lab Ver. 1.0B (MediBeacon Inc.)

Image Processing:

• Leica Application Suite X (LAS X) (Leica Microsystems Inc.)

• Zen Blue Edition (Carl Zeiss Microscopy GmbH)

Statistics:

• JMP 13 (JMP Inc.)

• Microsoft Excel 2010 (Microsoft Inc.)

2.1.3 Chemicals and commercial kits

Table 2: *Chemicals, commercial solutions and kits used in the experiment.*

Name of product	*Company*	*Catolog Number*
Sodium hydroxide (NaOH)	Merck	106462
Ethylenedinitrilotetraacetic acid (EDTA)	Sigma-Aldrich	1233508 USP
Tris base	Sigma-Aldrich	TRIS-RO Roche
Hydrochloric Acid (HCl) 37%	Sigma-Aldrich	258148-2.5L
Platinum™ Hot Start PCR Master Mix (2X)	Invitrogen	13000012
Nuclease-Free Water (not DEPC-Treated)	Invitrogen	AM9932
UltraPure™ Agarose	Invitrogen	16500100
Acetic acid (glacial) 100%	Merck	1000631000
Xylene Cyanol FF	Sigma-Aldrich	X4126-10G
Bromophenol Blue	Sigma-Aldrich	B0126-25G
Sodium dodecyl sulfate (SDS)	Sigma-Aldrich	862010
Glycerol	Sigma-Aldrich	G9012-500ML
UltraPure™ Ethidium Bromide, 10 mg/mL	Invitrogen	15585011
Streptozocin (STZ)	Sigma-Aldrich	S0130-5G
Water for injections (5ml)	Braun	PL 03551/0077
ROMPUN® 2 %	Bayer	6770081
Ketamin ® 2 %	Bayer	2645528
Pellet food I3C	FUJIFILM Wako Chemicals	S5904-P012
Paraformaldehyde (PFA)	Sigma-Aldrich	158127-3KG
NaCl	Sigma-Aldrich	S7653-1KG

Name of product	Company	Catolog Number
KCl	Sigma-Aldrich	P9333-500G
Na2HPO4	Sigma-Aldrich	NIST2186II
KH2PO4	Sigma-Aldrich	NIST200B
Sodium Hydroxide 1N (NaOH)	SAFC	59223C
Hydrochloric acid 1N (HCl)	Sigma-Aldrich	H9892-1L
Sucrose	Sigma-Aldrich	S0389-1KG
2-Methylbutane (Isopentane)	Sigma-Aldrich	M32631-1L
Liquid Nitrogen		
40% Acrylamide Solution	BIO-RAD	1610140
2% Bis Solution	BIO-RAD	1610142
16% Paraformaldehyde Solution	Thermo Fisher Scientific	15710
Sodium acrylate 97%	Sigma-Aldrich	408220-100G
2,2'-Azobis[2-(2-imidazolin-2-yl)propane]dihydrochloride (VA-044)	FUJIFILM Wako Chemicals	925-41020 - VA-044
Bovine Serum Albumin (BSA)	Sigma-Aldrich	F9665-50ML
4-(1,1,3,3-Tetramethylbutyl)phenyl-polyethylene glycol (Triton™ X-100)	Sigma-Aldrich	X100-500ML
m-Xylene ≥99% (Xylol)	Sigma-Aldrich	296325-1L
Ethanol	Merck	1009832511
Hematoxylin solution	Merck	1051741000
Eosin Y	Sigma-Aldrich	E4009-25G
Periodic acid ACS reagent, 99%	Sigma-Aldrich	375810-100G
Schiff's reagent	Sigma-Aldrich	3952016-500ML
Hematoxylin Solution, Mayer's	Sigma-Aldrich	MHS16-500ML
Azocarmine G	Sigma-Aldrich	A1091-25G
Aniline ≥99.5%	Sigma-Aldrich	242284-100ML
Tungstophosphoric acid hydrate	Merck	100582.01
Aniline Blue diammonium salt	Sigma-Aldrich	415049-25G
Orange G	Sigma-Aldrich	O7252-25G
Tissue freezing medium	Leica	14020108926
ProLong™ Diamond Antifade Mountant	Invitrogen	P36970

2.1.4 Primers for genotyping

The TGRNeph-hAT1R were genotyped using the following primers:

Forward primer: 5'-GAA GGA ACC TTA CTT CTG TGG-3'

Reverse primer: 5'-TCT TGT ATA GCA GTG CAG C-3'

The Cyp1a1ren2 rats were not genotyped since the transgene was integrated in the Y-chromosome so that all male rats of this line harbored the transgene.

2.1.5 Antibodies

Table 3: *Primary and secondary antibodies used in this research.*

Name	Species Raised / Raised-Against	Use	Company	Cat.No.	Excitation Wavelength
Podocin	Rabbit	1st	Sigma	p0372-200ul	X
Collagen 4	Rabbit	1st	Progen	10760	X
Nephrin	Guinea Pig	1st	Progen	GP-N2	X
VDAC	Mouse	1st	Abcam	ab14734	X
Alexa 546	Chicken Anti-Rabbit	2nd	Life Technologies	A10040	546
Alexa 647	Chicken Anti-Mouse	2nd	Invitrogen	A-21463	647
Alexa 594	Chicken Anti-Rabbit	2nd	Life Technologies	A-21442	594
Alexa 633	Goat Anti-Rabbit	2nd	Life Technologies	A-21070	633
Alexa 594	Donkey Anti-Goat	2nd	Life Technologies	A11058	594

2.1.6 Solutions prepared

Acetic Alcohol

- 10ml acetic acid

- Make up to 1L with 96% ethanol

Aniline Alcohol

- 1ml aniline oil

- Make up to 1L with 96% ethanol

Aniline Blue-Orange G solution

- 5g aniline blue

- 20g orange G

- 800ml ddH$_2$O

- 80ml acetic acid

- Make up to 1L with ddH$_2$O

0.1% Azocarmine G

- 1g azocarmine G
- 800ml ddH$_2$O
- Heat for 1 hour then cool to room temperature
- 6ml glacial acetic acid
- Make up to 1L with ddH$_2$O, filter

Blocking Solution (IHC)

- 1g BSA
- 50µl Triton X-100
- Make up to 50ml with PBS

0.2M Cacodylate buffer

- 42.8g Sodium Cacodylate
- Fill up to 1L with ddH$_2$O
- pH to 7.4 with either 0.2M HCl or 0.2M NaOH

10x DNA loading buffer

- 4g Sucrose
- 2.5mg Bromophenol Blue
- 10ml TE buffer

0.5M EDTA (pH 8.0)

- 186.1g EDTA
- 800ml ddH$_2$O
- pH to 8.0 with NaOH
- Make up to 1L with ddH$_2$O, autoclave

Karnovsky Fixative

- 2g paraformaldehyde
- Dissolve in 25ml ddH$_2$O by adding 2-3 drops of NaOH, heating to 70°C and stirring

- Cool to room temperature

- 5ml 25% glutaraldehyde

- Make up to 100ml with 0.2M cacodylate buffer

- pH to 7.4 with HCl

4% Paraformaldehyde

- 40g paraformaldehyde

- 100ml 10x PBS

- 700ml ddH_2O

- Add 3-4 drops of concentrated NaOH

- Heat with stirring until dissolved

- pH to 7.4 with NaOH

- Fill up to 1L with ddH_2O

- Filter and store at -20°C

10x Phosphate Buffered Saline (PBS)

- 80g NaCl

- 2g KCl

- 2.4g KH_2PO_4

- 14.4g Na_2HPO_4

- Add 800ml ddH_2O

- pH to 7.4 with HCl

- Fill up to 1L with ddH_2O, autoclave

1x Phosphate Buffered Saline (PBS)

- 100ml 10x PBS
- Fill up to 1L, autoclave

Phosphotungstic acid

- 50g phosphotungstic acid hydrate

- Make up to 1L with ddH_2O

Proteinase K

- 100mg proteinase K

- 10ml ddH$_2$O, aliquot and store at -20°C

RNase A

- 100mg RNase A

- 10ml 10mM sodium acetate

- Heat to 100°C for 15 minutes, cool to room temperature

- Adjust the pH to 7.4 with 1M Tris-HCl

- Aliquot and store at -20°C

18% Sucrose

- 90g Sucrose

- 50ml 10x PBS

- Make up to 450ml with ddH$_2$O

50x TAE Buffer

- 242g Trizma base

- 57.5ml acetic acid

- 100ml 0.5M EDTA (pH8.0)

- Make up to 800ml with ddH$_2$O

- pH to 8.5 with concentrated NaOH

- Make up to 1L with ddH$_2$O, autoclave

Tail Buffer

- 50ml 1M Tris-HCl (ph 8.0)

- 200ml 0.5M EDTA

- 20ml 5M NaCl

- 100ml 10% SDS

- Make up to 1L with ddH$_2$O, autoclave

1M Tris-HCl

- 121g Trizma base

- 800ml ddH$_2$O

- Use concentrated HCl to get to desired pH

- Make up to 1L with ddH$_2$O, autoclave

2.2 METHODS

2.2.1 Animals

All animal studies were conducted in accordance with federal and local laws and were approved by the Regierungspräsidium Karlsruhe, Land Baden-Württemberg (G77/17, G76/18).

The animals were bred and housed in our own animal facility at the Medical Faculty Mannheim. The animal experiments were performed on three rat lines; ZSF-1 rats, Sprague Dawley rats and crosses of TGRNeph-hAT1R and TGRCyp1a1Ren2 rats. Male ZSF-1 (Lepr^{fa}/Lepr^{cp}/Crl) ob/ob rats and their lean controls were purchased from Charles River Company, and Sprague Dawley rats were purchased from Janvier. The ZSF-1 rat is an F1 hybrid from crossing lean female fatty diabetic rats (ZDF; +/fa) with lean male spontaneously hypertensive heart failure rats (SHHF/Mcc-facp; +/fa, +/+)[117]. For the eperiments 8-10 rats/group were used if not other indicated.

The TGRNeph-hAT1R rat, which specifically overexpresses the AT1R in podocytes, was developed in our own group[39] and the TGRCyp1a1Ren2 rat, which carries an I3C dietary inducible transgenic renin gene incorporated in the Y-chromosome, was developed by Prof. John Mullins, Edinburgh[94, 97]. Two-month-old male Sprague Dawley rats were rendered diabetic by using a single dose of STZ (35 mg/kg, i.v.). Untreated rats served as controls. After 10 weeks and 7 months, urine was collected for 24 hours using metabolic cages with water and food access ad libitum, after which blood was taken.

ZSF1 rats spontaneously develop diabetes. 10 ob/ob and 8 control rats were used in the experiment. In ZSF1 rats, renal function, glucose status and blood pressure were

determined between the ages of 8 weeks and 40 weeks at monthly intervals. Urine samples were collected at 8, 12, 13, 16, 22, 27, 30, 33, 37 and 40 weeks of age.

In order to compare the effects of hypertension with the synergistic effects of hyperglycemia and hypertension on the same genetic background and to study the role of AT1R signaling in these disease conditions, we crossbred female heterozygous TGRNeph-hAT1R rats with male TGRCyp1a1Ren2 rats to obtain male transgenic Cyp1a1Ren2 rats either carrying (TGR) or not carrying (Wild) the Neph-hAT1R transgene in addition. Renin transgene expression was induced by the 0.125% I3C supplementation in the food. Blood pressure increased within 24 hours. Male rats not treated by I3C were normotensive. Diabetes was induced by a single dose of STZ (60 mg/kg, i.p.). This breeding procedure resulted in 50% Neph-hAT1-TG/Cyp1A1Ren2a-TG (TGR) and Neph-hAT1-wt/CypARen2a-TG male rats (Wild) [**Figure 5**].

All the rats used in this experiment have been housed in a social cage (3-4 rats for per cage). Cages were cleaned twice per week for controls (CTRL) and HBP rats while the cages that held diabetic rats were cleaned 3-4 times per week due to excessive urine production. Autoclaved sawdust and some paper were used as bedding material, and some enrichment (nesting material, wood particles and some piece of paper) was provided to enhance the social activities of the rats. Pellet food and water was provided ad libitum, and all cages were controlled daily by animal house staff. The rooms housing animals were kept at 22°C ± 1°C temperature and 60 ± 10 % of relative humidity, with a 12 hours alternate light and dark cycle and 100 % fresh air exchange.
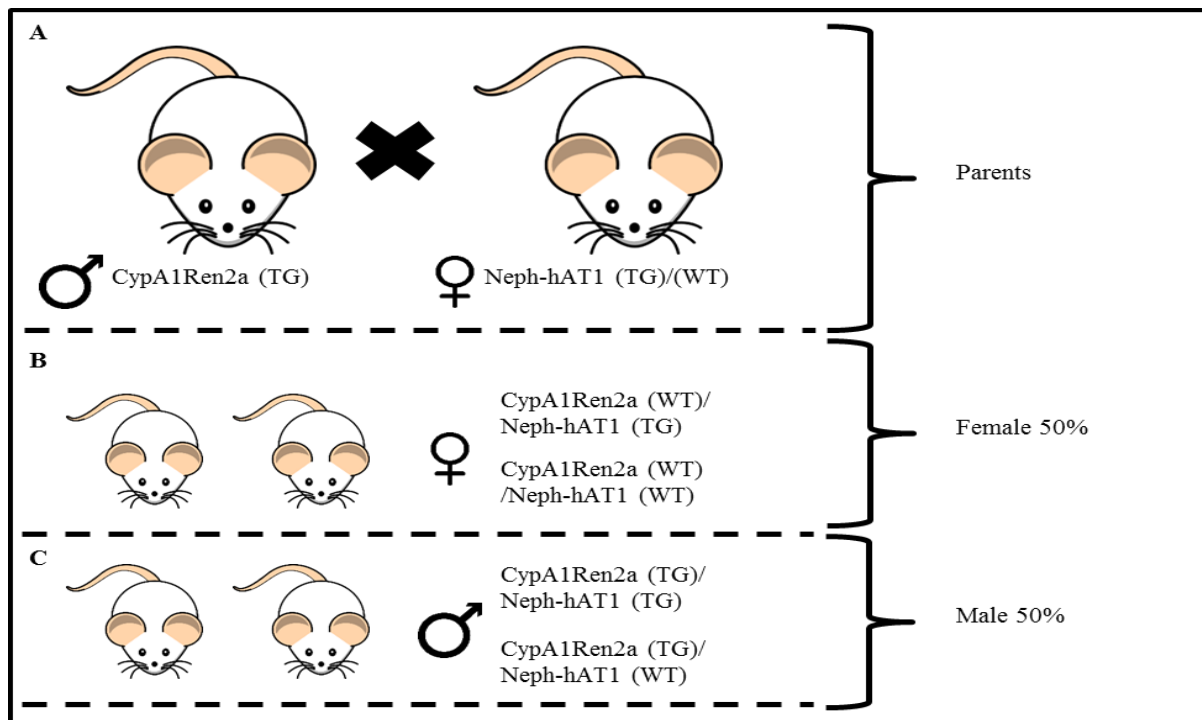
Figure 5: *Mating schema to create double transgenic male rats.* A- Male rat which carries inducible renin gene (Cyp1A1Ren2a) and the female rat which carries Neph-hAT1R transgene (Neph-hAT1 TG/WT). B- Female offspring which do not carry the CypA1Ren2a transgene, but they are either Neph-hAT1 (TG) or Neph-hAT1 (WT) for AT1 R transgene. C- Male offspring which all carries the CypA1Ren2a transgene, but they are either Neph-hAT1 (TG) or Neph-hAT1 (WT) for AT1R transgene.

2.2.2 DNA isolation and genotyping

DNA samples for genotyping were extracted from the tissue samples collected during ear markings. Samples were placed into PCR tubes and incubated in 75μl of 25mM NaOH and 0.2 mM EDTA solution for 1 hour at 98°C. Then, samples were cooled on ice for 15 minutes after which 75μl of 40mM Tris-HCl (pH 5.5) was added. Samples were then centrifuged at 4000 g for 3 minutes. 100μl aliquots were transferred to new PCR tubes, and 2μl of each aliquot was used for genotyping by PCR.

After the PCR reaction, samples were run on a 1.5% agarose gel at 100V for 25 minutes at room temperature. The gel was then imaged by UV light to record positive (Transgenic, or TGR) and negative (Wild Type, or WT) rats.

2.2.3 Design of HBP and diabetes experiments

Male Neph-hAT1-tg/Cyp1A1Ren2a-tg (TGR) and Neph-hAT1-wt/CypARen2a-tg (Wild) 6 weeks old rats were divided into six experimental groups (CTRL-TGR, CTRL-Wild, HBP-TGR, HBP-Wild, D-HBP-TGR, D-HBP-TGR). In D-HBP rats, diabetes was induced at the age of 6 weeks by intraperitoneal injection of 60mg/kg

STZ. After two weeks, D-HBP and HBP rats received pellet food supplemented with 0,125% I3C until the end of the experiment to induce HBP. Control rats were fed with standard pellet food. Finally, the animal experiments were terminated after 8 weeks when the rats were 14 weeks old [**Figure 6**].
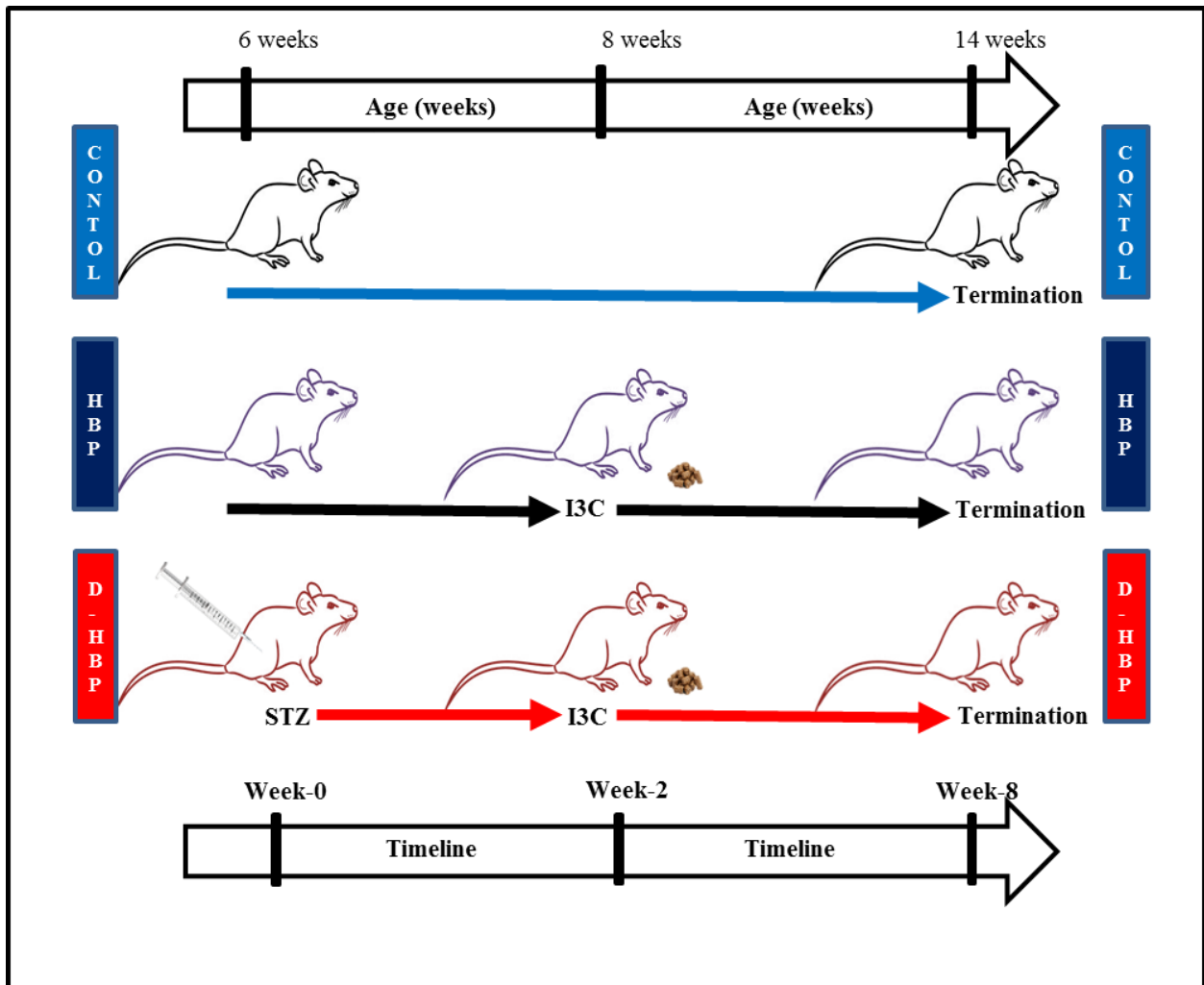
Figure 6: *Demonstration of the experimental timeline.* Control rats were not treated. HBP rats were fed by pellet food, which contains 0,125% Indole-3-Carbinol (I3C) 2 weeks after the beginning. D-HBP rats were intraperitoneally injected with 60mg/kg of streptozocin at the beginning of the experiment, then fed by pellet food which contains 0,125% Indiole-3-Carbinol (I3C) 2 weeks after. All rats were sacrificed 8 weeks later.

2.2.4 Health monitoring

Blood glucose concentration, blood pressure, body weight and rat grimace scale were monitored during the experiment to evaluate the health condition of the rats[118]. Blood pressure was measured using a tail-cuff once per week while blood glucose concentration and body weights were measured twice per week. The appearance

and social behavior of the rats were observed twice per week and evaluated according to the rat grimace scale.

2.2.5 Induction of diabetes

Diabetes was induced by administrating of a single intraperitoneal dose of STZ (60 mg/kg). Bodyweight, blood glucose level and behavior of the rats were monitored until the end of the experiment.

2.2.6 Induction of hypertension by Indole-3-carbinol

Hypertension was induced by dietary application of pellet food supplemented by 0.125% I3C (cat.no. S5904-P012, ssniff Spezialdiaten GmbH), which induced transgenic renin expression in the Cyp1A1Ren2a rat model as previously described[211]. Blood pressure was then monitored by tail-cuff plethysmography twice per week.

2.2.7 Metabolic cages

All experimental rats (CTRL, HBP and D-HBP) were placed in metabolic cages for 24 hours to collect urine samples and to evaluate water and food consumption. Powder food and water were supplied ad libitum. All rats in the metabolic cages were monitored every 8 hours for health. Blood plasma was taken in parallel. Clinical data from plasma and urine were determined to evaluate renal function, calculate GFR and the degree of proteinuria and albuminuria for each rat.

2.2.8 Transcutaneous measurement of the GFR

The GFR was measured transcutaneously using a GFR device in four rats/group in the second (2 weeks after diabetes induction and just before HBP induction) and sixth weeks (4 weeks after induction of hypertension) of the experiment [**Figure 7**]. The rats were anesthetized by isoflurane vapor. Hairs were removed using a shaving machine followed by incubation with hair loss cream (Cat.no. 86725 (867250860115), Nivea) for 3 minutes to get rid of fine hairs. Hairless skin was washed by distilled water and the rat was incubated for 10 minutes at 37°C. After the determination of the body weight, the transcutaneous GFR device was placed on the naked skin. FITC-Sinistrin (3mg/100g) was injected intravenously in the tail. The rat was then placed into a fresh cage and received pellet food and some enrichments

but no water. The GFR was measured for 2 hours. The data were saved in CVS format and then processed by MPD Studio (Ver. RC14, MediBeacon Inc.) to calculate the half-life.
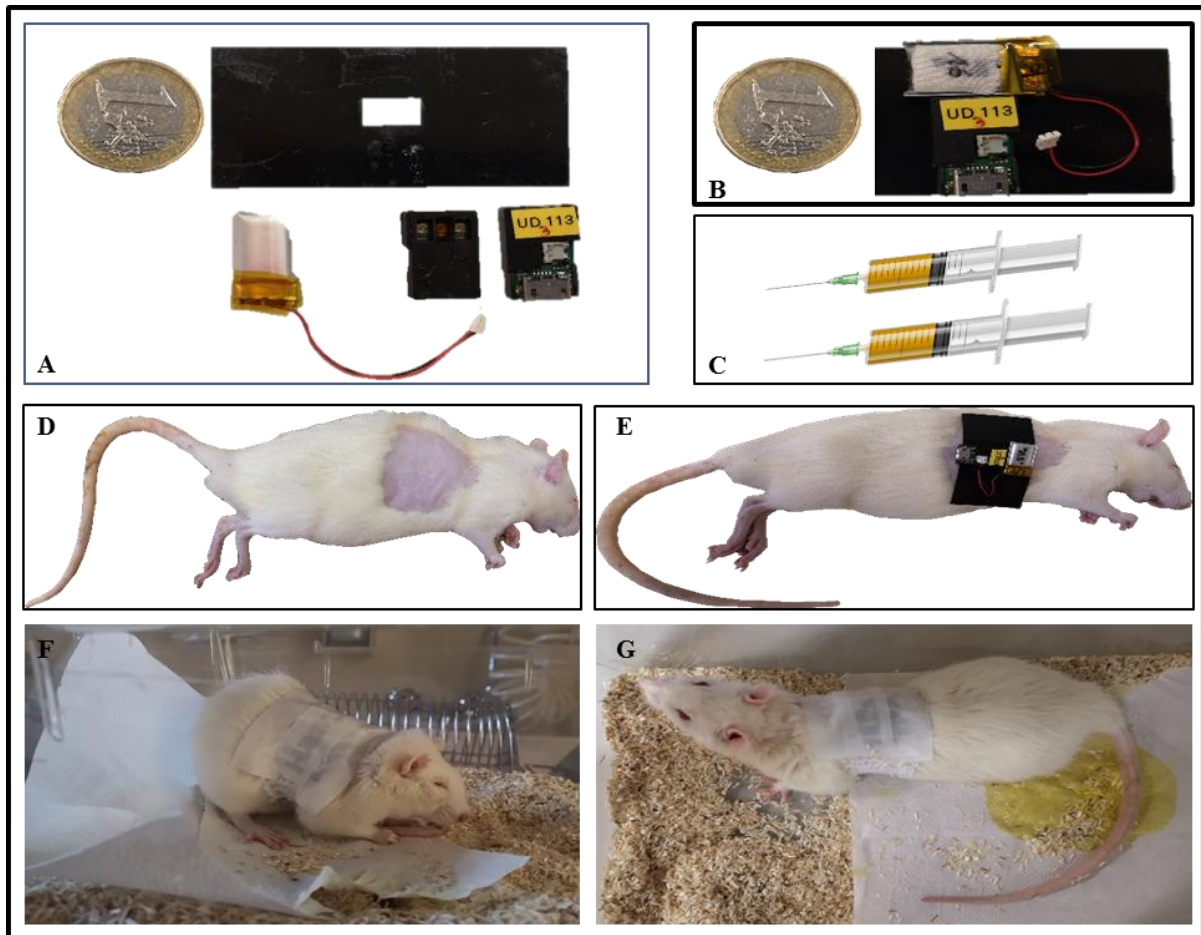
Figure 7: *Setup for transcutaneous GFR measurement.* A- the components of transcutaneous GFR measurement device; 1- two-sided tape with a small square hole, 2- battery and 3- device. B- Assembly of the device on the two-sided tape. C- Prepared FITC-Sinistrin before injection. D- Shaved rat after anaesthetization. E- The assembled device stuck over the shaved area before FITC-Sinistrin injection. F- The rat immediately after wake up. G- The rat urinated after a while.

2.2.9 Creatinine clearance as an estimate of the GFR

The creatinine clearance was calculated using the following formula.

$$GFR = \frac{[UCr * V]}{SCr} * \frac{1000}{1440}$$
$$GFR = ml/min$$

** Creatine clearance tends to exceed the correct GFR by 10 to 20 percentage.

UCr is urinary creatine concentration, V is urine produced in 24 hours, SCr is serum creatine concentration.

2.2.10 Termination of the experiment and eample collection

The experiments were terminated at the age of 14 weeks, namely 8 weeks after STZ injection and 6 weeks after induction of hypertension. Rats were anesthetized with 5mg/kg of Ketamine ® 2% and 100mg/kg of ROMPUN® 2 % (xylazine based drug) mixture. After the rat became unresponsive to the withdrawal reflex, the dissection procedure was started. The right kidney was collected before perfusion, placed into a 2ml tube as pieces and immediately frozen with liquid nitrogen. Then, the rat was sacrificed by retrograde total body perfusion with the fixative 2 % paraformaldehyde (PFA) in PBS, pH 7.4, containing 0.05% glutaraldehyde (GDA) for 3 min at a pressure of 220 mmHg as previously described[119]. Kidney, heart and liver were harvested for light microscopy. The perfused left kidney was divided into five pieces using a matrice. One thin middle part for paraffin embedding and a thick middle part for expansion microscopy were placed into 4% PFA, and incubated overnight at 4°C. Other thin slices from the mid parts were placed into karnovsky fixative for electron microscopy. The remaining two end pieces were saturated overnight in 18% Sucrose in PBS and then frozen in isopentane at -30°C followed by liquid nitrogen.

2.2.11 Post fixation and paraffinization

Fixed samples were placed into plastic cassets for post-fixation and paraffinization procedures. Samples were then incubated in 4% Formalin for 1.5 hour twice and followed by incubation of 70% ethanol, 80% ethanol, 96% ethanol, 99% ethanol twice, 100% xylol twice and liquid paraffin (60°C) 3 times for 1.5 hours each. Samples were then embedded into paraffin blocks and left to cool.

2.2.12 Clinical parameters

All the physiological parameters obtained from blood plasma and urine were measured by the core facility of the ZMF by the use of a cobas C 311 analyzer (Roche Diagnostics) except urinary albumin data. This was measured by the core facility using an albumin elisa kit (peroxidase-conjugated rabbit IgG antibody, Cat.no.55775, Abcam) and an elisa reader (Infinite® 200 PRO Plate Reader, Tecan Trading AG).

2.2.13 Histological staining and sample examination

2.2.13.1   Hematoxylin and Eosin staining

Hematoxylin and eosin stain (abbreviated as H&E stain) is one of the principal tissue staining methods used in histology. The aim of the staining is to make tissue sections, which is naturally transparent, visible and distinguishable under the light microscope. H&E stain consists of two histological stains: hematoxylin and eosin. The hematoxylin (cationic dye) stains cell nuclei blue, and eosin (anionic dye) stains the extracellular matrix and cytoplasm pink.

To stain the samples with H&E, 3 µm sections were cut by microtome and placed on slides und were dried at 60°C for 1 hour then cooled down for 10 minutes at room temperature. The sections were incubated 3 times in xylene for 5 minutes for deparaffinization, and then the samples were incubated in the following series of ethanol concentrations- 100%, 96%, 80%, 70% and ddH2O for 2 minutes each. Thereafter, they were stained by hematoxylin for 4 minutes, washed with tap water for 10 minutes, and incubated for 2 minutes in eosin solution. The sections were dehydrated by washing in ddH2O for 1 minute, and then the samples were incubated in the following series of ethanol solutions- 70%, 80%, 96% and 3 times in 100% ethanol for 2 minutes. Finally, samples were incubated 3 times in xylene for 5 minutes each. Stained samples were mounted with polylysine.

2.2.13.2   Periodic acid–Schiff staining

Periodic acid–Schiff (commonly known as PAS) is a staining technique which is used to detect polysaccharides, mucosubstances such as glycoproteins and glycolipids.

To perform this staining, 3 µm sections cut by microtome and placed on glass were incubated at 60°C for 1 hour then cooled down for 10 minutes at room temperature. The sections were incubated 3 times in xylene for 5 minutes for deparaffinization, and then the samples were incubated in the following series of ethanol concentrations- 100%, 96%, 80%, 70% and ddH2O for 2 minutes each. Thereafter, they were incubated in 0.5% periodic acid solution for 5 minutes, washed in ddH2O for 1 minute, and then incubated in Schiff reagent for 15 minutes. Sections were washed under running tap water for 5 minutes, and then dehydrated in the following series of ethanol concentrations- 70%, 80%, 96% and 3 times in 100% ethanol for 2 minutes

each. Finally, the samples were incubated 3 times in xylene for 5 minutes each. Stained samples were then mounted with polylysine.

2.2.13.3   Heidenhain's AZAN stain

Heidenhain's stain, or Heidenhain's AZAN trichrome stain, is a staining methods in which three anionic dyes (azocarmine G, aniline blue and orange G) are used in cooperation with phosphotungstic acid (PTA). Azocarmine G stains nuclei, erythrocytes, fibrin, fibrinoid, acidophilic cytoplasm and epithelial hyalin red. Aniline blue and orange G counterstains collagen fibers, basophilic cytoplasm and mucus blue and orange.

3 µm sections were incubated at 60°C for 1 hour then cooled down for 10 minutes at room temperature. The sections were incubated 3 times in xylene for 5 minutes for deparaffinization, and then the samples were incubated in the following series of ethanol concentrations- 100%, 96%, 80%, 70% and ddH2O for 2 minutes each. Then the samples ware washed in in 0.1% azocarmine G solution for 20 minutes at 56°C followed by a wash in running tap water for 2 minutes. The intensity of the staining was controlled by 3 short (10 seconds to 1 minute) washing steps with aniline alcohol until the staining of the nucleus and cytoplasm were distinguishable. After that, the reaction was stopped by the acetic acid solution. The collagen content in the sample was then stained by incubating in 5% phosphotungstic acid for 20 minutes, washed in running tap water, and lastly incubated in aniline blue-orange G solution. The samples were dehydrated by ddH2O wash, and cleared by washing twice in 96% ethanol and then incubated twice in 100% ethanol for 2 minutes and twice in xylene for 5 minutes. Stained samples were then mounted by polylysine.

2.2.13.4   Determination of the damage index

The damage indexes were calculated using AZAN stained tissue section. We designated five categories of glomerular damage G0 – G5, whereby G0 characterized healthy glomeruli and G5 sclerotic glomeruli. An average of 180 glomeruli per rat were evaluated.

2.2.13.5 Electron microscopy

The preparation of the samples and electron microscopy was performed by Prof. Gröne, DKFZ and Prof. Kriz, Medical Faculty Mannheim, University Heidelberg using standard techniques.

2.2.13.6 High-Resolution light microscopy

Thin-section light microscopy was performed by Prof. Kriz, Medical Faculty Mannheim, University Heidelberg, as previously described[14]. With a diamond knife, 0.5 µm thick sections were obtained and stained with methylene blue and used for high-resolution light microscopy.

2.2.14 Expansion microscopy and immunohistochemistry

2.2.14.1 Expansion microscopy for kidney samples

Kidney samples were incubated overnight in 4% PFA thereafter placed into Amplification Hydrogel Solution (AHS) in a 50 ml falcon tube wrapped with foil and incubated on a shaker for 2-3 days at 4°C (AHS: tissue ratio = 10:1). After that, samples were placed into a 6 well plate filled with AHS. Then the solution was covert by mineral oil to avoid oxygen in the air. The plate was incubated in a humidified chamber at 37°C for 2 hours polymerization. After the polymerization step, the tissue containing gel was trimmed to minimize volume, using a sharp razor blade. Next the gel was washed for 2 hours at room temperature in 1xPBS with shaking. The samples were further processed by cutting 500 µm slices using a vibratome and were then placed into a 24 well plate with 1xPBS. All the slices were then stored at 4°C in 1x PBS. Clearing of the tissue was achieved by removing the lipids due to incubation of the samples in 6 well plates in a wet chamber in denaturation solution with SDS for 12 hours at 70 °C, followed by further 12 hours at 95°C (1mm thick tissue 2x 24hr). The denaturation step should not be too short; otherwise, it blunts the expansion, and not too long; since then, the tissue becomes too fragile. Thereafter the samples were washed 2-4 hours in 1x PBST with shaking at room temperature to eliminate denaturation solution. After this step, denatured samples were transparent and fragile. These samples can be kept for 6 months at 4°C for long term storage.

2.2.14.2 Immunohistochemistry for expansion microscopy and imaging samples

Denatured and 1x PBS washed samples were cut into small pieces, and accordingly placed into 24 well plates containing 1 ml of 1x PBS in each well. Then, 1x PBS was replaced with 500 µl blocking buffer (2% BSA in 1x PBS with 1% Triton X-100). Thereafter, samples were incubated overnight at 37°C in a humidified chamber. The blocking buffer was then replaced with 350 µl of primary antibody solution, which contained blocking buffer and primary antibody in a ratio indicated on the table (**see 2.1.5**) and incubated overnight. Later on, samples were washed 3 times for 10 minutes each. Then, the samples 350µl of secondary antibody solution was added and incubated overnight, and then washed 3 times for 20 minutes each. Samples were then ready to proceed with the first imaging at the confocal microscope.

For expansion, the PBS needs to be carefully removed and the sample is placed into a 10 ml plate with an excess of deionized water for 1-2 days at room temperature. The water is changed 3-4 times during this period. Then the samples were again imaged at the confocal microscope. The expanded tissue consists of more than 90% of water, thus it is transparent and the RI index matches to water (RI 1.33). Autofluorescence is strongly reduced. For imaging, the gels were placed into a 3 mm plate with a glass bottom and immobilized with 2% low melt agarose in water to prevent movement during imaging. For imaging 10x, 20x, and 63x water immersion objectives were used. Thereafter, the tissues were shrunken by placing it into 1xPBS for further storage. For repeated immunohistochemistry, the shrunken sample is destained by incubation in denaturation solution 6-16 hr at 70°C, thereafter wash 3x in PBST each for 2hr at 37°C. Then the next immunohistochemistry is started as described above.

2.2.14.3 Expansion factor and distortion

In tissue expansion technique for microscopy, one of the biggest challenge is to evaluate the expansion factor. To this end, we compared the maximal longitudinal and transverse glomerular diameters/glomerulus and measured 50 glomeruli/rat from both, non-expanded frozen H&E stained tissue and expanded tissue from the same kidney, which was podocin stained. Then for each kidney the mean values for both, non-expanded frozen tissue and expanded tissue samples, were calculated. The

ratio between the mean of expanded glomeruli and the mean of the non-expanded glomeruli was calculated as the expansion factor for an individual rat. Morphometric measurements in expanded tissues (podocyte FP width's) were then divided through the individual expansion factor. The ratios between the longitudinal and transverse glomerular diameters were calculated for each glomerulus to determine the distortion.

2.2.14.4   Structured Illumination Microscopy (SIM)

Structured Illumination Microscopy (SIM) analysis of the podocyte slit membrane density was performed by Prof. N. Endlich, University Greifswald, Fa. Nipoka using previously described technique[106]. For the quantification of the FP structure they developed a software-based approach named Podocyte Exact Morphology Measurement Procedure (PEMP) and measured the filtration slit density (FSD), which highly correlated inversely with FP width.

3 RESULTS

3.1 Kidney pathologies in classical rat models of diabetes

3.1.1 Effect of STZ induced diabetes on the rat kidney

Previous experiments in our research group demonstrated that STZ-induced diabetes in Sprague Dawley rats only causes minor alterations in the kidney, even after 7 months of diabetes. **Table 4** shows significantly altered clinical data from the urine and plasma of diabetic rats, 10 weeks and 7 months after the induction of diabetes, relative to age-matched controls. Diabetic rats showed features typical of type-1 diabetes, including diuresis and increased water and food consumption. The urinary albumin excretion, an early indicator of diabetic nephropathy, was slightly increased 10 weeks after diabetes induction (4.5 mg/24hr vs. 0,45mg/24hr in controls) and progressed only moderately during a 7 month period of diabetes (7.48 vs. 0.53mg/24hr in controls). The renal histology did not reveal any pathological changes in kidneys morphology [**Figure 8**], although metabolic alterations in tubular epithelial cells occurred already 4 weeks after induction of diabetes. Periodic acid staining (PAS) and oil red staining revealed increased lipid and glycogen deposits within tubules suggesting a disturbed cellular metabolism. Moreover, increased proliferation was noted, as shown by Ki-67 immunohistochemistry [**Figure 9**]. Overall, SD rat kidneys show resistance to STZ-induced diabetes and only very early signs of DN can be induced.

Table 4: *Clinical data from the plasma and urine of Sprague Dawley rats 10 weeks and 7 months, respectively, after induction of diabetes (by STZ injection, 35 mg/kg i.v.). Data are mean ± SD; *p<0.05 vs. control, **p<0.01 vs. control, ***p<0.001 vs. control, n= 5 rats/group.*

Parameter	10 weeks STZ-diabetes		7 months STZ-diabetes	
	Control	Diabetes	Control	Diabetes
Urine, ml/24 hr	14.9 ± 4	142 ± 10,7***	16 ± 5.7	275 ± 26.4***
u-glucose, mg/24 hr	4.4 ± 2	131482 ± 393941**	57.1 ± 25.5	194225 ± 38031**
u-protein, mg/24hr	13 ± 3	13 ± 14	28.2 ± 9.3	30.9 ± 19.6
u-albumin, mg/24hr	0.45 ± 0.034	4.58 ± 4.59*	0.53 ± 0.022	7.48 ± 5.17*
p-urea, mg/dl	38.1 ± 10	60.9 ± 9.7*	39.6 ± 0.9	64.0 ± 6.0**
p-creatinine, mg/dl	0.33 ± 0.014	0.26 ± 0.02**	0.36 ± 0.05	0.23 ± 0.01**
p-protein, mg/dl	62.5 ± 2.1	54 ± 5.1	65 ± 4.2	57 ± 3.3
p-glucose, mg/dl	146 ± 1.4	576 ± 6.7***	136 ± 4.9	745 ± 80***
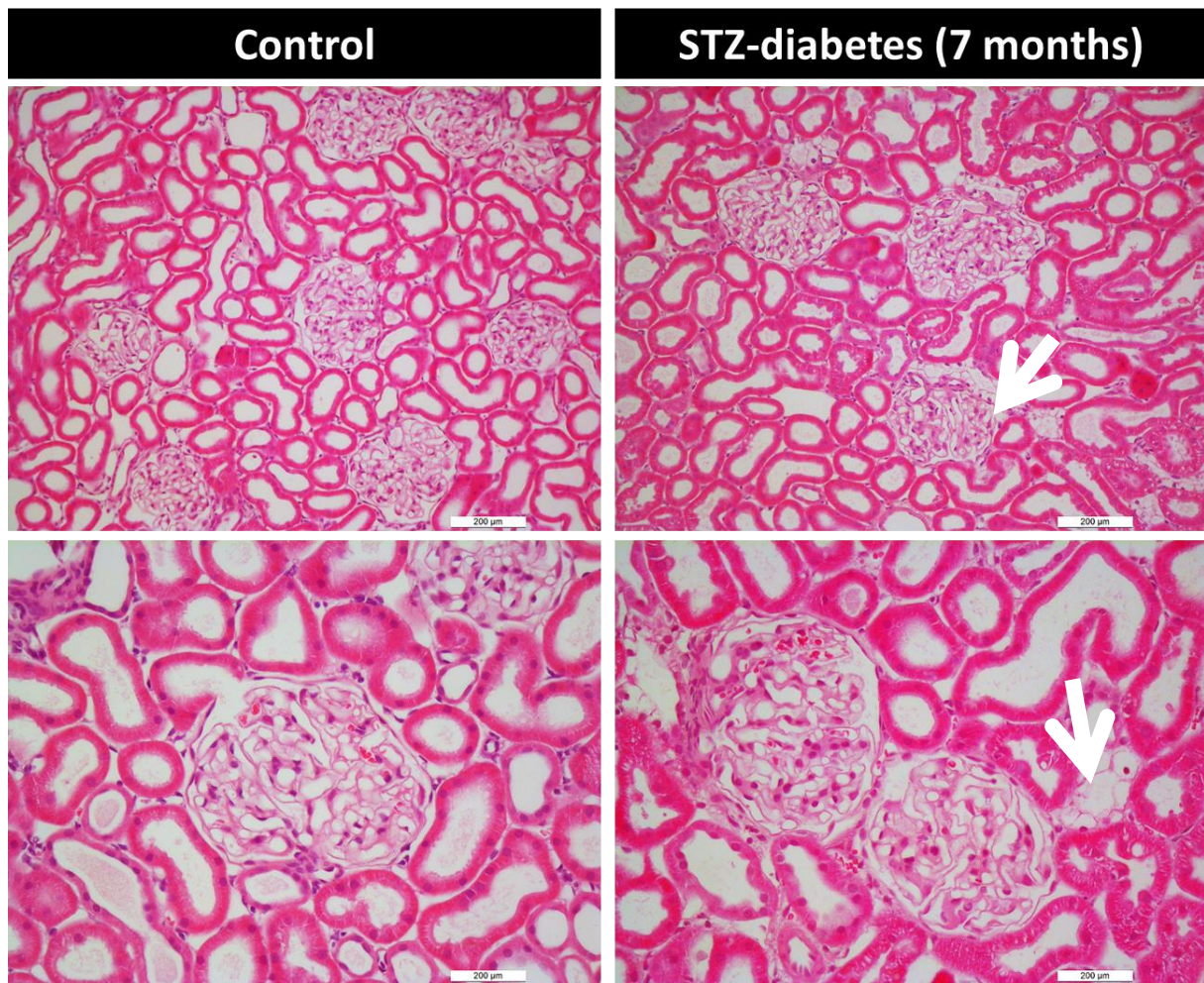
Figure 8: *Histological evaluation of diabetic and control kidney samples 7 months after diabetes induction by STZ in SD rats.* There were no visible structural pathohistological changes in the glomeruli and tubuli of both control and diabetic samples. However, in diabetic samples, Armanni-Ebstein lesions, indicating glycogen accumulation, were observed in selective renal epithelial cells.
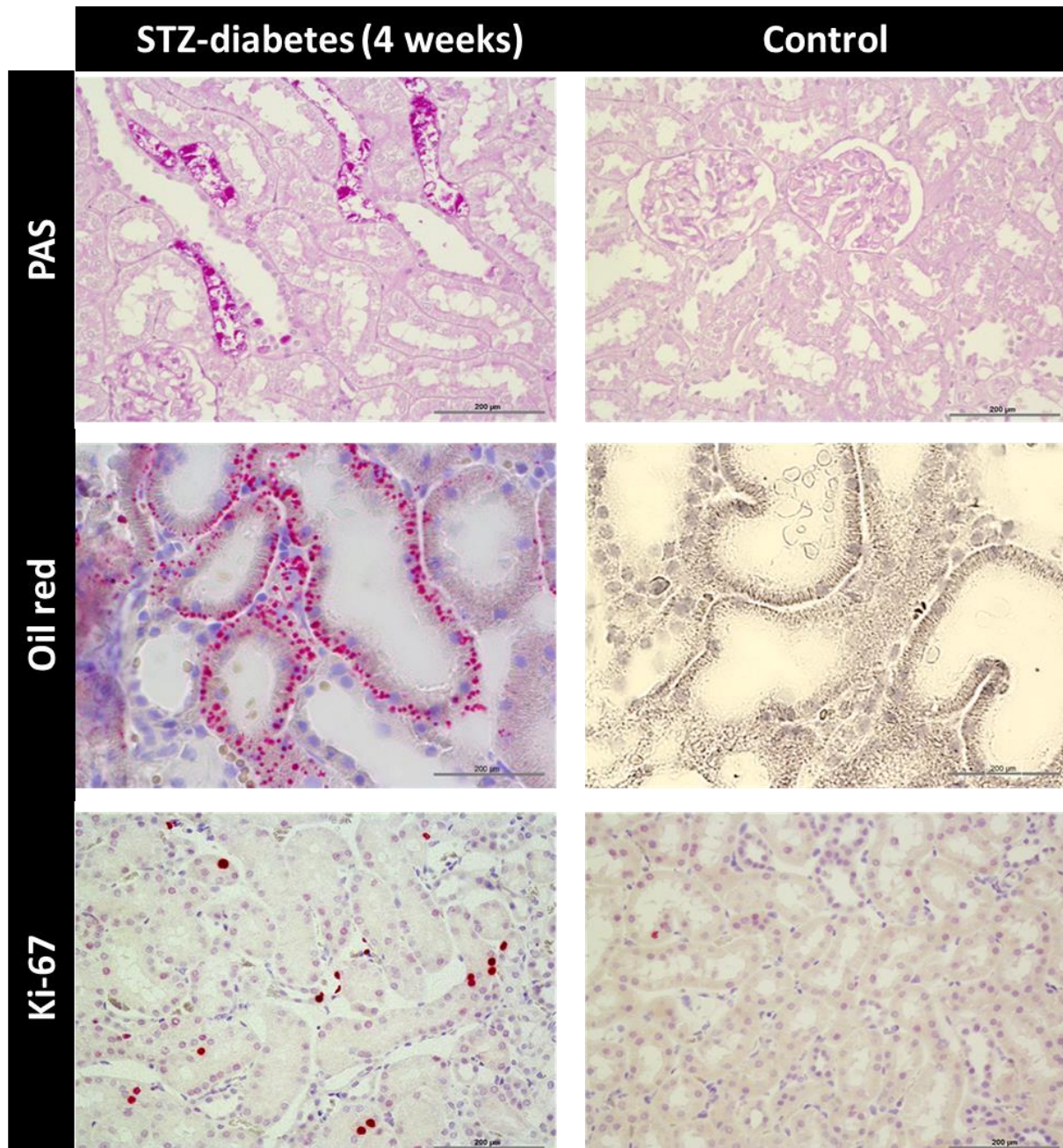
Figure 9: *Histological examination of the diabetic and control kidney samples 4 weeks after diabetes induction by STZ in SD rats.* Periodic acid staining (PAS) stained some tubules in the diabetic kidney samples, but not in control (CTRL). Oil droplets were also observed in renal tubules. Furthermore, Ki-67, a proliferation marker, stained in diabetic kidney samples, especially in tubules, indicating increased proliferation in tubular epithelium. ** Scale bar is 200µm for each sample.*

3.1.2 Renal pathologies in the ZSF1 rat, a model for type II diabetes

Although a number of experimental diabetic mouse and rat models exist, only those with additional pathologies like obesity or hypertension, develop severe renal injuries that mimic human DN. Moreover, in humans, DN is often associated with

45

hypertension or obesity. In the current thesis, we studied the renal function and phenotype of the ZSF-1 rat (ob/ob). The ZSF-1 rat (Leprfa,Leprcp/Crl) is a F1 hybrid from crosses between lean fatty diabetic female rats (ZDF; +/fa) and lean spontaneously hypertensive heart failure male rats (SHHF/Mcc-facp;+/fa,+/+). The ZSF1 rat spontaneously develops Type 2 diabetes, including renal damage modeling diabetic nephropathy. However, similar to other spontaneous rodent models with DN, hyperglycemia is combined with metabolic syndromes including obesity, cardiac failure and hypertension. Lean rats with the same genetic background were used as non-diabetic controls studied. Pathophysiological parameters during the progression of the disease are shown in **Table 5**. The rats started to become diabetic, obese and hypertensive at the age of 3 months. The urinary albumin excretion started to increase at the same age. At the age of 10 months, severe albuminuria with urinary excretion of 304 mg albumin/24hr vs. 0.6 mg albumin/24hr in controls was manifested. The loss in renal function correlated with the histological alterations in the kidneys consistent with DN, including arteriolar thickening, tubular atrophy, interstitial fibrosis and mesangial expansion and sclerosis in the glomeruli of 10 months old ob/ob rats [**Figure 10** and **Figure 11**]. Renal sections of ob/ob rats and their age-matched lean controls were stained with AZAN or PAS and showed severe renal damage in the ob/ob rats. In AZAN staining, the connective tissue was stained blue, whereas proteins and their intra-tubular casts were stained red. More than 50% of glomeruli show severe mesangial proliferation and FSGS.
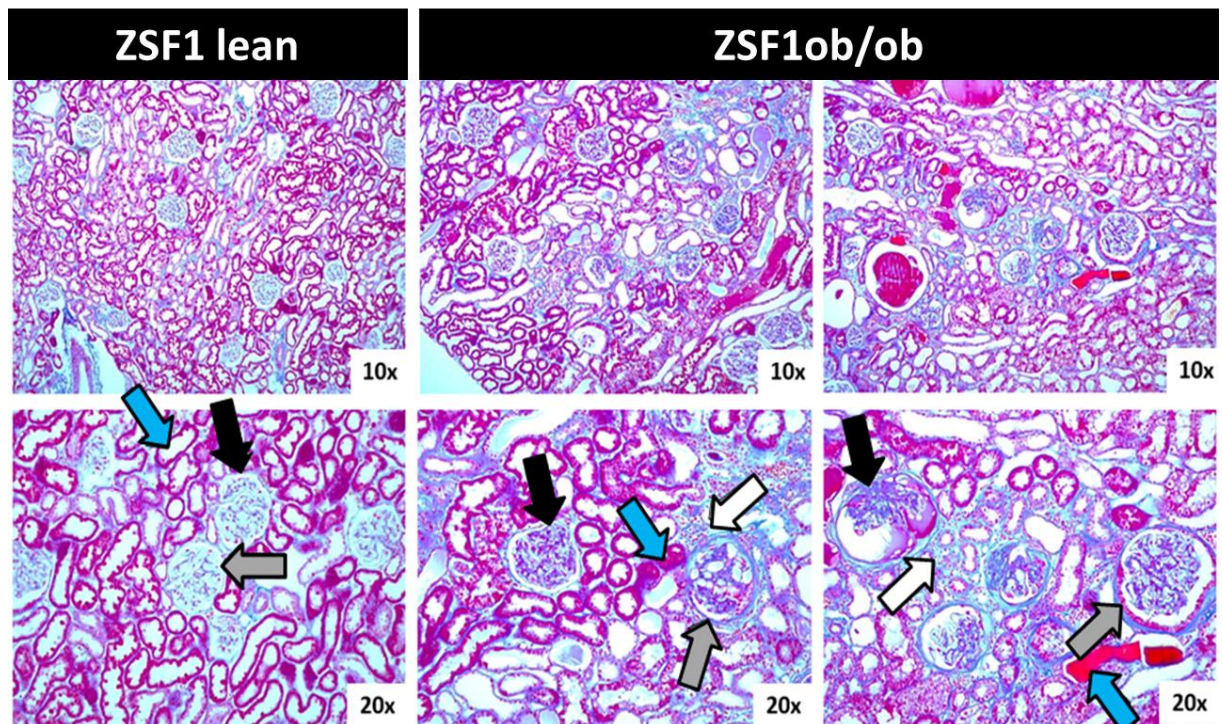
Figure 10: *Heidenhain's AZAN staining of the ZSF1 lean and ob/ob rats' kidney.* Blue arrows show the lumen of tubules which is stained red in ob/ob rats' kidney sample indicating protein casts while no staining observed in lean one. Black arrows indicate the adhesion of glomeruli to Bowman's capsule and FSGS which is not observed in lean rats. Grey arrows point out the thickening of Bowman's capsule which is not found in lean rats. White arrows show the accumulation of connective tissue fibers in ob/ob rat kidney. *Proteins are stained as red/violet, and connective tissue fibers are stained blue.*
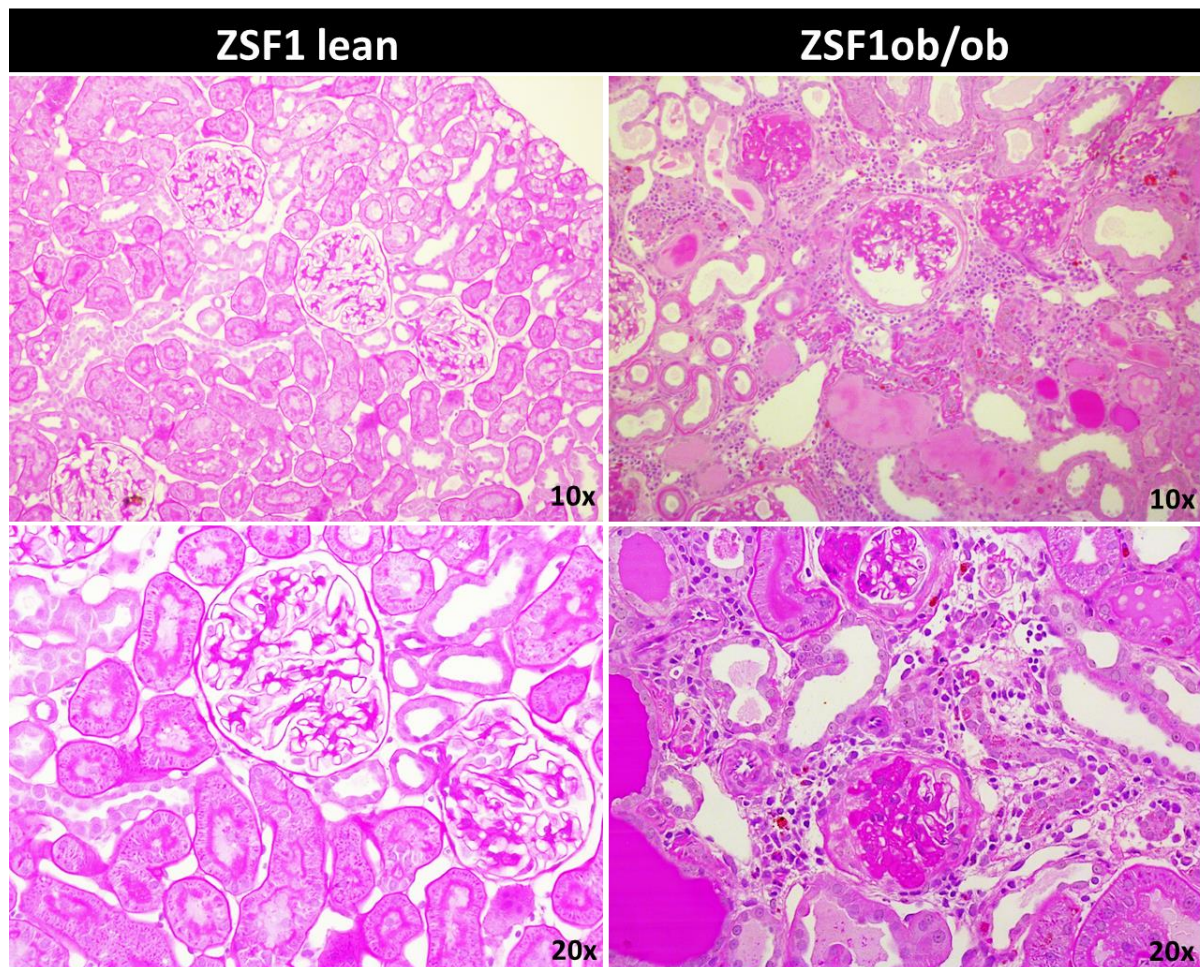
Figure 11: *Periodic acid staining of ZSF1 lean and ob/ob kidney samples.* There are significant differences between lean and ob/ob rats' kidneys. Accumulation of protein casts in tubules of ob/ob rats' kidney (indicated with black arrows) are the sign of protein leakage. Mesangial expansion and sclerosis in the glomeruli and massive interstitial fibrosis are also seen.

The striking differences between the renal phenotypes of the STZ-induced diabetic SD rats and the diabetic ZSF1 rat with metabolic syndrome lead us to address the hypothesis that, in the STZ-diabetic SD rats, additional factors are required to initiate renal pathologies.

Thus, in the next experiment, we wanted to dissect the effect of hypertension from a combined effect of hypertension and hyperglycemia and, in addition, to study the contribution of AT1R signaling in the podocytes to the progression of the disease. Therefore, we created different rat models using the same genetic background and the same treatment conditions.

Table 5: *Clinical parameters obtained from lean and ob/ob rats*. Parameters are summarized as mean ± SD. To confirm the data statistically, a student's t-test was performed. Differences were considered significant with *p < 0.05. The lean group represents a non-diabetic control. The age is indicated in weeks.

Group	Body Weight [g]									
	Week 8	Week 12	Week 13	Week 16	Week 22	Week 27	Week 30	Week 33	Week 37	Week 40
Lean	277 ± 30	356 ± 13	367 ± 12	407 ± 14	445 ± 23	487 ± 20	492 ± 18	505 ± 20	516 ± 22	510 ± 25
OB/OB	296 ± 15	462 ± 22	475 ± 24	529 ± 29	566 ± 33	599 ± 42	614 ± 44	631 ± 48	647± 51	657 ± 57

Group	Urinary Glucose Level [mg/24hr]									
	Week 8	Week 12	Week 16	Week 22	Week 27	Week 30	Week 33	Week 37	Week 40	
Lean	0.3 ± 0.3	2.9 ± 1.0	3.2 ± 0.3	2.7 ± 0.9	3.2 ± 0.9	2.7 ± 1.2	2.8 ± 1.4	2.1 ± 1.1	3.2 ± 0.7	
OB/OB	3.1 ± 0.4	3011 ± 689	4629 ± 1064	1385 ± 1209	8419 ± 1395	7623 ± 2266	7566 ± 1368	4034 ± 247	2885 ± 1687	

Group	Blood Pressure [mmHg]									
	Week 12	Week 13	Week 16	Week 20	Week 25	Week 31	Week 33	Week 35	Week 37	Week 41
Lean	157.5 ± 8.4	162.3 ± 5.9	163.1 ± 6.1	157.2 ± 5.2	152.3 ± 5.4	148.2 ± 6.9	144.0 ± 3.4	147.0 ± 5.5	148.6 ± 6.1	145.3 ± 3.6
OB/OB	141.5 ± 6.0	168.2 ± 5.0	177.0 ± 6.9	164.3 ± 11.2	165.6 ± 5.4	172.3 ± 6.8	172.3 ± 5.6	171.3 ± 5.2	175.4 ± 5.2	178.7 ± 7.2

Group	Urinary Creatinine [mg/24hr]									
	Week 8	Week 12	Week 16	Week 22	Week 27	Week 30	Week 33	Week 37	Week 40	
Lean	5.92 ± 0.98	10.77 ± 0.79	11.25 ± 1.72	11.23 ± 1.75	14.76 ± 1.66	13.14 ± 1.45	14.73 ± 1.43	13.96 v 2.27	16.32 ± 2.02	
OB/OB	3.81 ± 0.02	6.31 ± 1.02	7.24 ± 1.06	7.11 ± 1.38	9.88 ± 1.82	10.24 ± 1.72	10.44 ± 1.41	8.02 ± 1.53	10.48 ± 1.51	

Group	Urinary Protein [mg/24hr]									
	Week 8	Week 12	Week 16	Week 22	Week 27	Week 30	Week 33	Week 37	Week 40	
Lean	13.98 ± 3.97	16.28 ± 3.01	15.27 ± 3.21	11.21 ± 3.53	13.51 ± 1.90	10.58 ± 2.25	15.67 ± 6.20	7.37 ± 3.41	14.24 ± 3.06	
OB/OB	8.25 ± 0.69	10.45 ± 5.19	44.19 ± 16.49	163.5 ± 48.67	257.2 ± 64.45	321.2 ± 97.82	356.2 ± 105	298.7 ± 116	373.9 ± 167	

Group	Urinary Albumin [µg/24hr]									
	Week 8	Week 12	Week 16	Week 22	Week 27	Week 30	Week 33	Week 37	Week 40	
Lean	221.8 ± 51.56	206.8 ± 35.26	255.5 ± 53.61	302.0 ± 94.47	695.4 ± 774	1394 ± 240	268.2 ± 144	349.0 ± 186	682.7 ± 420	
OB/OB	1106 ± 137	2529 ± 346	24619 ± 5763	119861 ± 33545	152174 ± 41867	279378 ± 104839	258551 ± 118225	104345 ± 87634	304758 ± 104906	

3.2 Hypertension and AT1R overexpression in podocytes synergistically stimulate rapid progression of glomerulosclerosis in STZ- diabetic rats

3.2.1 Development of the rat models

In order to compare the effects of hypertension with those of combined STZ-diabetes and hypertension under identical conditions, we used a transgenic Cyp1a1Ren2 rat which carries a transgenic renin gene under the control of the cytochrome P4501a1 promoter and is located at the Y-chromosome. Transgene expression is induced by dietary supplementation with I3C which results in a dose-dependent hypertension within 24 hr. To mimic the natural progression of human DN, we induced hypertension after the induction of STZ-diabetes. In addition, we aimed to study the contribution of AT1R signaling in podocytes to renal damage. Therefore, we crossed a second transgenic rat line, the TGR Neph-hAT1, with the Cyp1a1Ren2 rats before starting the experiments. The Neph-hAT1 rat specifically overexpresses the AT1R in the podocytes, which leads to slowly progressing glomerulosclerosis in aged rats. The breeding procedure and experimental program are illustrated in **Figure 12**. The experiments started at the age of 6 weeks and were finished at the age of 14 weeks, a period before the TGRNeph-hAT1 rats start to develop disturbances in renal function and morphology. Since the Cyp1a1Ren2 transgene is located in the Y chromosome, all of the male progenies carry this transgene. Consequently, heterozygous female TGR Neph-hAT1 were crossed with male TGR Cyp1a1Ren2 to generate the genotypes Cyp1a1Ren2/Neph-hAT1TGR and Cyp1a1Ren2/wildtype. Then, the resulting male rats were subjected to the experiment while female rats were used for breeding. 6 weeks after birth, 60mg/kg of streptozotocin (STZ) was injected to the diabetic groups while others had no treatment. To induce hypertension two weeks after STZ injection, half of the non-treated group and half of the STZ-injected group received an I3C supplemented diet until the end of the experiment in order to induce hypertension. Hereby, we have created the following experimental groups: CTRL-TGR, CTRL-Wild, HBP-TGR, HBP-Wild, D-HBP-TGR and D-HBP-Wild [**Figure 12D**]. Since the Cyp1a1Ren2 gene is silent when not induced by I3C, only rats harboring the transgenic AT1R were called "TGR" and rats without the transgenic AT1R are called "Wild".
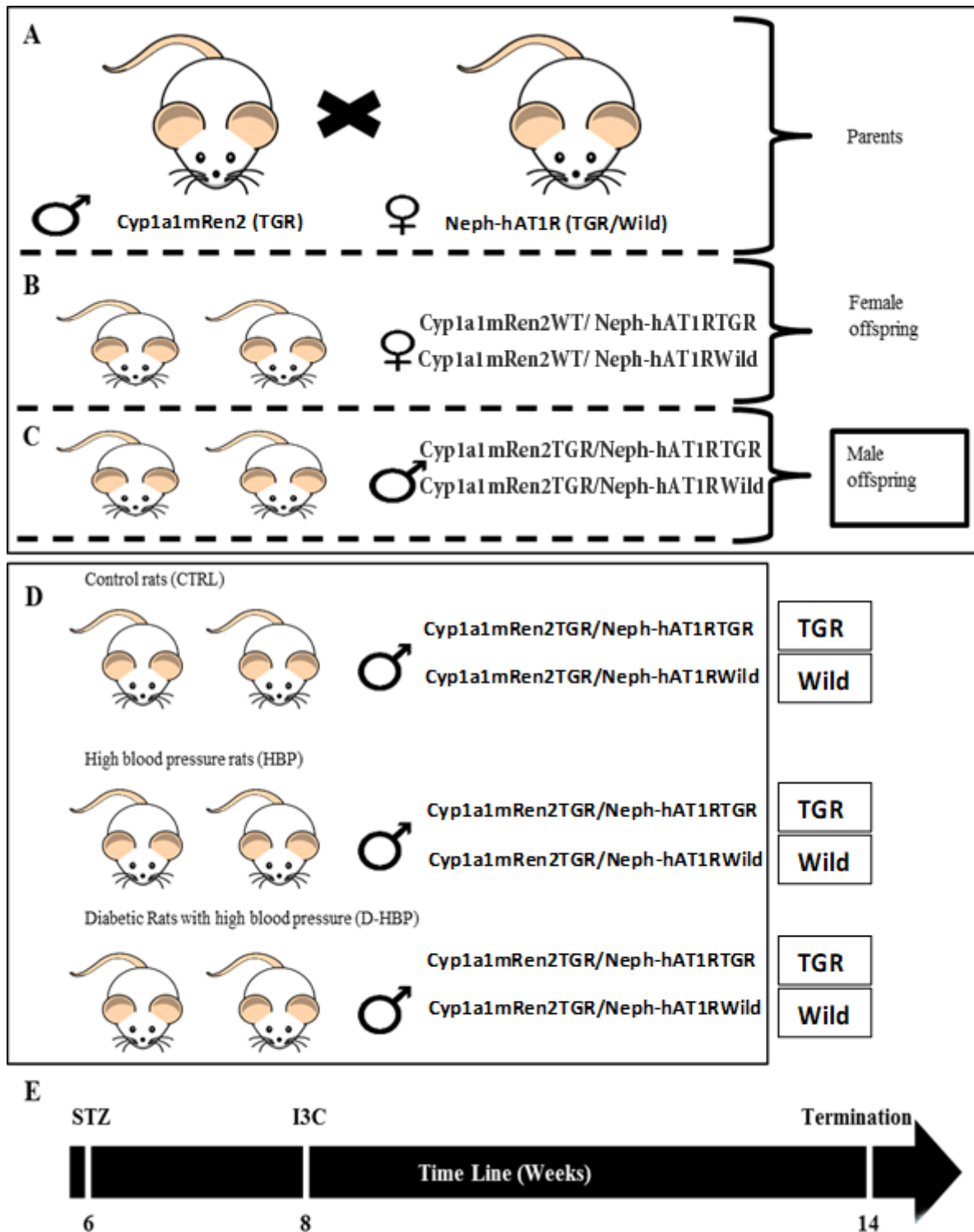
Figure 12: *Mating scheme to create double transgenic rats and experimental groups.* A- The male rat which carries the inducible renin gene (Cyp1a1Ren2) and the female rat which carries the Neph-hAT1 receptor overexpressing gene (Neph-hAT1 TGR/Wild). B- The female offspring which do not carry the CypA1Ren2a transgene but are either Neph-hAT1 (TGR) or Neph-hAT1 (Wild) for the AT1 receptor transgene. C- The male offspring which all carry the Cyp1a1Ren2 transgene but are either Neph-hAT1 (TGR) or Neph-hAT1 (Wild) for the AT1 receptor transgene. D- Three experimental groups that have both Neph-hAT1 (TGR) and Neph-hAT1 (Wild) were designed each with TGR and Wild subgroup.

3.2.2   AT1R overexpression in podocytes does not affect hyperglycemia and blood pressure levels

During the experiment, we regularly monitored blood glucose concentration and alterations in body weight and blood pressure. We also monitored water and food consumption and urine production using metabolic cages. Of note, there was no difference with regard to all of these parameters between CTRL-TGR and CTRL-Wild rats, indicating that AT1R overexpression alone did not affect any of the physiological parameters during the time of the experiment. In addition, the transgenic inducible renin gene did not affect any of these parameters in the controls, indicating that it is not expressed in the absence of I3C [**Figure 13, 14, 15** and **16**]. These facts were an important precondition for the experimental aim to dissect the effects of hypertension from those of combined hyperglycemia and hypertension and to specify the role of AT1R in podocytes in these pathologies.

STZ induced hyperglycemia in all treated rats while non-treated rats did not show any changes in blood glucose concentration throughout the experimental period. The blood glucose levels did not differ between the treated groups – D-HBP-Wild and D-HBP-TGR [**Figure 13**]. Diabetic rats showed the typical features of type-1 diabetes, including diuresis, increased water consumption and body weight loss, which also did not differ between D-HBP-TGR and D-HBP-Wild [**Figure14, 15** and **20**].   Blood pressure increased within 24 hours after induction and stayed stable until the end of the experiment. There was no difference in blood pressure between HBP and D-HBP and between TGR and Wild groups [**Figure 16**].
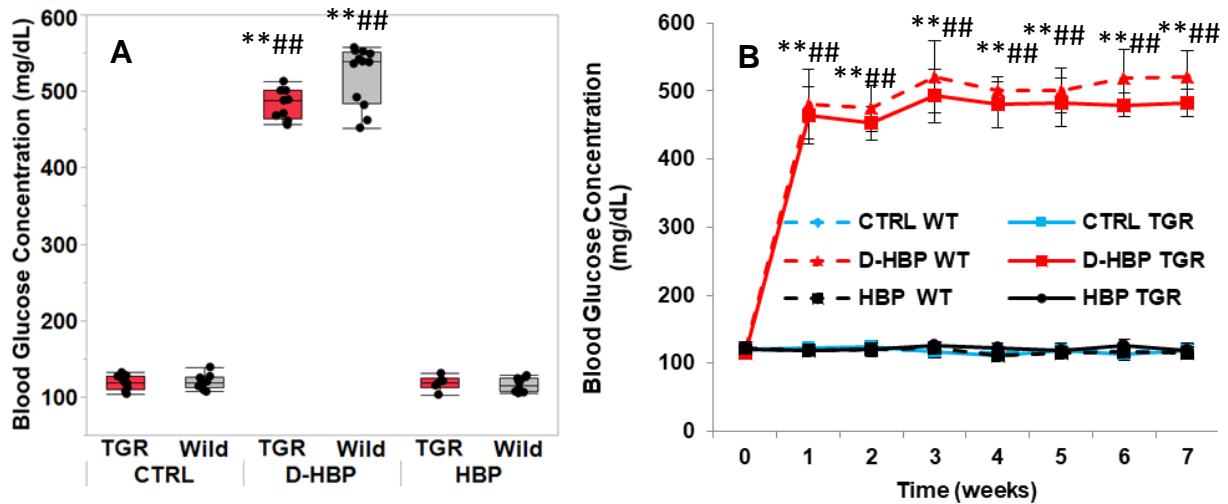
Figure 13: *Blood glucose concentration.* A- Blood glucose of the rats two weeks after the STZ injection. Blood glucose levels rapidly increased in the D-HBP group due to the STZ injection while it remained steadily low for CTRL and HBP rats regardless of the genotype. B- Progressive measurement of blood glucose concentration of the rats from the beginning of the experiment to the end of the experiment. No significant differences have been observed between TGR and Wild in the same experimental group.
*** $p < 0.01$ vs. CTRL, ##$p < 0.01$ vs. HBP.*
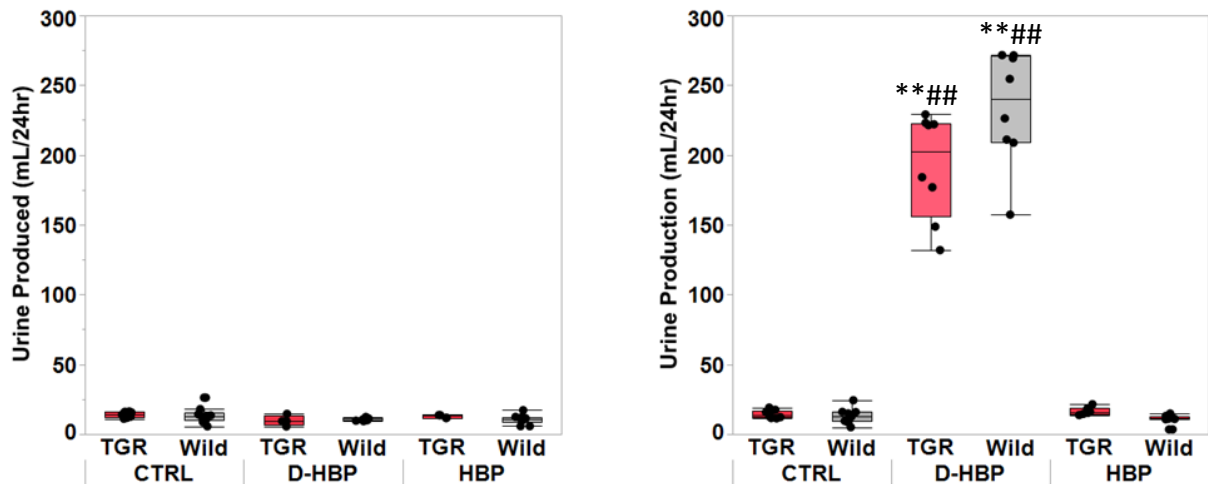
Figure 14: *Urine production per 24 hr.* A- Urine production is normal in all groups before starting the experiment. B- Both genotypes in the D-HBP group show polyuria at a similar level at the end of the experiment. No significant differences have been observed between TGR and Wild in the same experimental group. *** $p < 0.01$ vs. CTRL, ## $p < 0.01$ vs. HBP.*
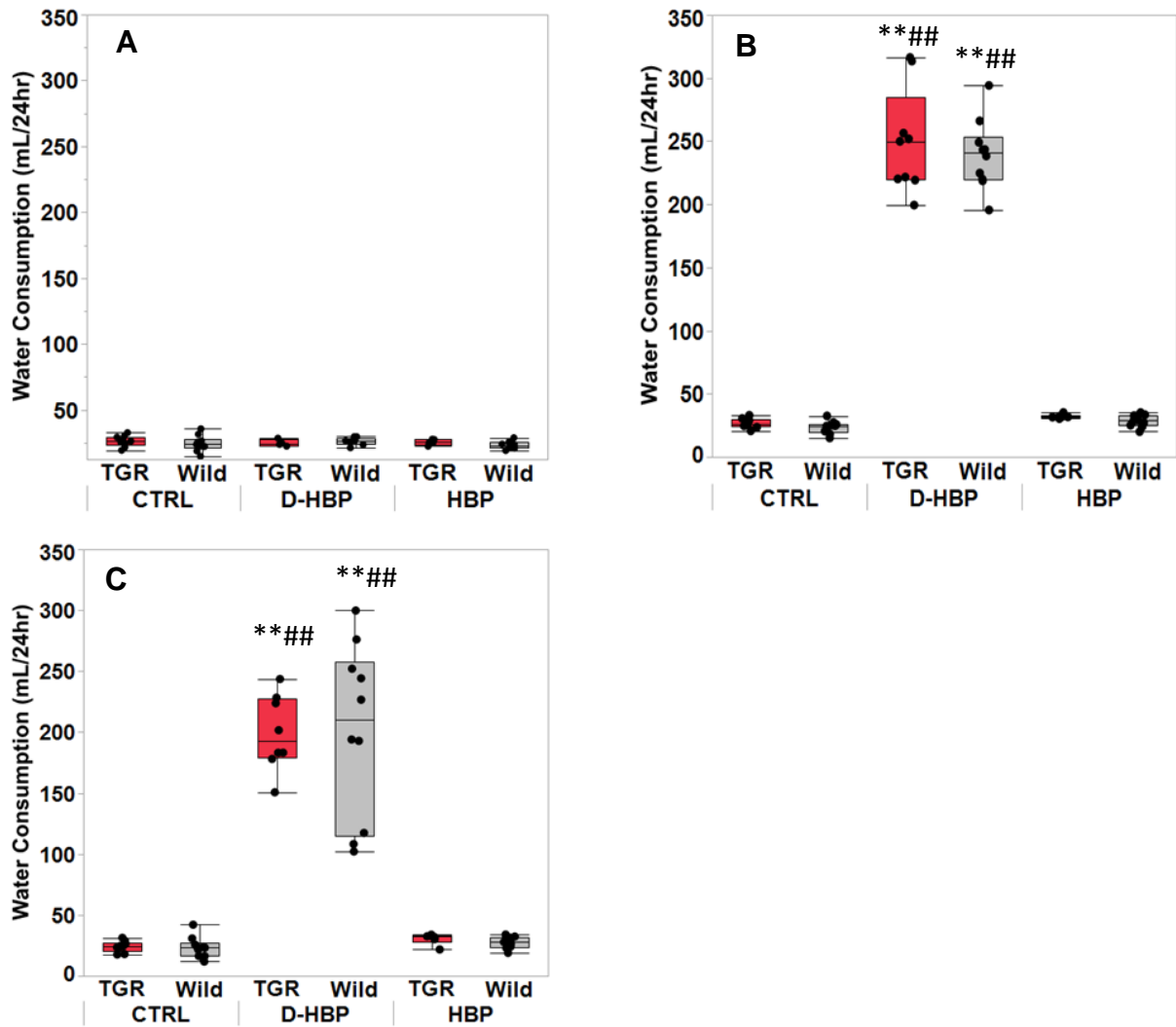
Figure 15: *Water consumption during the experiment.* A- Water consumption of the rats at the beginning of the experiment, before STZ injection. B- Water consumption of the rats two weeks after STZ injection and before I3C intake. D-HBP rats consumed significantly more water than CTRL and HBP rats. C- Water consumption of the rats at the end of the experiment, six weeks after STZ injection. CTRL and HBP rats do not show any changes in water consumption while it was significantly greater in the D-HBP group. No significant differences were observed between TGR and Wild rats in the same experimental group. ** $p < 0.01$ vs. CTRL, ##$p<0.01$ vs. HBP.
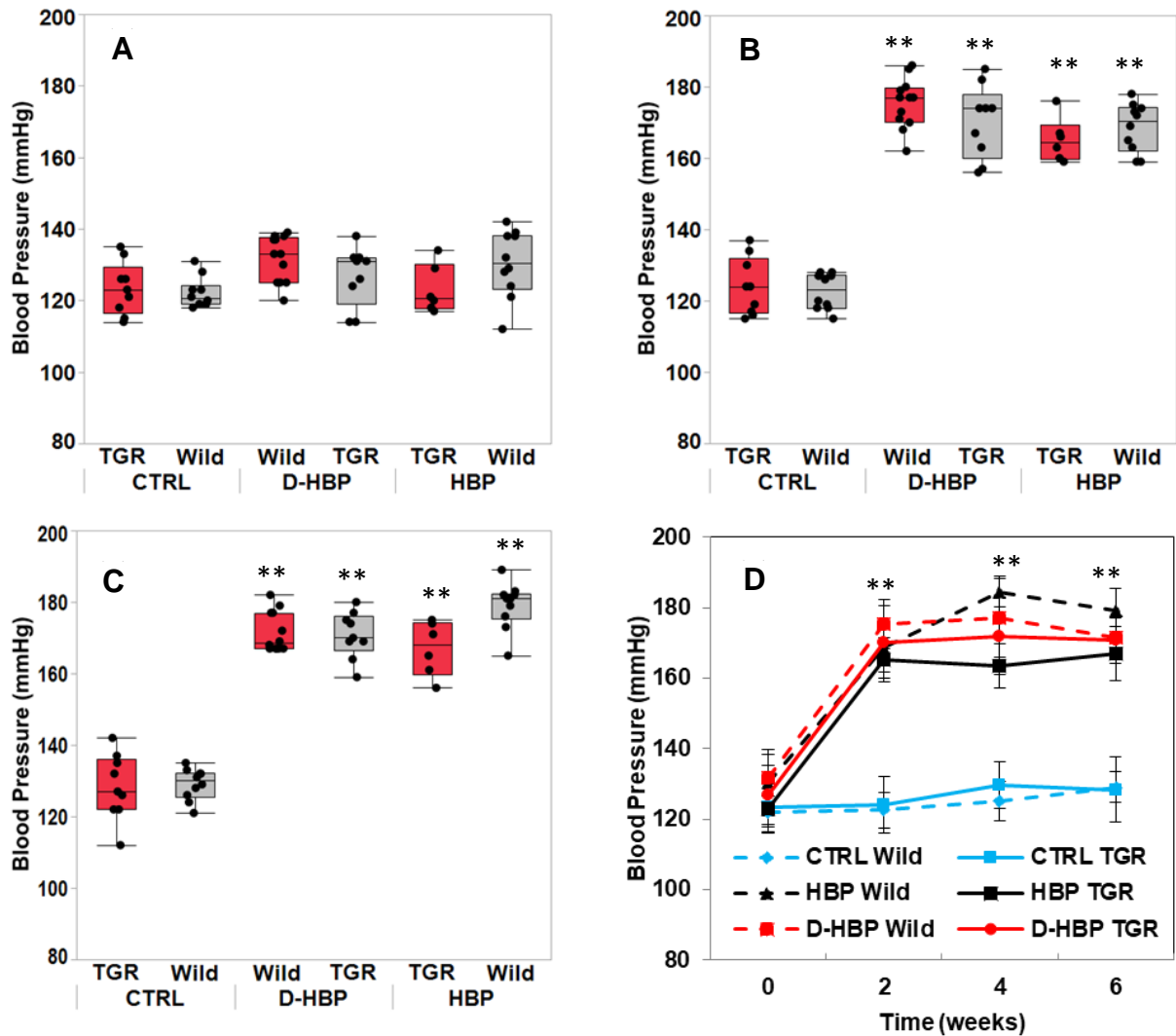
Figure 16: *Blood pressure of rats.* A- Blood pressure of all rats at the beginning of the experiment. No differences were observed. B- Blood pressure of the rats after I3C intake. Blood pressure of the rats which received I3C dramatically increased within 24-48 hours. C- Blood pressure of the rats at the end of the experiment, 6 weeks after I3C intake. All the rats which received I3C have shown a comparable steady high blood pressure until the end of the experiment. D- Blood pressure changes over the time. No significant differences were observed between TGR and Wild rats in the same experimental group and between HBP and D-HBP groups. ** *p< 0.01 vs.CTRL.*

3.3 Hyperglycemia and hypertension together aggravates renal damage, which is further enhanced by AT1R in podocytes

3.3.1 Renal function

In order to evaluate renal function throughout the experimental period we studied clinical parameters in blood plasma and 24hr urine and performed transcutaneous measurements of GFR using fluorescein isothiocyanate (FITC)-Sinistrin. **Figure 17** demonstrates a strong increase in the half-life of FITC-sinistrin clearance in the D-HBP groups, indicating a significant drop in GFR. In contrast, the GFR was only

slightly decreased in the HBP-TGR group when compared with controls. Of note, the GFR dropped significantly more rapidly in the D-HBP-TGR compared to the D-HBP-Wild rats. Thus, activated AT1R signaling in podocytes seems to be an important determinant in the progression of glomerular damage, specifically in DN.

The decline in the GFR corresponds well with the increase in the albumin and protein excretion/24 hours [**Figure 18**]. The urinary protein and albumin excretions were moderately increased in the HBP-TGR but not in the HBP-WT group. In contrast, corresponding to the decline in GFR, the albuminuria increased dramatically in the D-HBP groups. Again, the severity of albuminuria was significantly more pronounced in the D-HBP-TGR than in the D-HBP-Wild group, supporting the detrimental role of AT1R signaling in podocytes for the progression of DN.
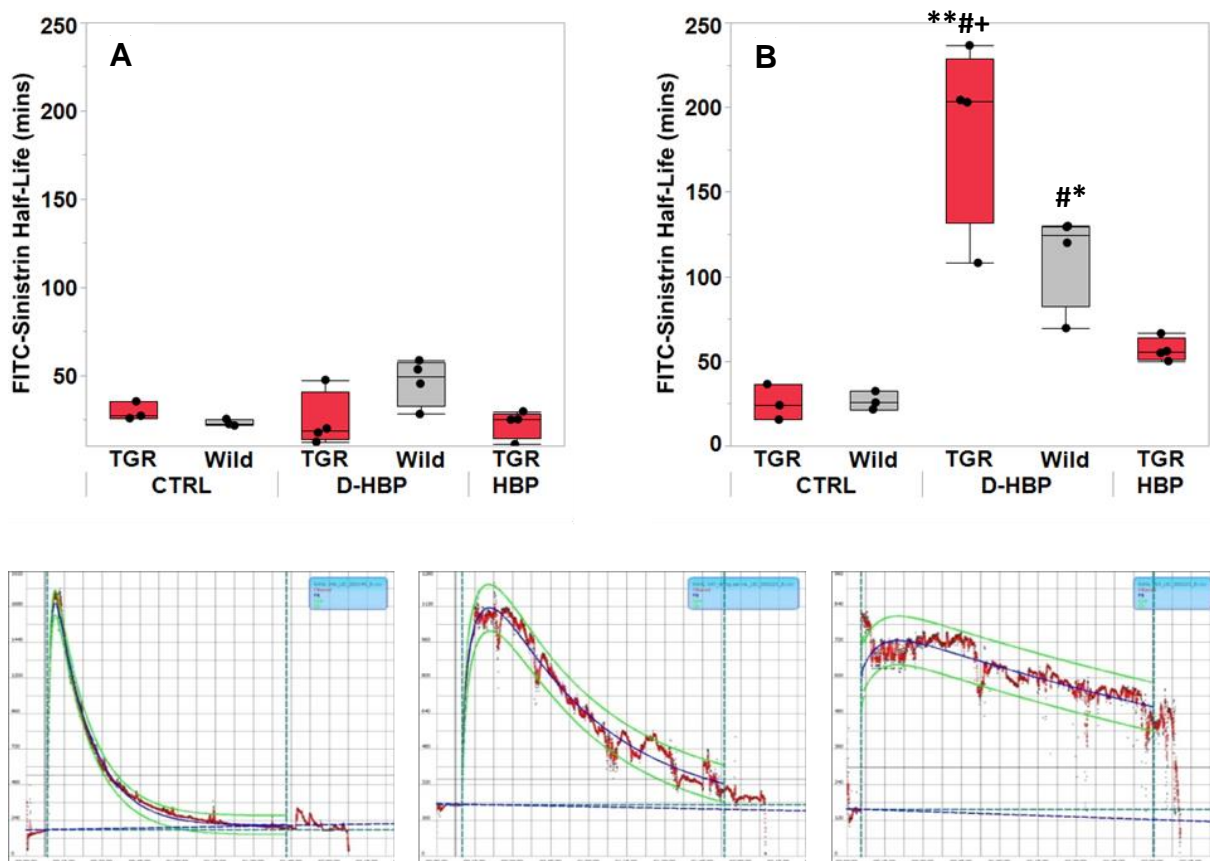
Figure 17: *Transcutaneous GFR measurement by FITC-Sinistrin half-life.* A- Two weeks after the induction of diabetes. No significant differences were observed among the experimental groups. B- 4 weeks after IC3 intake. There is no difference in GFR between CTRL-TGR and CTRL-Wild. In the D-HBP group, GFR dropped significantly in both TGR and Wild rats; however, the drop is significantly more pronounced in the TGR compared to Wild rats. FITC-Sinistrin half-life was slightly increased in HBP-TGRs compared to the CTRL rats. * p< 0.05 , ** p < 0.01 vs. CTRL, #p<0.05 vs HBP, + p<0.05 vs Wild
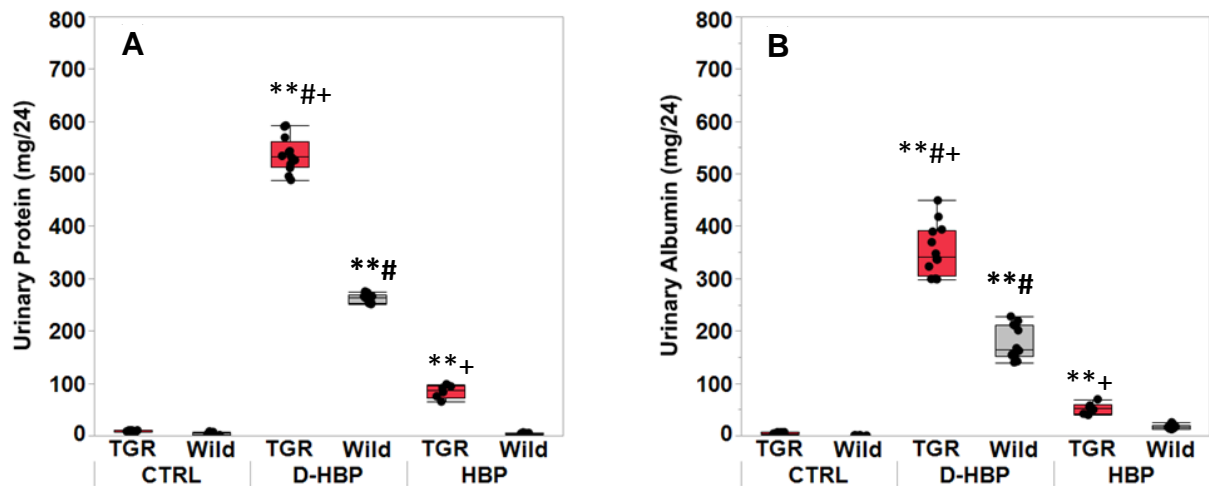
Figure 18: *Urinary protein and albumin excretion at experimental week 7.* In D-HBP rats, there is a considerable increase in both, urinary protein and albumin excretion vs. CTRL and HBP rats. This increase is significantly more pronounced in D-HBP-TGR than in D-HBP-Wild rats. Both parameters were also slightly increased in HBP-TGR rats while HPB-Wild and CTRL rats did not differ.
*** p< 0.01 vs. CTRL, #p<0.05 vs HBP of the same genotype, + p<0.05 vs Wild of the same group.*

The deterioration of renal function resulted in increased plasma urea levels in the D-HBP groups [**Figure 19**] when compared with the CTRL and HBP groups. There was no difference between plasma urea levels of HBP and CTRL groups. In contrast, the plasma creatinine levels decreased in the D-HBP groups, which was probably a result of muscle weight loss due to diabetes. In addition, plasma cholesterol and triglyceride levels were significantly increased in the D-HBP groups. This increase was highest in the D-HBP-TGR group. Interestingly, a moderate increase in plasma cholesterol was also observed in the HBP-TGR group in contrast to the HBP-Wild group, when compared with CTRL.
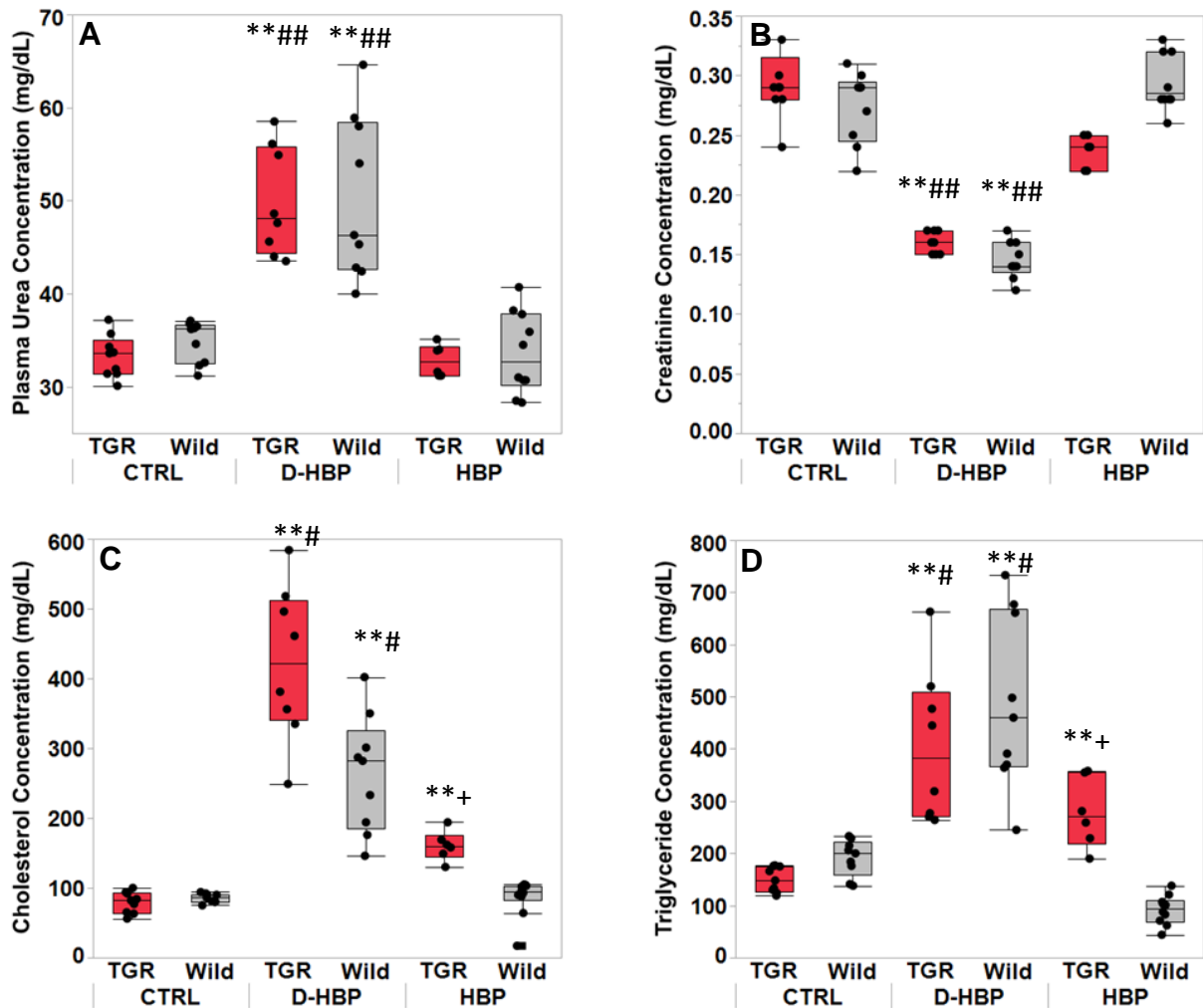
Figure 19: *Urea, Creatinine, Cholesterol and Triglyceride concentration in blood plasma at experimental week 7.* A- Plasma urea concentration. D-HBP group have shown the highest urea concentration in plasma while both CTRL and HBP group shown no difference among. There was no significant difference between TGR and wild in any corresponding group. B- Plasma creatinine concentration. Here, plasma creatinine concentration was the lowest in D-HBP group while CTRL and HBP group have shown the same level of creatinine concentration. C- Plasma cholesterol concentration. Unlike CTRL group, D-HBP and HBP rats have revealed increased cholesterol level in plasma. Interestingly, TGR rats have significantly shown the highest cholesterol concentration in their corresponding groups. D- Triglyceride concentration in blood plasma. Here, triglyceride concentration revealed increase in D-HBP-TGR, D-HBP-Wild and HBP-TGR groups.
** $p < 0.01$ vs. CTRL, #$p < 0.05$ vs HBP of the same genotype, + $p < 0.05$ vs Wild of the same group.

3.3.2   Renal structure and morphology

At the end of the experiments, kidneys were harvested for histological evaluation. **Figure 20** shows an increase in the kidney/body weight ratio in the D-HBP groups, which might indicate hypertrophic growth. However, it is more probable that the decreased body weights in the D-HBP groups account for the increased ratio. The absolute kidney weights did not differ between the groups.

In order to verify whether hypertension or diabetes was associated with glomerular hypertrophy, we stained kidney sections with hematoxylin and eosin and determined the glomerular area. **Figure 20** shows that, at the end of the experiment, the glomerular area did not differ between non-treated CRTL-TGR and CRTL-Wild. Thus, at that age, transgenic overexpression of the AT1R did not affect glomerular growth in untreated rats. However, in the HBP group, we observed a significant increase in glomerular size in HBP-TGRs comparable to that in D-HBP rats but not in the HBP-Wild. These data indicate that the level and/or duration of hypertension in this experiment were insufficient to cause hypertrophic growth per se in HBP-Wild. However, the overexpression of the AT1R in podocytes together with hypertension in the HBP-TGR group stimulates glomerular hypertrophy. In contrast, both D-HBP groups, independent from their genotype, show significant glomerular hypertrophy. Consequently, the synergistic actions of diabetes and hypertension are required to induce hypertrophic growth of the glomerular tuft. There was no difference in the glomerular area between the hypertrophic glomeruli of the HBP-TGR, D-HBP-TGR and D-HBP-WT groups. Thus, glomerular hypertrophy alone cannot explain the significant differences in the renal function we observed between these groups.
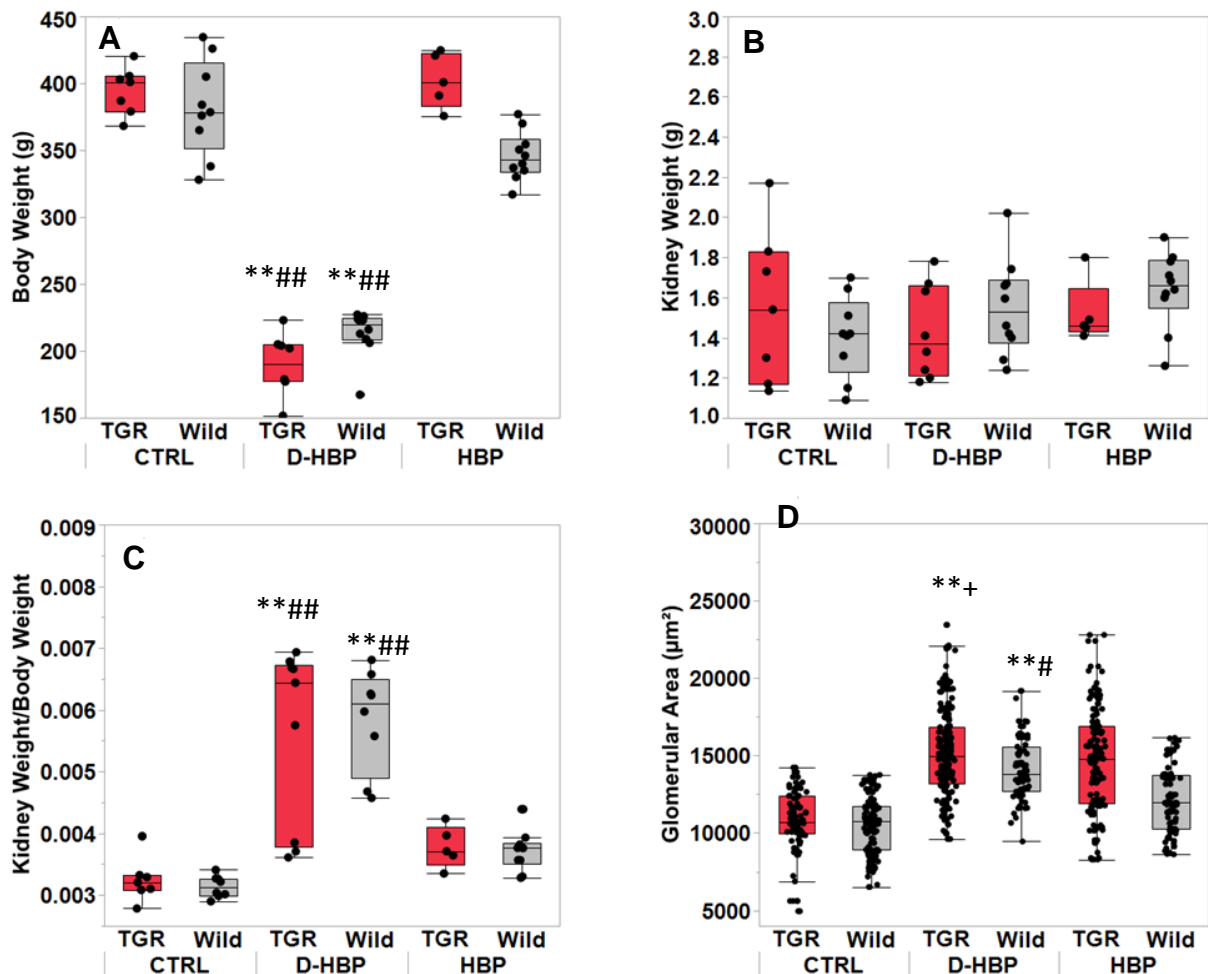
Figure 20: *Bodyweight (BW), kidney weight (KW), the ratio of BW/KW and glomerular area.* A-Bodyweight of experimental rats. No difference has seen between TGR and Wild rats in corresponding groups. However, rats in D-HBP group shown the lowest body weight. B- Kidney weight of the rats. C-BW/KW ratio. Here, D-HBP group have shown the highest value in ratio due to diabetes dependent the weight loss. D- Glomerular area. D-HBP and HBP rats have shown enlarged glomerular area. TGR rats in both groups have shown a slightly bigger glomerular area than the wild ones.
** p< 0.01 vs. CTRL, #p<0.05 vs HBP of the same genotype, + p<0.05 vs Wild of the same group.

To study the glomerular lesions in more detail, Richardson's staining of semi-thin kidney sections and electron microscopy were performed by Prof. Kriz, Neuroanatomy, Medical Faculty Mannheim and by Prof. Gröne DKFZ, Heidelberg. Light microscopy [**Figure 21**]. Electron microscopy [**Figure-22**] images of glomerular profiles from a D-HBP-TGR show the acute injuries we found in this group and partially in the HBP rats. **Figure 21 A, B, C** and **E** show prominent mesangial expansion, which might represent a first reaction to the increased blood pressure. In **Figure 21B**, huge hypertrophied podocytes are visible, indicating a compensatory reaction for the possible loss of podocytes. Detached, viable podocytes protruding into the urinary orifice are shown in **Figure 21C**. **Figure 21D** shows irregular

60

unfolded large capillaries, indicating that the supporting function of the mesangium is impaired. This causes an extension of the glomerular tuft close to the parietal epithelial cells, promoting the attachment of podocytes and might initiate focal tuft adhesion to the Bowman's capsule. **Figure 21E** demonstrates a significant tuft adhesion comprising almost two-thirds of the tuft and massive mesangial expansion. Shear stress drags the glomerular tuft towards the tubular opening. Bottle shaped podocytes, likely a result of high shear stress due to the rapid flow of the filtrate which makes the podocytes prone to detaching. In **Figure 21F**, advanced massive mesangial expansion and numerous detached podocytes in the Bowman's space can be observed. On both sides of the glomerulus, massive intra-tubular protein casts are visible. **Figure 21G** shows advanced renal damage, comprising a collapsed glomerulus with tubulopathy. Although some of the pathologies were also observed in the HBP group, the frequency and severity of glomerular lesions were significantly increased in the D-HBP group, with the D-HBP-TGRs much more severe affected than the D-HBP-Wild rats. **Figure 21H** demonstrates that the majority of glomeruli were seriously damaged in the D-HBP-TGRs.
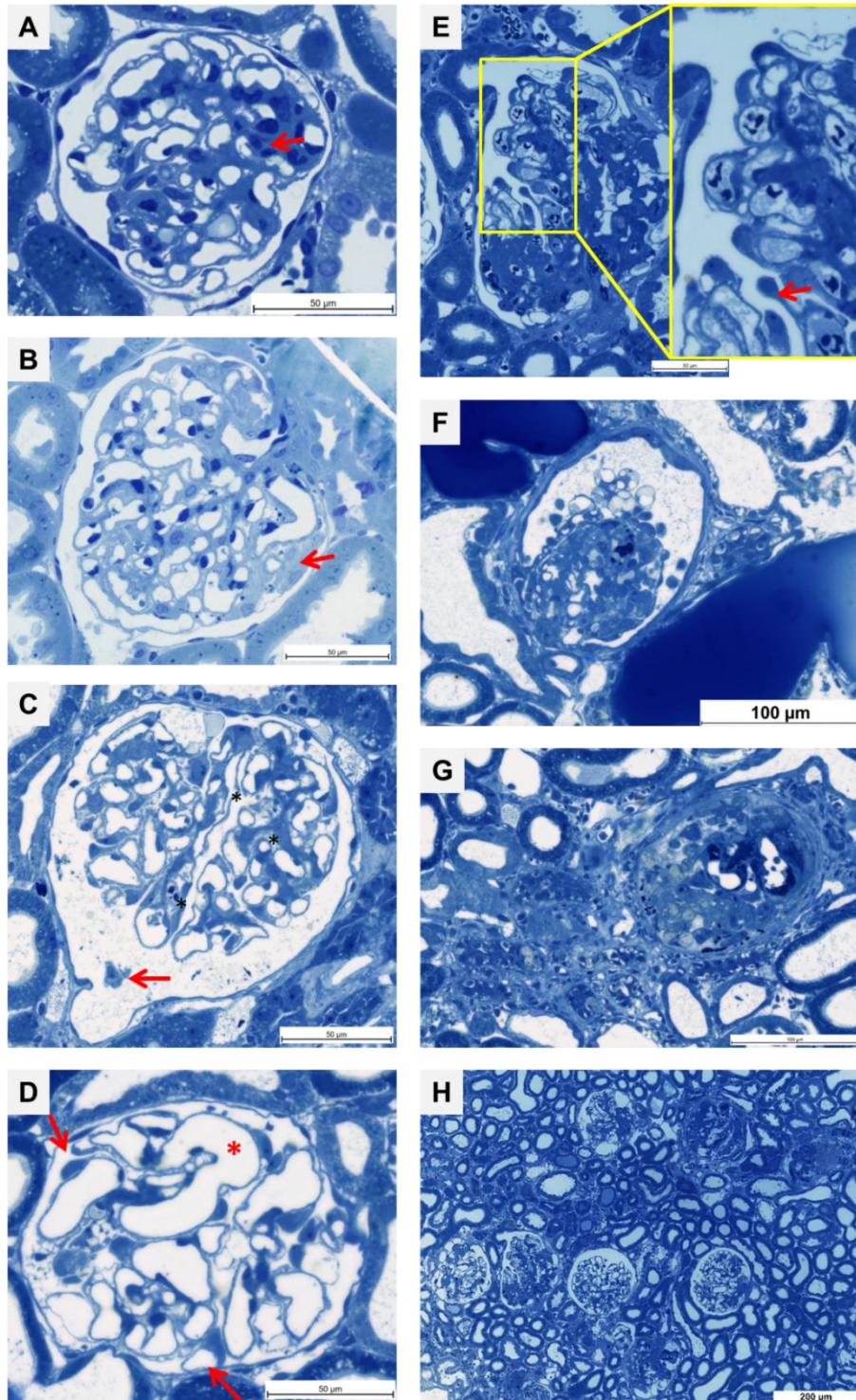
Figure 21: *Light micrographs of glomerular profiles in a D-HBP-TGR rat showing the crucial injuries.* A- Mesangial expansion, B- Mesangial expansion and hypertrophied podocytes C- Podocytes are protruding into the urinary orifice. D- Irregular large capillaries indicating that the supporting function of the mesangium is impaired. The glomerular tuft is expanded close to the parietal epithelial cells, promoting attachment of podocytes. E- Large tuft adhesion comprising almost two-thirds of the tuft. Mesangial expansion. Shear stress drags the glomerular tuft toward the tubular opening. Bottle shaped podocytes (arrow), likely a result of high shear stress due to the rapid flow of the filtrate – being prone to detachment. F- Massive mesangial expansion and detached podocytes in the Bowman's space. G- Collapsed glomerulus with tubulopathy H- Overview of a kidney region showing severe glomerular damage.

Electron micrographs are shown in **Figure 22**. Remarkable, we observed thickening of the GBM and deposition of worn-out GBM material in the mesangium of the D-HBP-TGRs similar to the findings of Kriz[14] in patients with DN [**Figure 22A**]. **Figure 22B** shows huge pseudocysts and in **Figure 22C** and **D** widened podocyte FPs can be observed. A complete FPE can be seen in two neighboring capillaries in **Figure 22E**. **Figure 22F** shows tuft adhesion to the Bowman's capsule.

In order to quantify the damage profile, we performed AZAN staining on renal sections. In **Figure 23,** representative pictures of glomeruli in the different experimental groups are shown. The most severe damage was found in the D-HBP-TGR group. PAS staining of D-HBP-TGR shows severe FSGS and massive intratubular protein casts.

For quantification, we designated five categories of glomerular damage from healthy (G0) to the most severely damaged with adhesions to the Bowman's capsule (G4). We evaluated an average of 180 glomeruli per rat. As shown in **Figure 24**, the most severe damage was found in the D-HBP-TGR group with 70.3 % of glomeruli were injured, including 26 % in the most severely damaged category G3 and G4. In contrast, in the D-HBP-Wild group, only 25.9 % of the glomeruli were injured and only 3.3 % of glomeruli were in the G3 and G4 group. The prominent damage in this group was restricted to mesangial expansion. In the HBP group, the glomerular injuries were significantly less than in the D-HBP group and the differences between TGR and Wild much less distinct (damaged glomeruli: 16,4% in HBP-Wild, 30% in HBP-TGR). These results correspond well with the functional data described above.
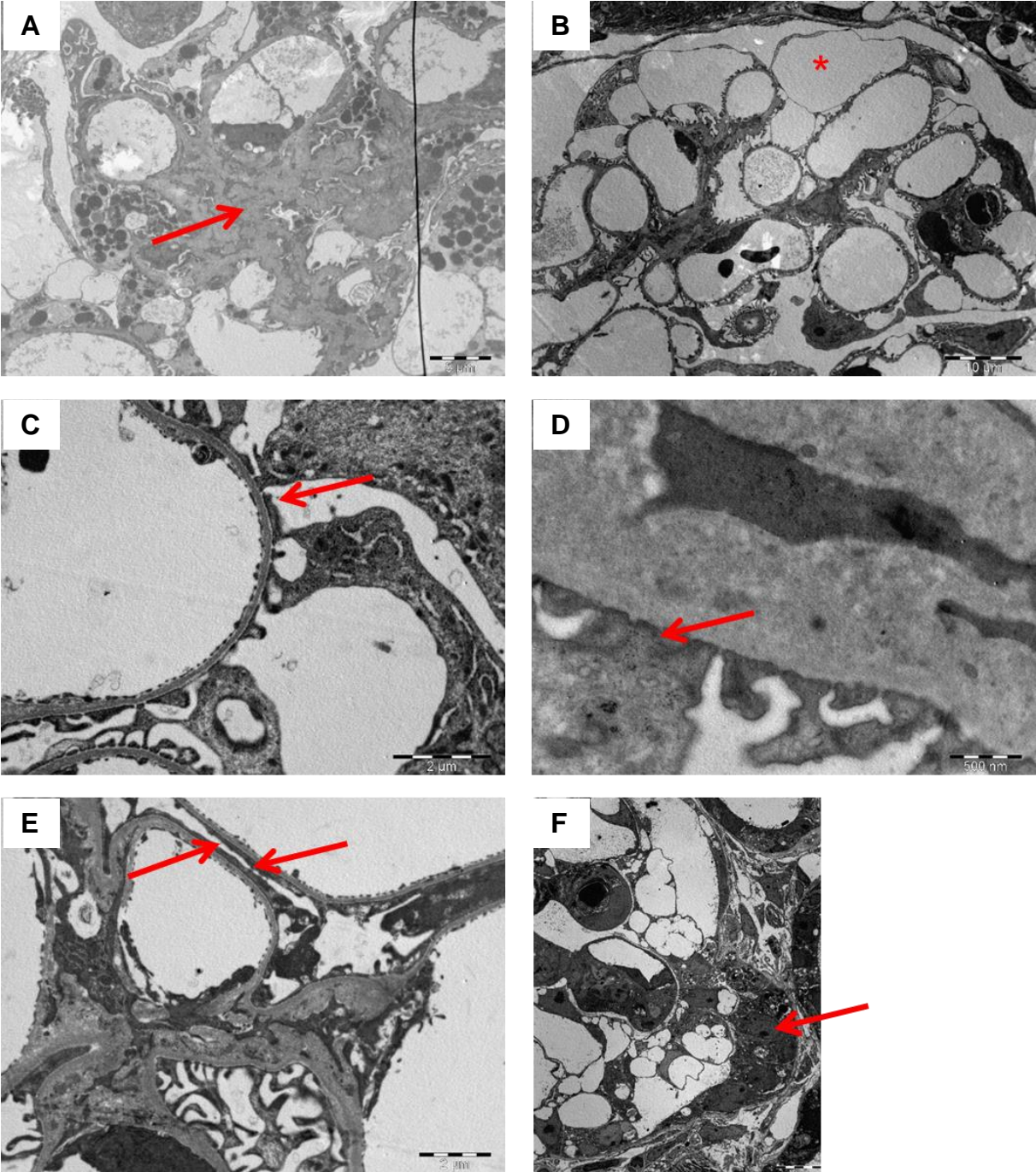
Figure 22: *Representative images of transmission electron microscopy (TEM) in a D-HBP-TGR rat.* A- Thickening of GBM and deposition of worn-out GBM in the mesangium B- Pseudocysts C+D- Widened podocyte FPs are attached to the GBM E- FPE at two neighboring capillaries F- Adhesion of the glomerular tuft to the Bowman's capsule.
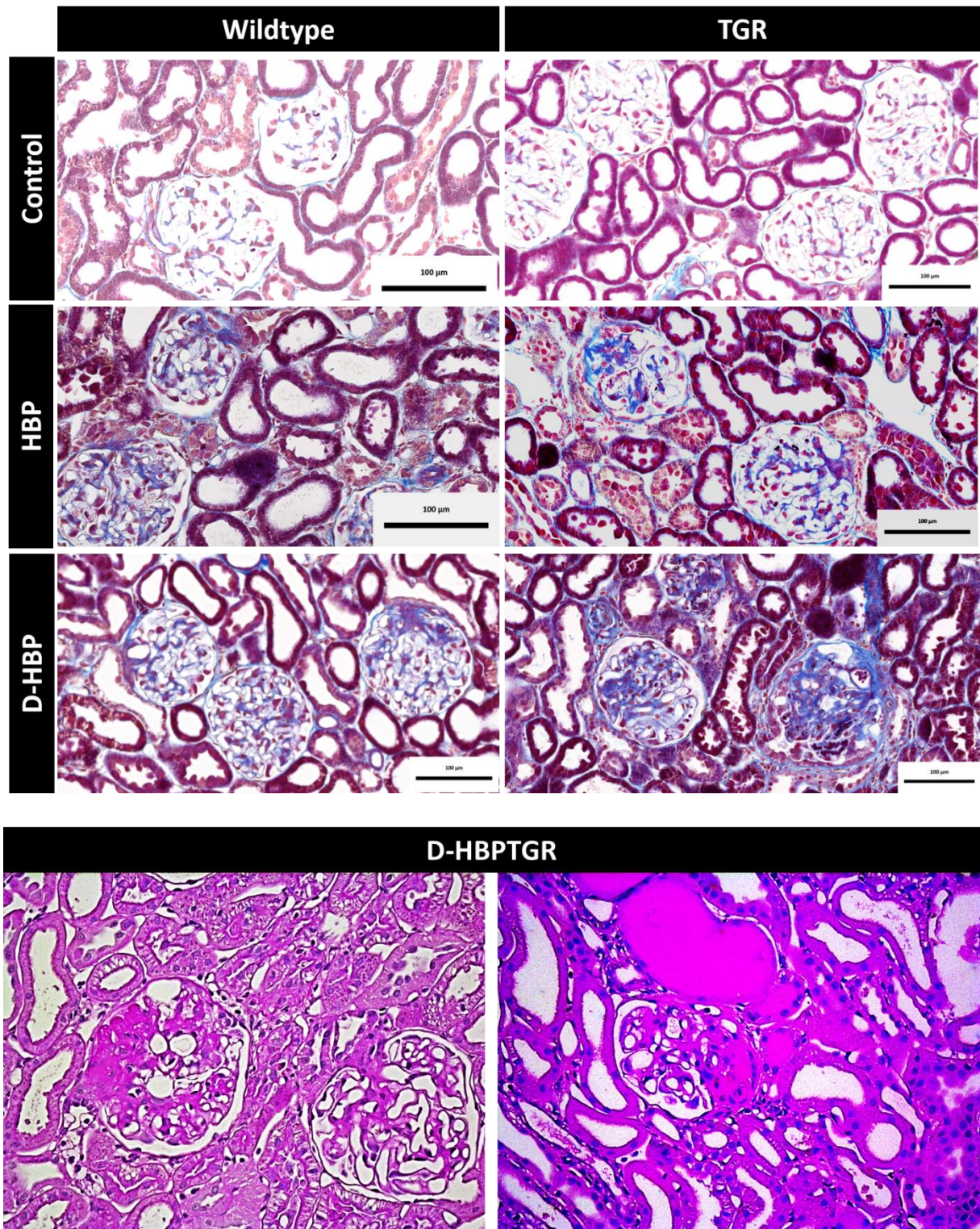
Figure 23: *Representative light microscopic images of renal damage in the different genetic and treatment groups.* **Top** (6 images): AZAN staining of the kidney sections reveals the most severe damage in the D-HBP-TGR group. **Bottom** (2 images): PAS staining of D-HBP-TGR kidney sections reveal massive FSGS and intratubular protein casts.
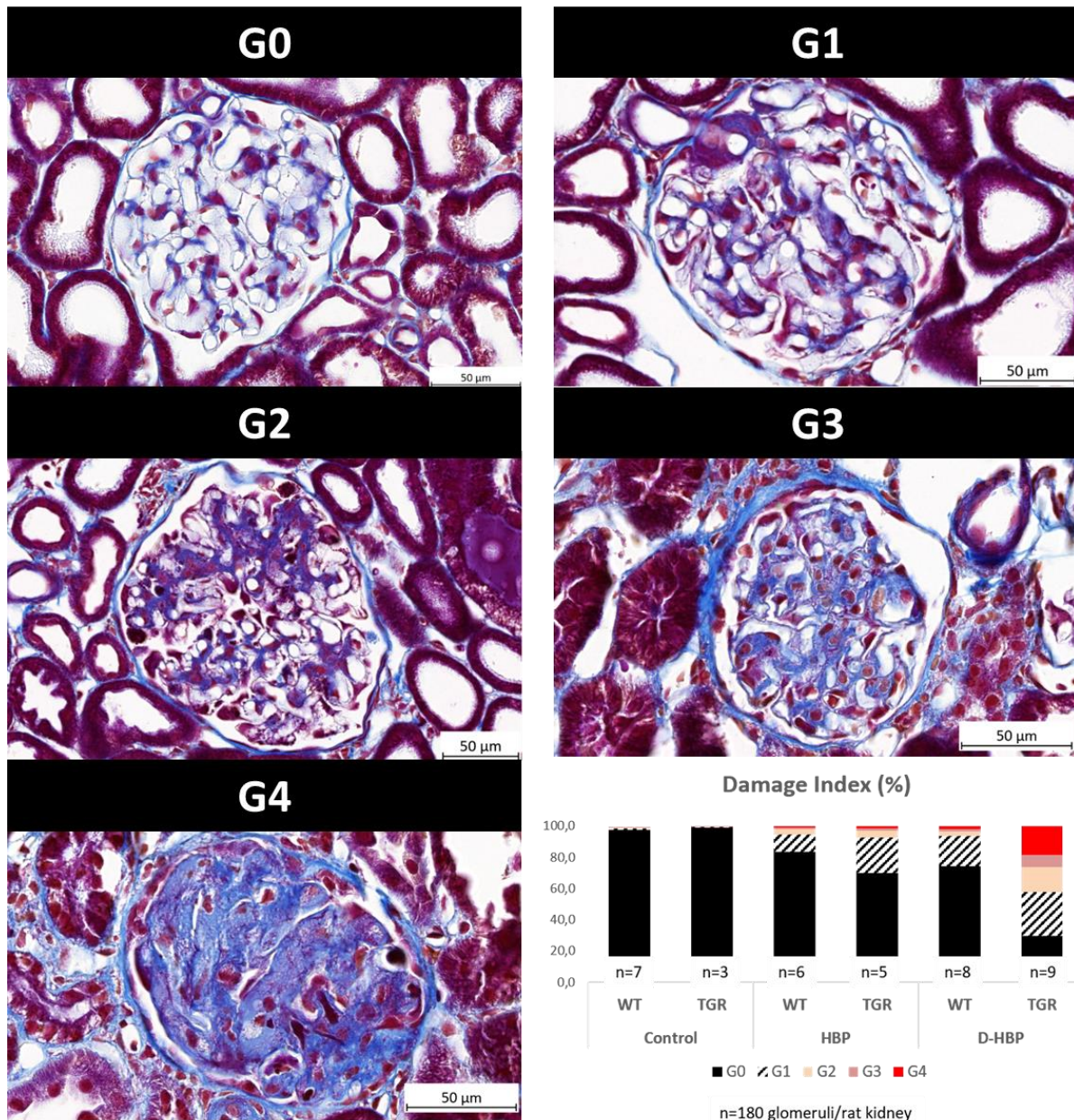
Figure 24: *Representative AZAN stained images for 4 categories used to determine the damage index (AZAN staining.* G0- healthy glomerulus stained fairly mild blue. G1- glomerulus stained mild blue representing the first signs of mesangial expansion. G2- moderately blue-stained glomeruli and mesangial expansion. G3- Severely blue-stained glomerulus and thickening in Bowman's capsule together with mesangial expansion. G4- mostly blue-stained glomerulus showing adhesion to the thickened Bowman's capsule. Damage index chart shows the distribution of the G0, G1, G2, G3 and G4 in percentages. D-HBP-TGR rats have had the most severely damaged glomeruli out of all groups.

3.4 Conclusion I

Our data demonstrate that the synergistic action of diabetes and HBP is required to induce rapid renal damage in diabetic rats since neither HBP alone nor STZ-diabetes alone was able to induce a comparable deterioration in renal function and morphology. AT1R overexpression in podocytes strongly accelerates the disease progression, specifically in D-HBP conditions.

66

3.5 Expansion microscopy enables nanoscale evaluation of the renal filtration barrier

The evaluation of characteristic histological lesions in the GFB, such as podocyte FPE and GBM thickening so far required electron microscopy, since the fine structure of the GBM is in the nanoscale range below 100 nm. Thus, it cannot be evaluated by light microscopy as the physical diffraction limit of optical microscopes prevents high-resolution imaging below 250nm. Recently developed Super-Resolution Microscopy solved this problem; however, it requires expensive microscope techniques and a highly skilled operator. In the present study, we aimed to use a recently developed technique ExM, to visualize and quantify alterations in the nano-scale structure of the GBM.

ExM has solved three very important problems in the field.

- It enabled the visualizing of nano-scale structures by the use of the fluorescent or confocal microscope.
- It enabled the labeling of the structure of interest using classical antibodies and immunohistochemistry.
- It enabled the volumetric evaluation of thick tissue slices and the creation of 3D models of the structure of interest at the nanoscale range.

3.5.1 Workflow of ExM on kidney samples

Our protocol is in principle based on a procedure described in 2018[111]. The workflow of our experiments is shown in **Figure 25** and described in more detail at the material and method section. After clearing and denaturation, the kidney sample has expanded roughly 1.8 times and becomes fragile. For immunohistochemistry, these slices were cut from the cortex to the medulla into different sections each containing cortical and medullary parts, which were used to stain with different antibodies or used to store at 4°C. Thereafter, samples were first imaged at the confocal microscope and then further expanded by placing the sample into ddH2O for 1 day. Compared to the original size, the kidney is finally expanded by roughly 4.5 times. The second and final imaging is then performed. The immunostaining before the final expansion has the advantage that lesser antibodies are needed, and the tissue gel is

less fragile. The expanded tissue consist of more than 90% water. Thus, the autofluorescence is strongly reduced. One sample can be repeatedly stained. Therefore, the tissue is shrunken again by placing it into 1x PBS, the antibody is removed due to repeating the denaturation step and the immunohistochemical staining procedure is repeated.
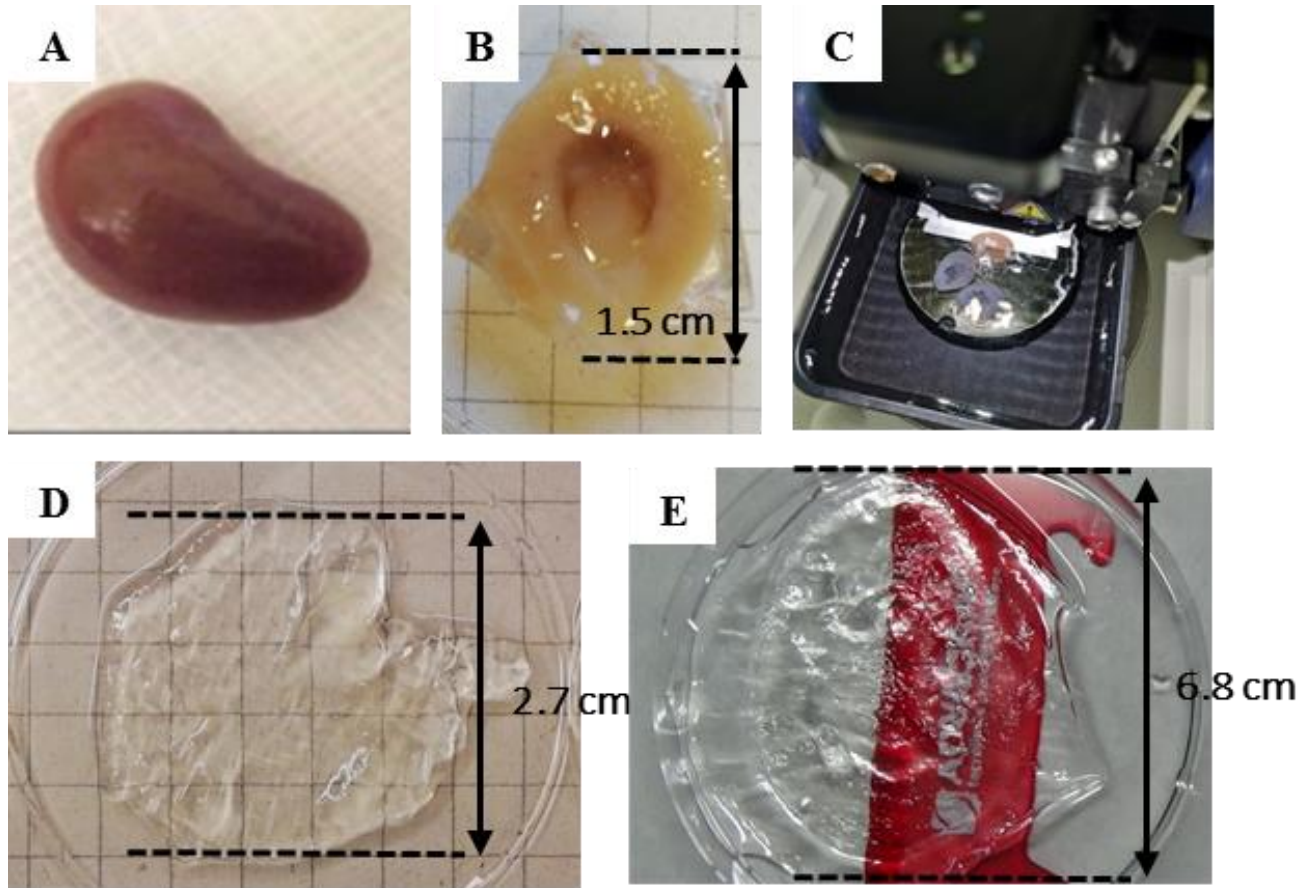
Figure 25. *Workflow for expansion microscopy.* A- Entire kidney sample after perfusion. Then, this kidney was cut into several pieces, and the mid-part was placed into AHS after overnight postfixation in 4% PFA at 4 °C. B- Kidney sample after polymerization of AHS solution at 37 °C. C- Polymerized sample was cut via vibratome at the desired thickness (1mm to 50 µm). D- Kidney slices after clearing and denaturation in denaturation solution at 70 and 95°C each for 12 hr (500 µm thickness). Then, the sample becomes transparent (and expanded approximately 2 fold). E- Sample placed into ddH2O and expanded. Immunostaining was performed after the denaturation.

3.5.2   Immunohistochemistry

To label the SD between the secondary FPs, we used nephrin, a major constituent of the SD. The intracellular tail of nephrin directly binds to podocin, which is located at the insertion site of the SD in the podocyte secondary FPs. We used podocin staining to outline the secondary FP. The width of the FP was determined by the distance between two podocin stains. A key feature of glomerular diseases is podocyte FPE, which includes the retraction of the secondary FP and is associated with their widening in **Figure 26**. Furthermore, we stained collagen IV, the main constituent of

the GBM which also label the Bowman's capsule. Co-staining of nephrin and collagen IV allows the study of glomerular tuft volume, the size of the Bowman's capsule and GBM thickening [**Figure 27**].
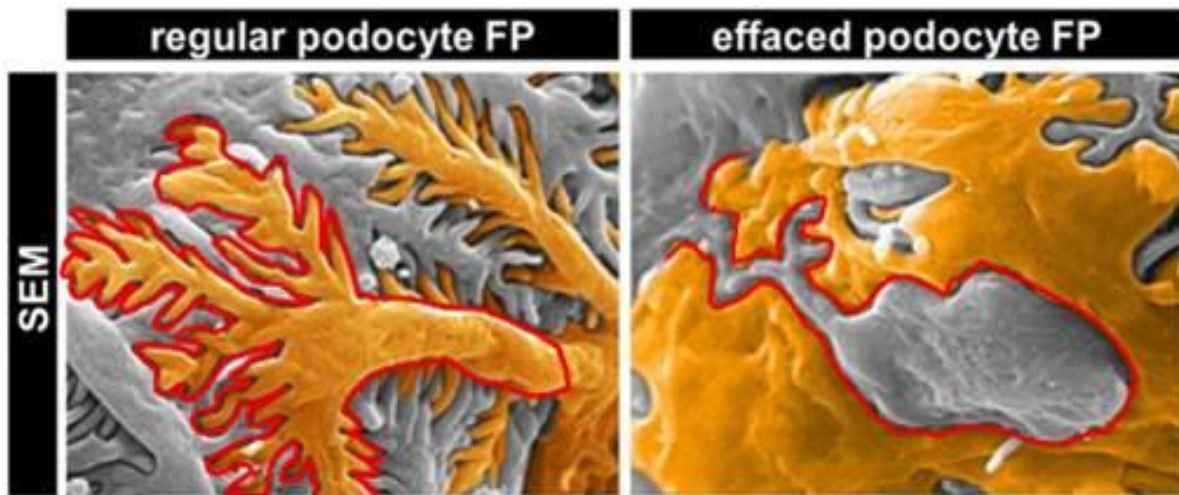
Figure 26: Arrangement of the podocyte foot process in Scanning Electron Microscopy (SEM). A- FPs are tightly attached and well organized. B- FPs are retracted and effaced. Red lines (drew by us) represent SD, namely nephrin. *Originally published in Endlich et al. 2018
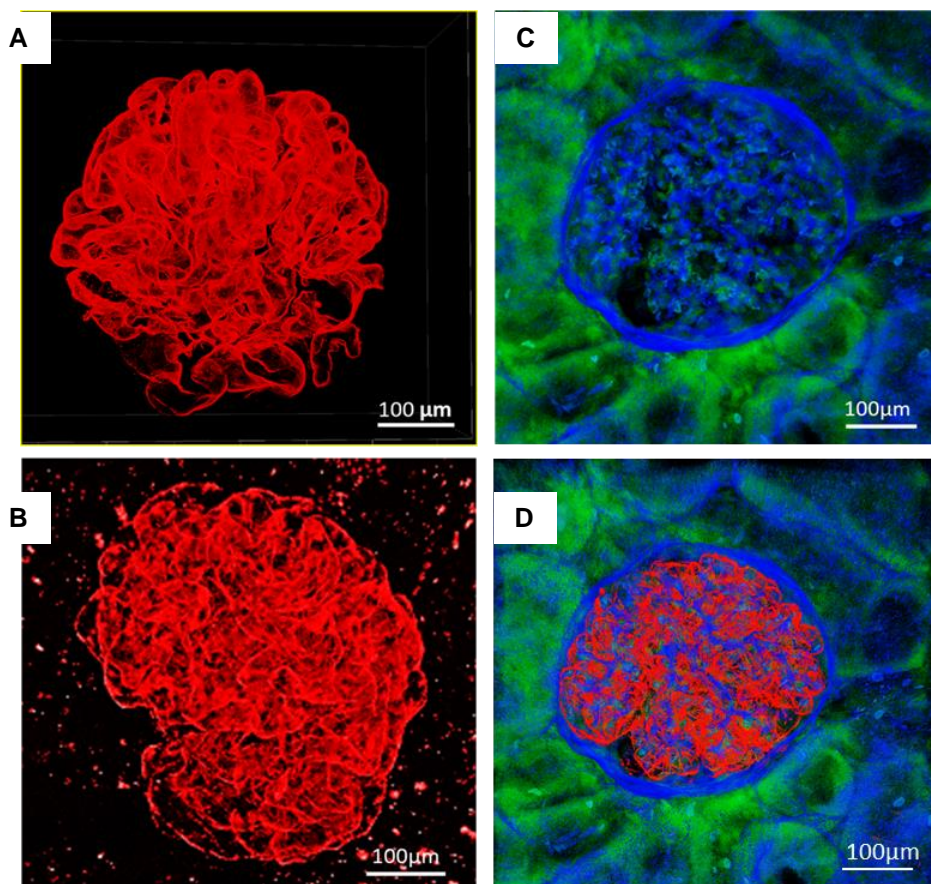
Figure 27: *Immunohistochemical staining of glomerular structures.* A- Podocin staining labels the membrane of the podocyte secondary foot processes outside of the capillary tuft. B- Nephrin staining labels the slit diaphragm and thus, generates a similar picture as the podocin staining. C- Collagen IV staining labels the basement membrane and parietal epithelium. D- Co-staining of nephrin and collagen IV.

3.5.3 Visualization of slit diaphragm and podocyte foot processes by ExM and confocal microscopy

The physical expansion of the tissue dramatically increased the resolution. **Figure 28** shows immunohistochemistry for podocin on a non-expanded 4µm kidney section and on an expanded 500µm section. The 4µm kidney section was stained with podocin and synaptopodin antibodies. The 500µm sections were stained with a podocin antibody and expanded using the ExM technique. The 4 µm samples were imaged by the use of a 63x (oil immersion) objective. The 500 µm samples were imaged using a 20x (water immersion) objective. Despite less magnification used to image the expanded tissue, the resolution was much higher than in the non-expanded tissue, as shown in **Figure 28**. ExM enabled the visualizing of the podocin-labeled podocyte FPs. **Figure 29** shows a comparison of podocyte FPs in rat kidneys we imaged by ExM and confocal microscopy with those generated by SIM, which was prepared by Prof. N. Endlich, University Greifswald, NIKOPA, Greifswald using the same tissue. It is clear that ExM provided a comparable resolution as SIM.

IHC Podocin-
Kidney 4 µm Slice
63x Objective
Oil immersion

IHC Podocin
Kidney after
expansion
500 µm Slice
20x Objective
Water immersion
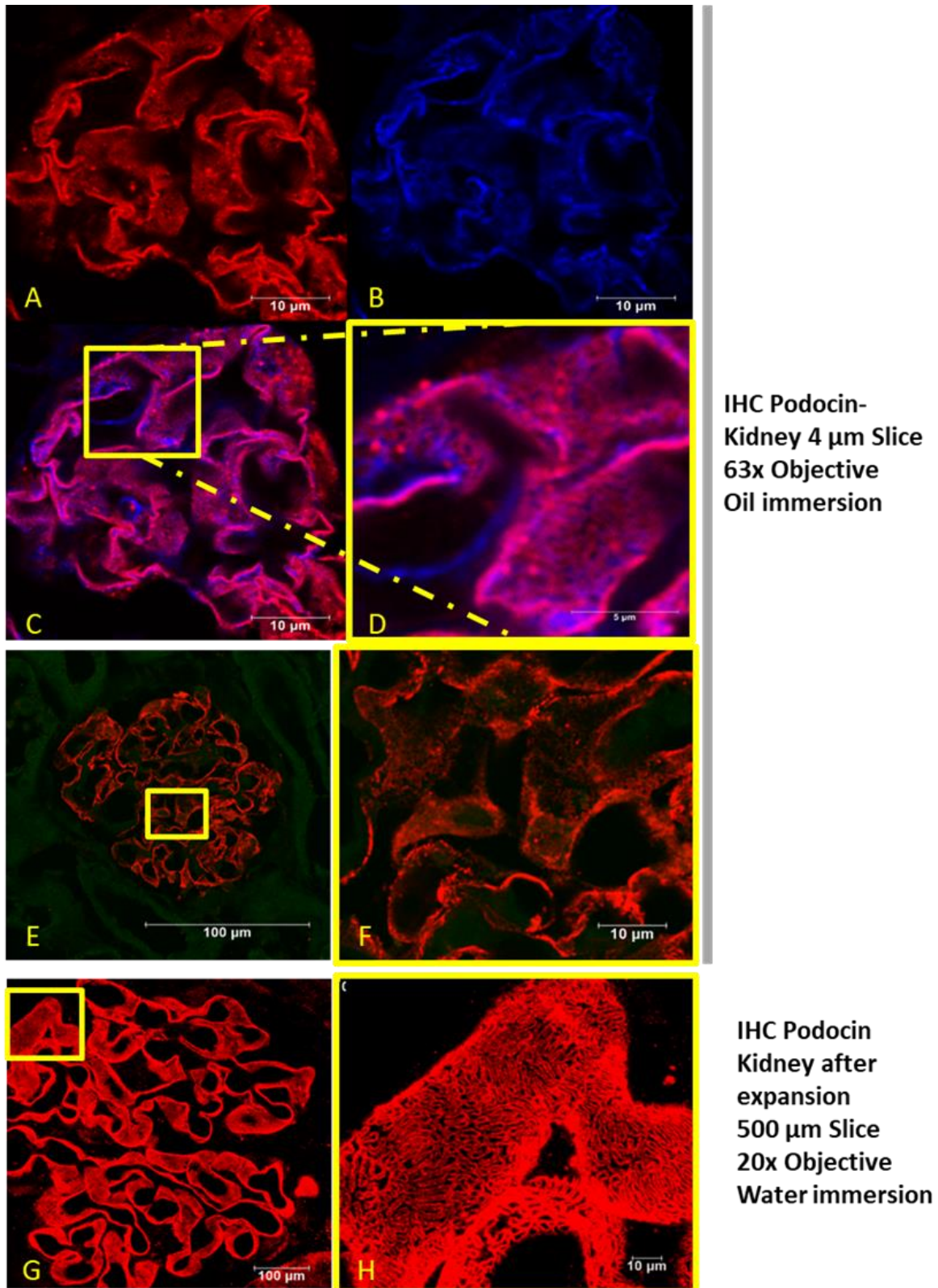
Figure 28: *Comparison of the resolution of the classical IHC to ExM.* A and B- 5µm thick sample stained with Podocin (red) and Synaptopodin (blue) by classical IHC (60x oil immersion objective).C- Merge image of A and B. D- Magnification of the podocyte foot process on 4µm thick sample stained with classical IHC. E- 4µm thick sample stained with podocin (red) by using classical IHC (63x oil immersion objective). F- Magnification of the area labeled on the image E. G- Podocin stained glomerular structure and podocyte foot process (stained red) in 500µm expanded kidney sample (20x water immersion). H- Magnification of the yellow labeled area on the image G.
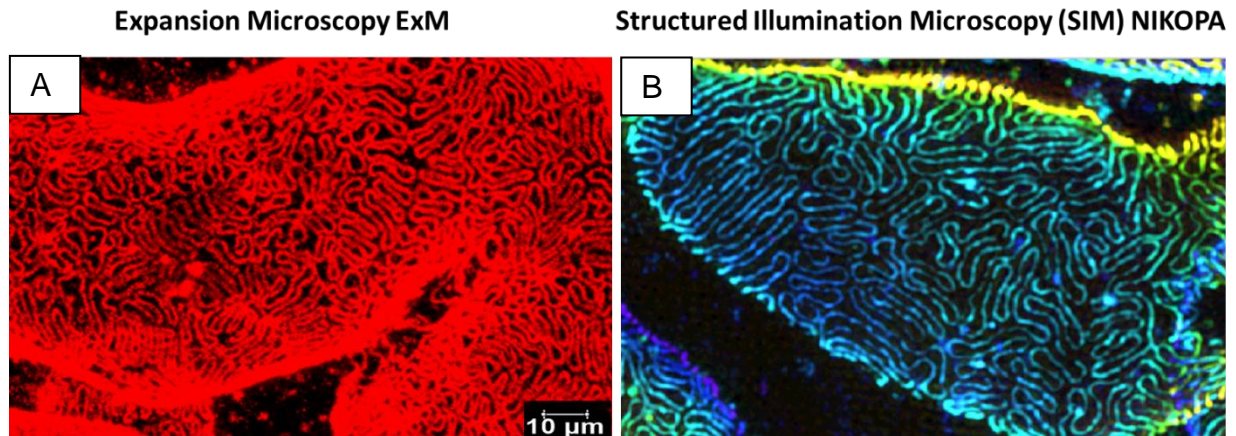
Figure 29: *Comparison of Expansion Microscopy technique (ExM) and Structured Illumination Microscopy (SIM)*. A- 500µm thick kidney sample stained with Podocin (red) and expanded (20x water immersion objective). B- Super-resolution microscopy images of the mouse kidney (**published by Endlich et al. 2018).

3.5.4 Expansion factor and distortion

An important issue we addressed was the determination of the expansion factor. The expansion factor was calculated for each individual rat and was used to normalize morphometric measurements. Moreover, we wished to evaluate whether ExM causes any distortion of the samples' structure, which might affect the results of morphometric measurements. From each rat, a part of the kidney was frozen for H&E staining and used as a "non-expanded control samples", and another part was used for ExM and stained for podocin. In both samples, the glomerular size was calculated, as shown in **Figure-30**. We measured the longitudinal and transverse diameters. Based on this, for each kidney, we calculated the expansion factor, which was later used to normalize the following morphometric measurements in the ExM tissues. The graphic illustration in **Figure-30** demonstrates that the average expansion factors were equal for longitudinal and transverse diameters. They correlated with r= 0.97.   Alike, the expansion factor did not differ between the different treatment groups and genotypes. Moreover, as shown in **Figure-31**, the increase in glomerular size in HBP or D-HBP vs. CTRL was comparable, independent of whether it was evaluated using H&E staining on non-expanded tissues or ExM. Thus, these data indicate that morphometric measurements in the expanded kidneys are trustable for the evaluation of changes in tissue structure due to disease. Additionally we calculated the ratios between both glomerular diameters for each glomerulus to evaluate a possible distortion of the tissue during expansion.

As shown in **Figure-31** the ratios were constant regardless of disease or whether using non-expanded or ExM tissue.
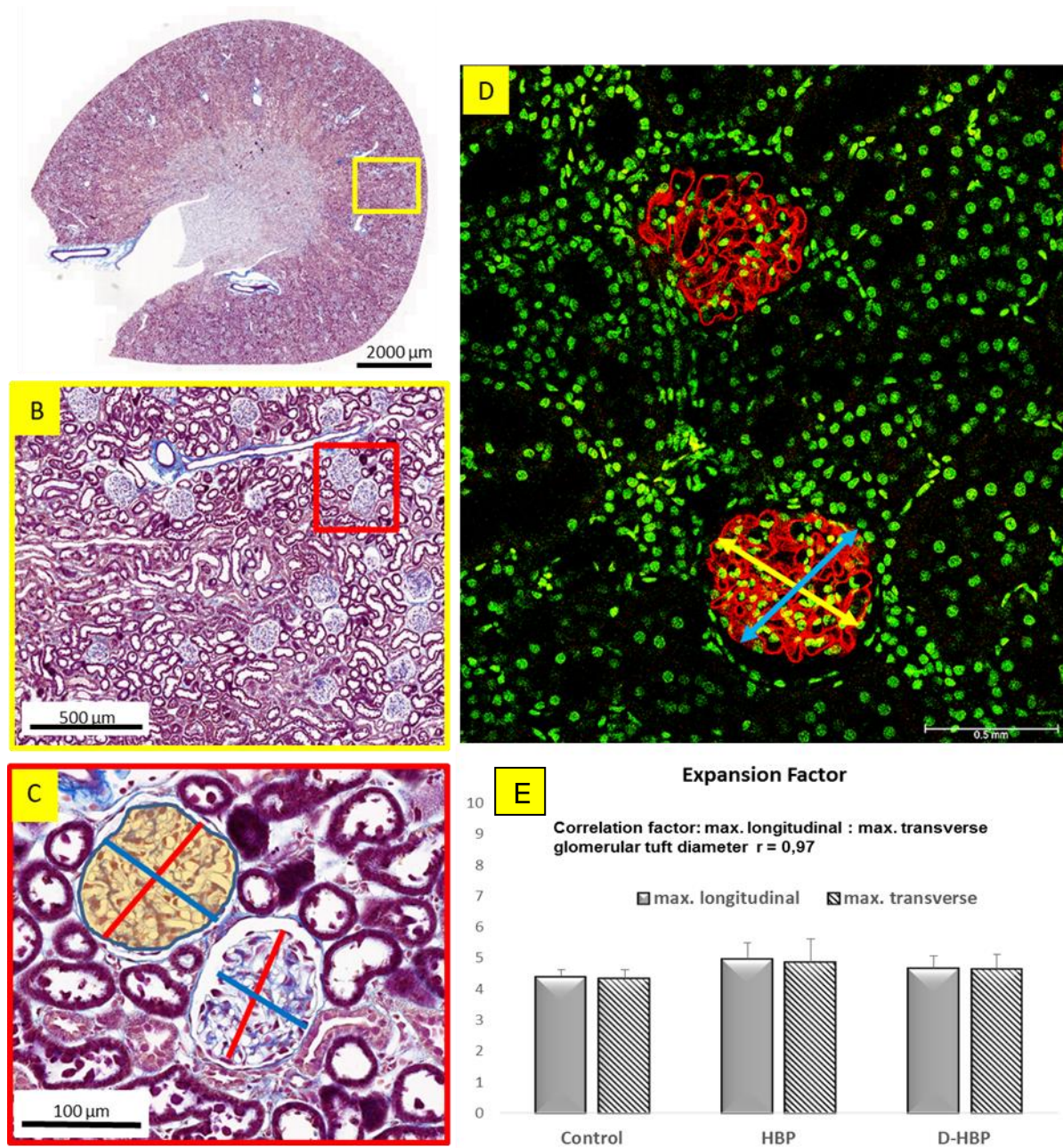
Figure 30: *Calculation of the expansion factor and evaluation of the expansion.* A- Entire scan of the kidney section stained by H&E. B- magnification of the yellow labeled area. C- Representation of the measurements on two glomeruli. D- Expanded kidney sample and measurement of two glomeruli. E- chart representing the average expansion factor among the groups.

Non-expanded frozen sections

max. longitudinal Diameter (µm)

max. transverse diameter (µm)

Ratio max. longitudinal : max. transverse diameter

Expanded sections (ExM)

max. longitudinal Diameter (µm)

max. transverse diameter (µm)

Ratio max. longitudinal : max. transverse diameter
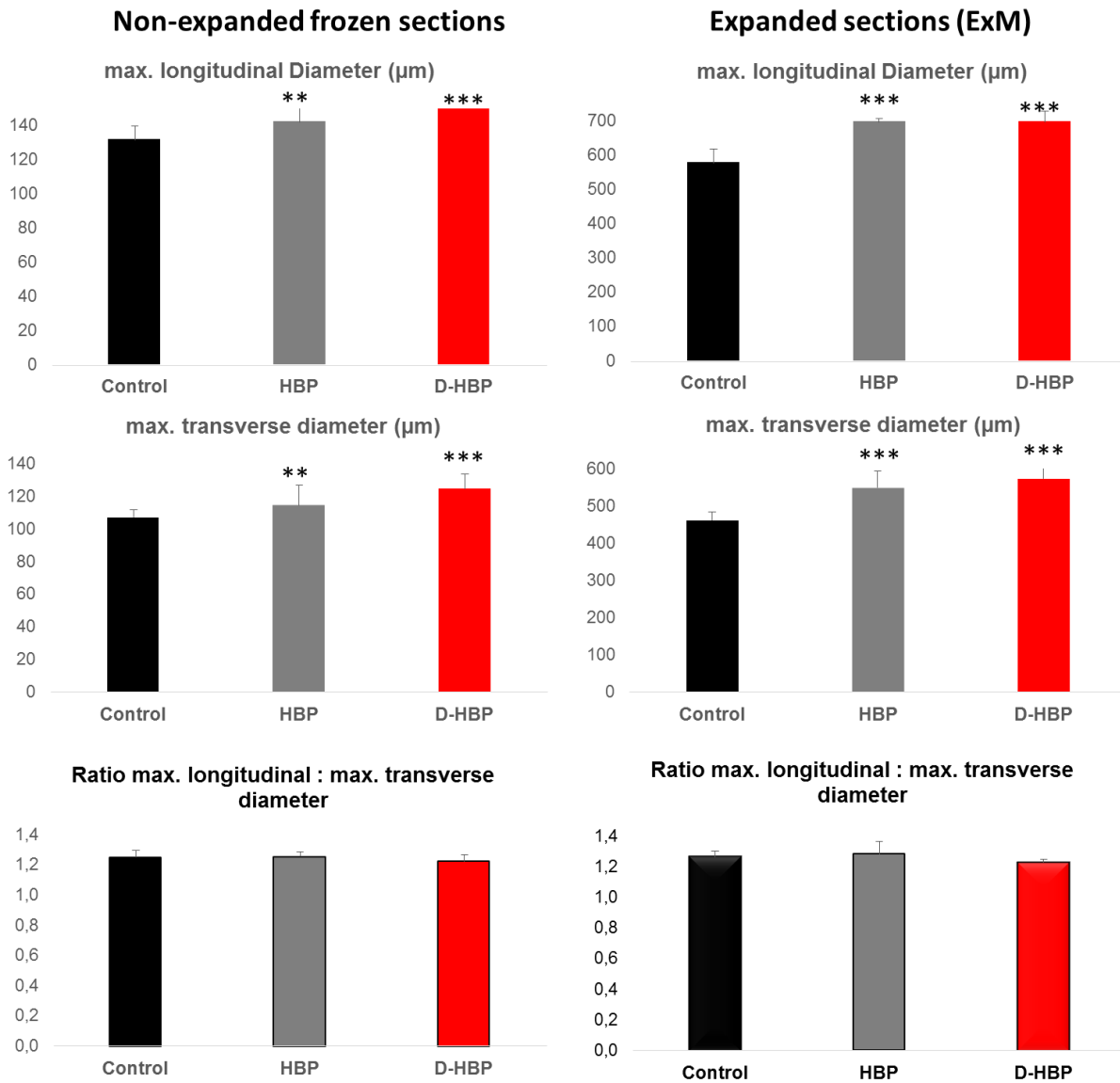
Figure 31: *Expansion factor and distortion.* Graphs showing the max. transverse and max. longitudinal glomerular diameters. Both are comparably increased in the HBP and D-HBP group vs. controls independently, whether measured in non-expanded or expanded tissue. In contrast, the ratios between the max. transverse and max. longitudinal glomerular diameters were similar in all groups, indicating that the tissue uniformly expanded.

3.5.5 Glomerular damage correlates with FPE - evaluated by ExM vs. SIM and electron microscopy

We used the described method to evaluate the podocyte FPs in order to quantify the FP widths. Widening of FPs is a feature of FP retraction and associates with DN. As shown in **Figure-32**, ExM and podocin staining permitted us to image a larger renal area and to evaluate a number of glomeruli in 3D at low magnification (10x 0bjective) [**Figure-32A**]. Individual glomeruli were selected and evaluated in more detail using the 20x objective [**Figure-32B**]. Then selected glomerular regions were investigated in even more detail using the 63x objective to evaluate the FPs [**Figure-32C** and **D**].
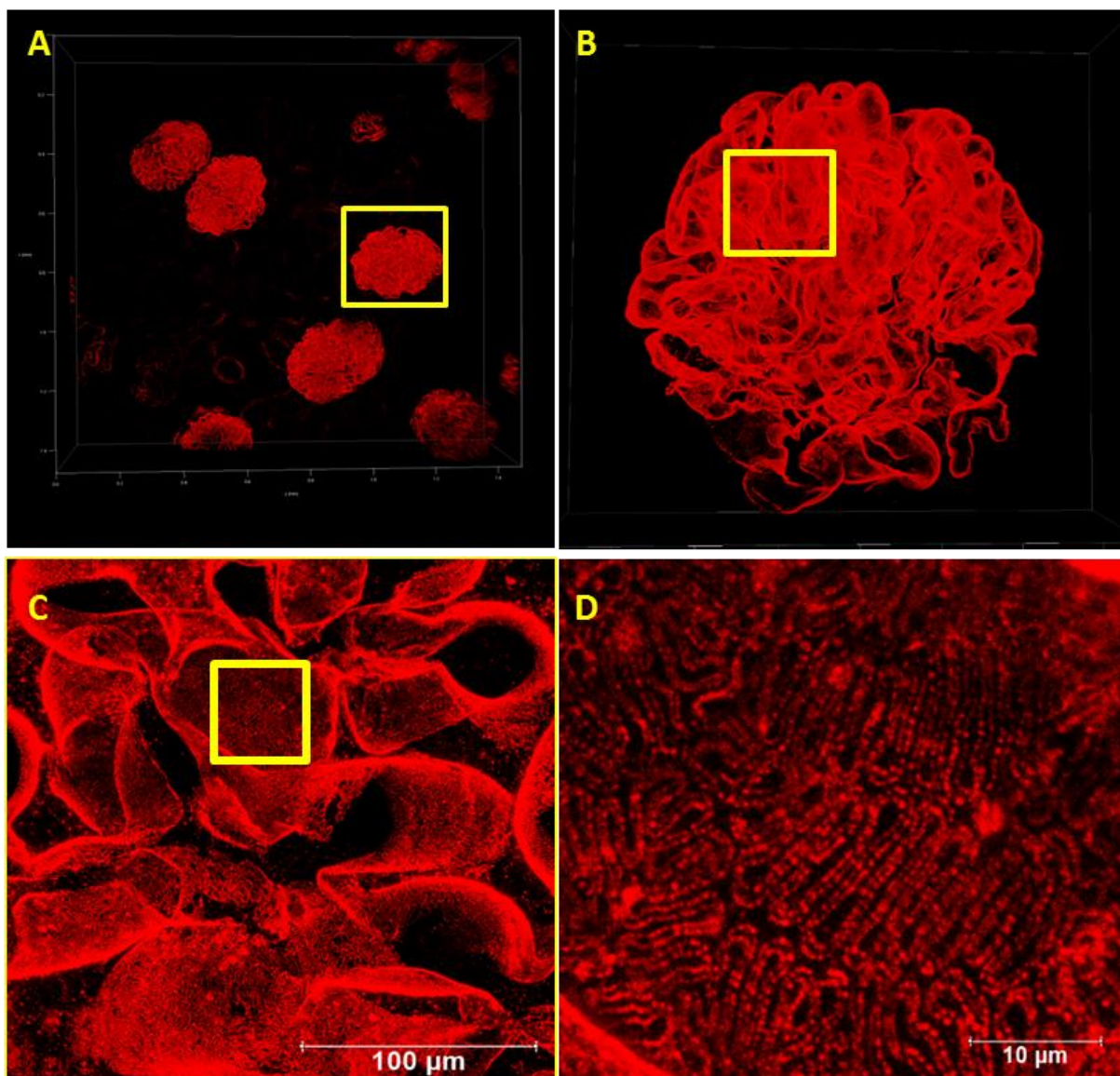
Figure 32: *Deep imaging of the podocyte foot process in expanded kidney sample.* A- 3D images of several kidney's glomeruli, 10x objective. B- 3D images of a single glomerulus, 20x objective. C- Magnification of the labeled area on the B, 63x objective. D- Further magnification of the labeled area on the image C showing podocyte foot processes and slit diaphragm, 63x objective.

Interestingly, using this method, we often found structures never previously described, as shown in **Figure-33** and which we cannot explain yet. These loops of interdigitating FPs, not anymore connected with the GBM, might represent a reservoir that is used to compensate pressure-related expansions of the capillary. These hypothesis needs to be further investigated.
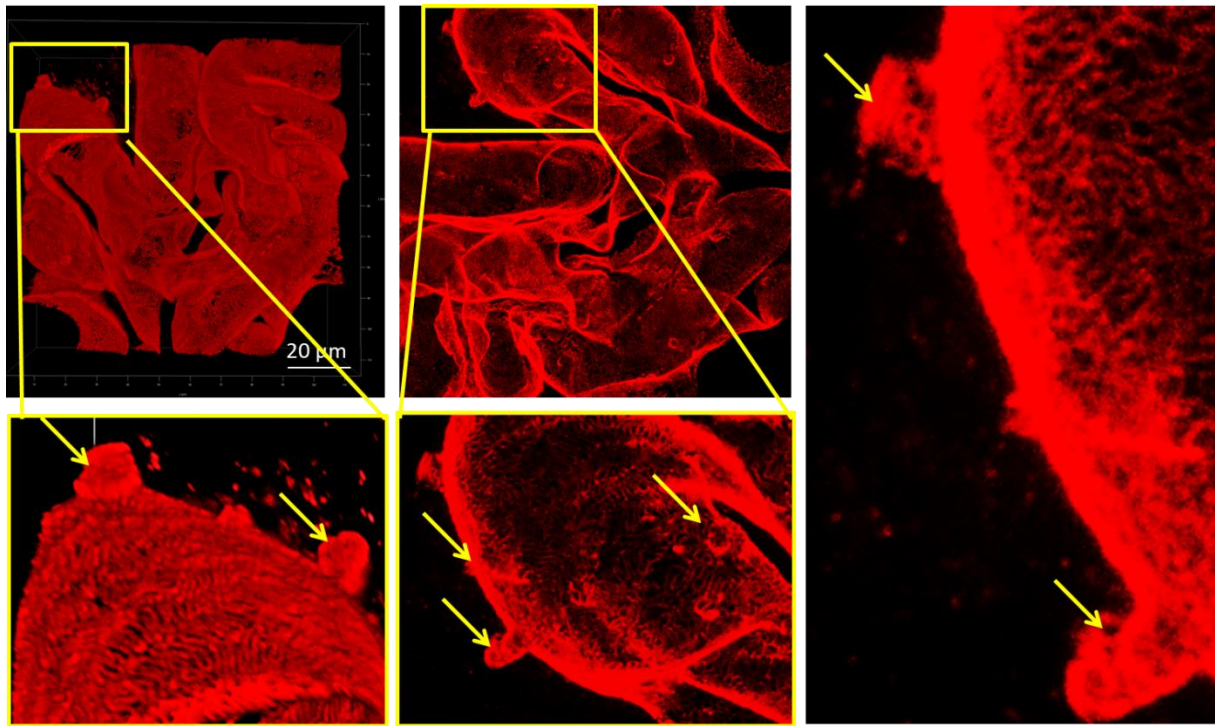
Figure 33: Figures showing intact interdigitating FPs which are not adhered to the GBM.

Figures-34 - 38 show representative images from the kidneys of CTRL-TGR [**Figure-34**], HBP-TGR [**Figure-35**] and D-HBP-TGR rats [**Figure-36 - 38**]. In CRTL rat kidneys, all the surfaces of capillaries are densely covered by long, narrow FPs interdigitating with each other [**Figure-34**].
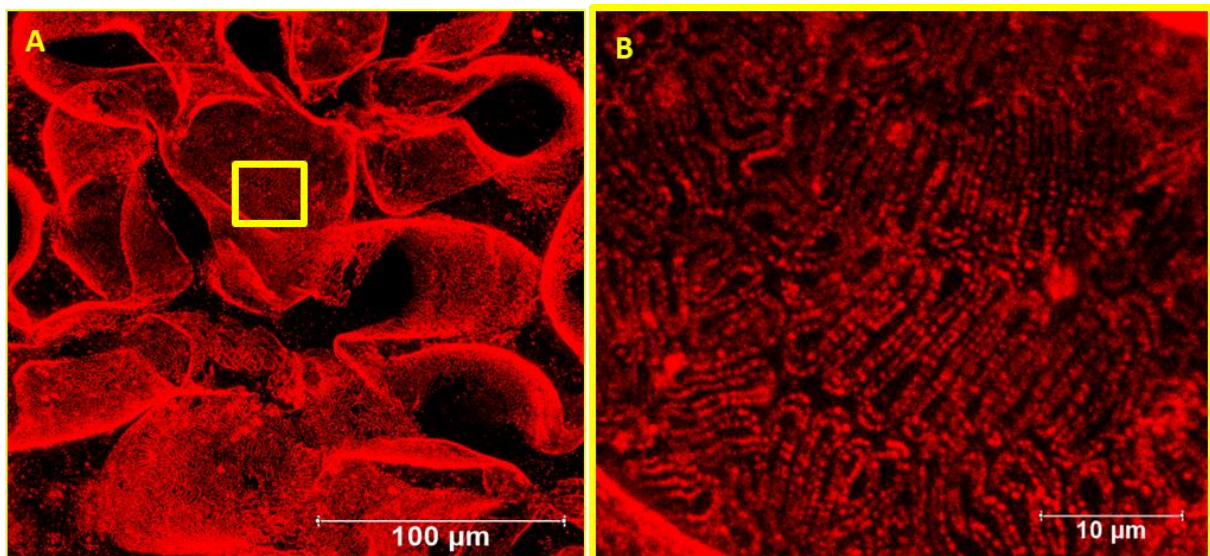
Figure 34: *Podocyte foot process of the expanded kidney sample in the CTRL group.* A- 3D image of a single glomerulus. B- Magnification of the labeled area in A.

In both, HBP-Wild and -TGR rat kidneys, the podocyte FPs network appear regular, the SD is intact and densely covers all capillaries, although the rats already developed to a certain degree albuminuria. However, it is obvious that the FPs widths are increased and the FPs are shorter **[Figure-35]**. In contrast, in D-HBP rats, specifically in D-HBP-TGR, we found severe injuries in the FP structure as shown in **Figure-36-38**. Within one glomerulus, there are areas of a still intact FP network with shortened and widened FPs, in other areas, the FPs are retracted, irregularly organized or podocin staining is completely lost indicating a complete FPE or not covered GBM with scarring.
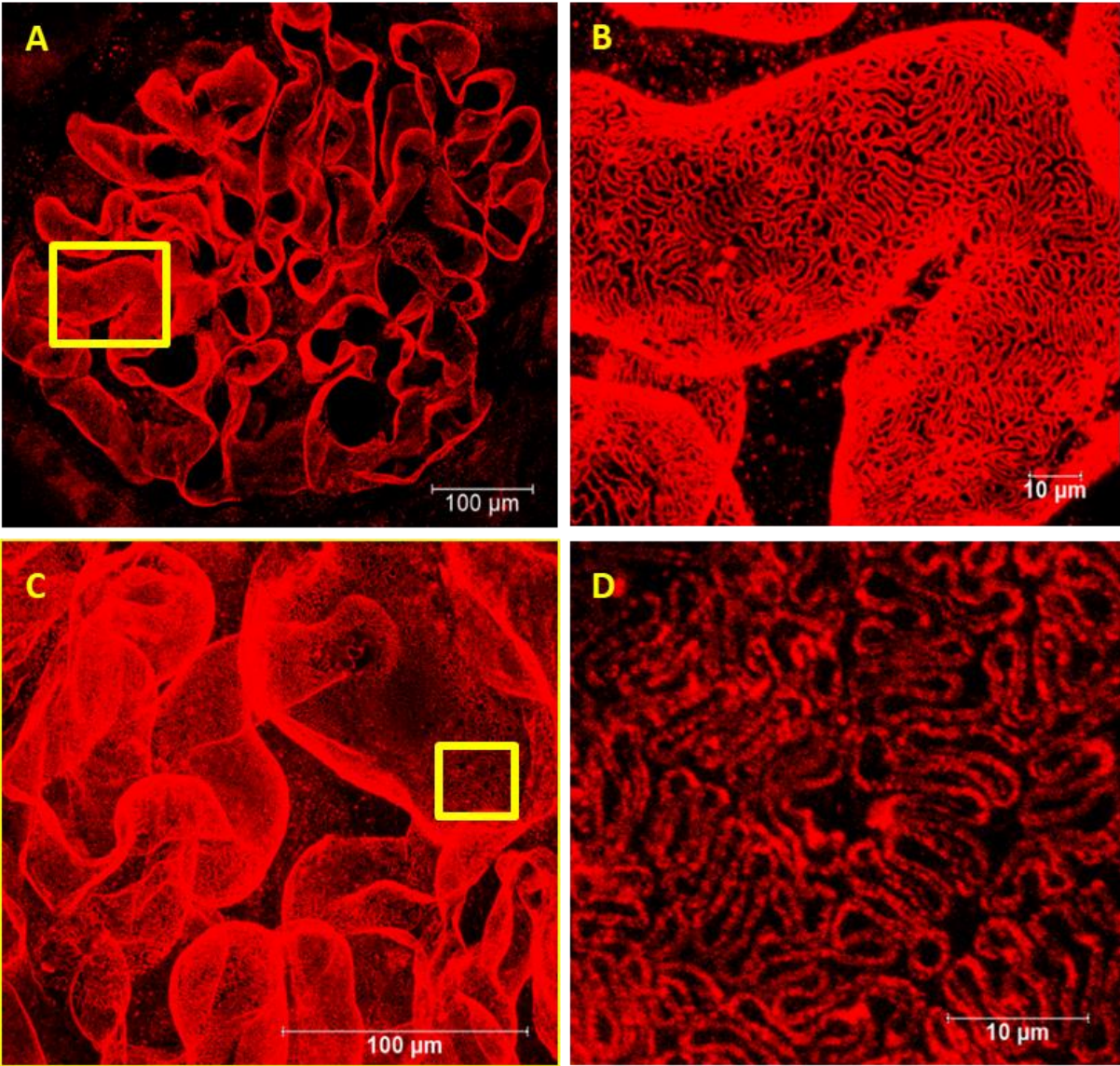
Figure 35: *Podocyte foot process arrangement of expanded kidney samples in the HBP group.* A-3D images of the kidney's glomerulus. B- Magnification of the labeled area in picture A. C- The 3D image of a kidney's glomerulus. D- Magnification of the labeled area on image C.
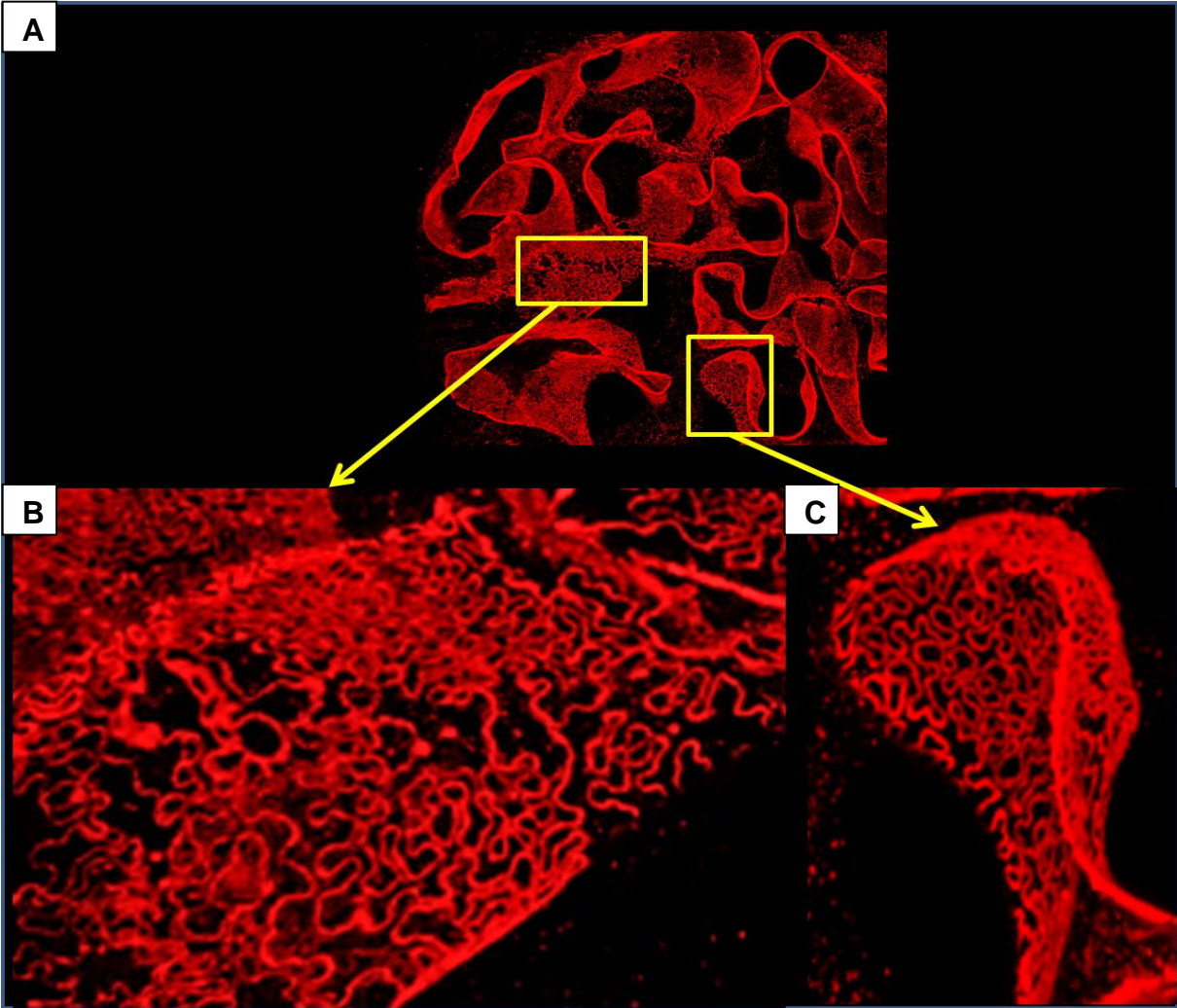
Figure 36: *3D representation of the FPs arrangement in D-HBP-TGR. A- 3D distant image of a glomerulus.* B- Magnification of the selected area with FPE. C- Magnification of the selected area to show ExM enables to visualize the arrangement of the fine structures in 3D, showing widened and shortened FPs.
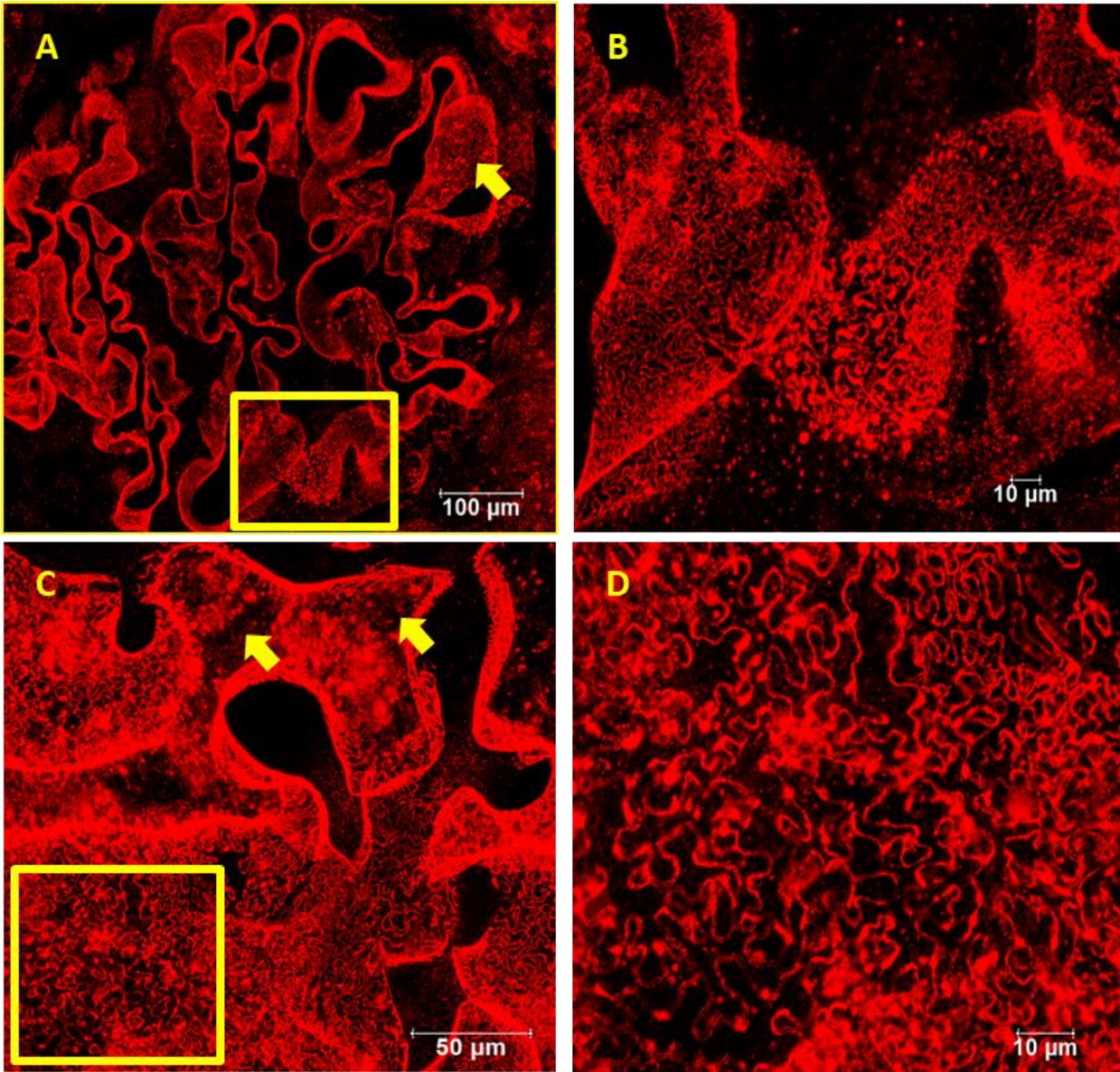
Figure 37: *Podocyte foot process arrangement of expanded kidney samples in the D-HBP-TGR group.* A- 3D overview image of the kidney's glomerulus. B- Magnification of the labeled area in picture A showing FPE. C- The 3D image of a kidney's glomerulus. Arrows indicate areas where the FPs structure is completely lost. D- Magnification of the labeled area on image C showing severe FPE.
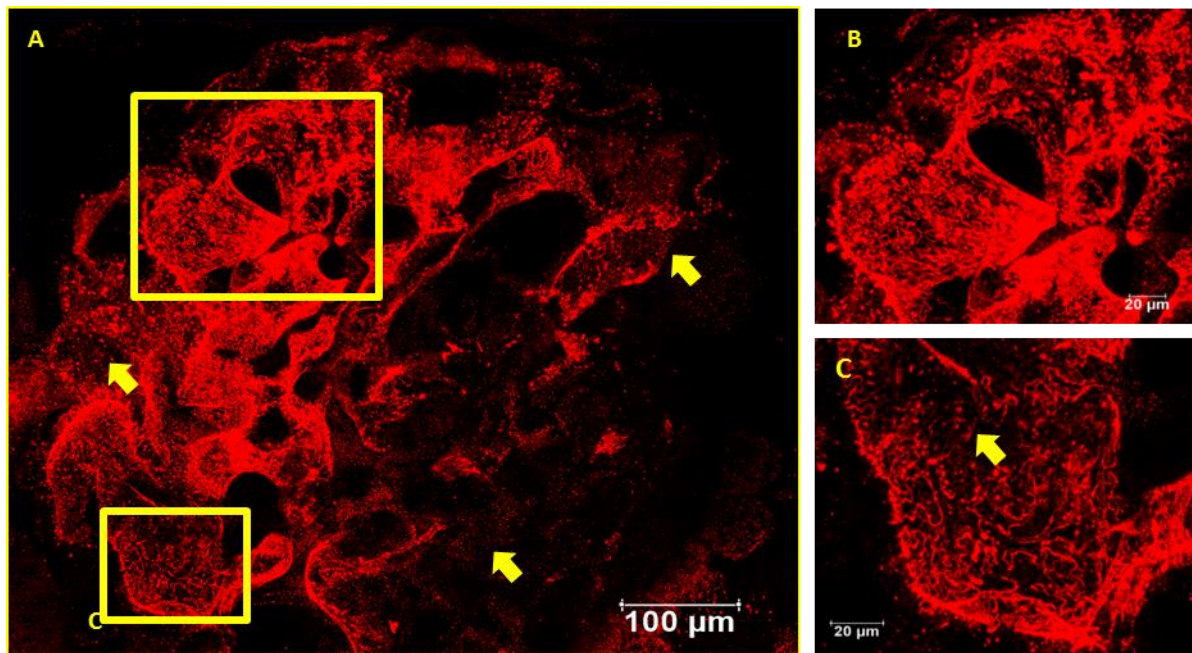
Figure 38: *Podocyte FP arrangement of expanded kidney samples in the D-HBP-TGR group.* A- 3D images of the kidney's glomerulus. B- and C- Magnification of the labeled area in picture A. showing severe FPE and loss of FP structure (arrows).

The FP widths were calculated by measuring the distances between the podocin stainings [**Figure 39**] of 150 FPs in 5 different regions of each of 2-3 glomeruli per rat.
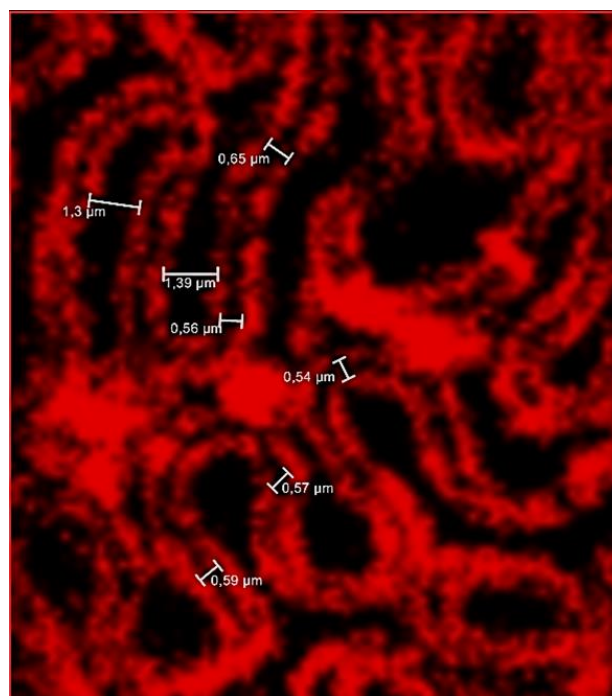
Figure 39: *Representative image showing the measurement of podocyte FP widths and SD widths.* Here, the space between podocyte foot processes are clearly shown by ExM.

Using paraffin sections from the same kidneys, the group of Prof. N. Endlich in Greifswald (University Greifswald/NIKOPA) determined the podocyte filtration slit density (FSD) by SIM and a software-based approach PEMP. They previously demonstrated a high correlation between the FSD and with FP width[106]. **Figure-40** shows representative ExM images of CRTL, HBP and D-HBP rat kidneys with podocin stained podocyte FPs in comparison to nephrin stained podocyte FPs imaged SIM. The resolution and quality of images using ExM are clearly comparable with SIM.
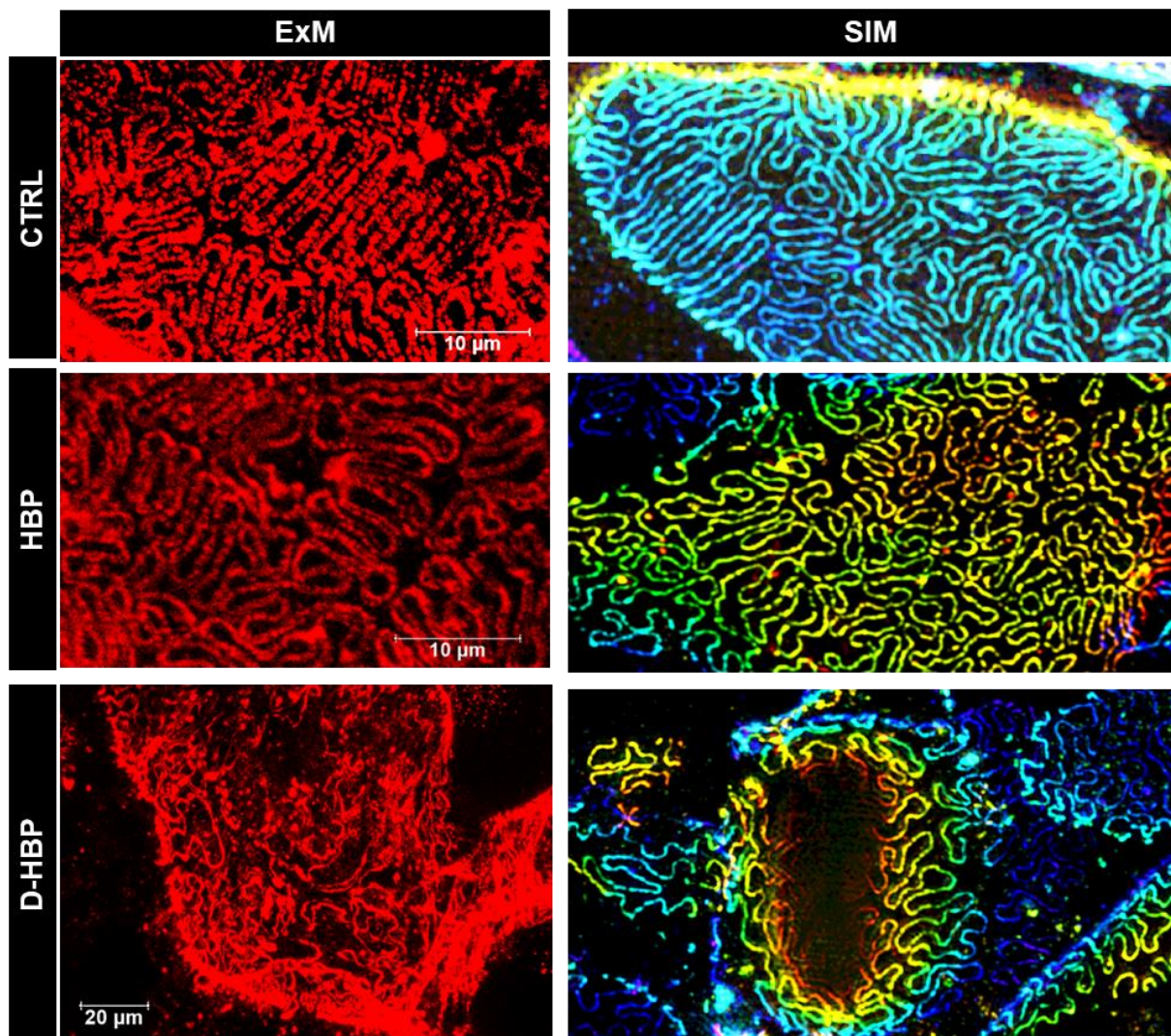
Figure 40: *Comparison of the FPs arrangement in ExM and SIM.* In ExM technique, we observed that CTRL group has relatively long FPs, and FPs are well organized; however, this organization is moderately altered in HBP rats. FPs are effaced and distorted in D-HBP rats. The same pattern is also observed by SIM technique, which was performed by N. Endlich, University Greifswald/NIKOPA

Figure 41 shows the calculated FP widths of TGR and Wild in the three experimental groups CRTL, HBP and D-HBP. Both TGR and Wild show a significant increase of

the FPs widths in HBP rats and a further significant increase in the D-HBP rats. Within the D-HBP group the TGR-FP-width is significantly increased vs. the Wild-FP-widths. The FSD data obtained by SIM and FP width obtained by ExM highly correlated with the correlation coefficient of r=-0.975. An increase in FP width corresponds to a decrease in FSD. Further, the FP width corresponds well with the damage index determined in paraffin sections, the albuminuria and the degree of GFR deterioration.
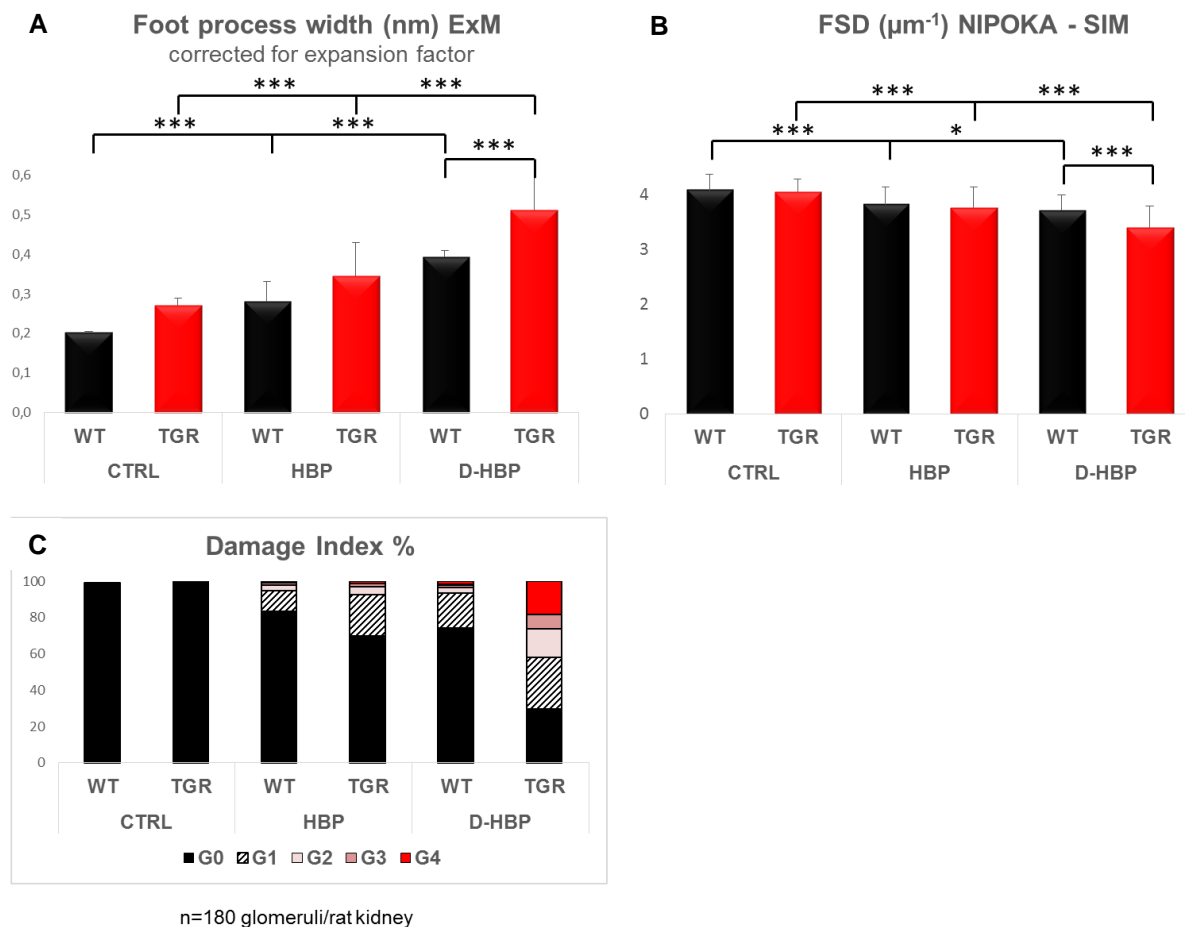
Figure 41: *Comparison of the SIM determined FSD and ExM determined FP widths.* A- Foot process widthd determined by ExM. Here, the D-HBP group has shown the greatest width, presumably due to the FPs retraction. B- Filtration slit density of the experimental rats determined by SIM and PEMP. Glomerular damage index (in percentage)

3.6 Conclusion II

Expansion microscopy is a useful tool for nanoscale evaluation of the GFB in rats with glomerular diseases and provides similar results concerning the FP architecture as SIM technology. The FP widths strongly correlate with increases in albuminuria and the damage index and decreases in GFR. Although HBP induced a certain

albuminuria, the FP architecture is preserved, however, FP widths are increased, and the FP lengths are shortened.

4   DISCUSSION

DN is a leading cause of end-stage renal disease and affects 30% of diabetic patients[116, 120]. Thus, 70% of diabetic patients are protected from DN, indicating that, besides hyperglycemia, DN requires additional factors to develop. Despite major advances in our understanding of the disease, the molecular pathogenesis of DN remains far from clear. A major barrier to further progress is the lack of a suitable diabetic animal model that mimics human DN. Existing diabetic models mostly exhibit only the earliest features of human DN[121]. Rodent models that develop pathohistological alterations in the kidney, like the ob/ob mouse or the ZSF1 rat, are also hypertensive and/or obese. Thus, it has been difficult to separate the hemodynamic from non-hemodynamic effects in vivo. DN is characterized by severe albuminuria, renal hyperfiltration, GBM thickening and glomerulosclerosis[115] and the currently first-line therapy is blocking Ang II.

The present study had two major aims. First, to develop suitable rat models to compare the effects of diabetes, hypertension and combined diabetes/hypertension on the kidney and to specify the role of Ang II signaling in podocytes in this context. Second, to establish and verify an ExM method, which enables the visualization of the podocyte FPs in these disease models and to quantify the degree of FPE. FPE of podocytes is a typical feature of DN and is associated with the leakage of the GFB. It requires electron microscopy to diagnose since the fine structure of GFB is in the nanoscale range.

The key findings of this study are;

1. For the development of DN in rats, HBP and hyperglycemia has to synergize, since neither HBP alone nor STZ-diabetes alone was able to induce a comparable deterioration of renal function and pathohistological alterations in the kidney. AT1R overexpression in podocytes strongly aggravated the renal damage in D-HBP rats and to a less degree also in HBP rats.

2. ExM is a useful tool for the nanoscale evaluation and quantification of the alterations in podocyte FPs architecture by light microscopy. The determined FPs

width strongly correlated with albuminuria, the damage index and the decreases in GFR.

4.1 Hyperglycemia do not induce diabetic nephropathy in SD rats

Previous experiments in our group characterized the effect of STZ diabetes on the kidneys of Sprague Dawley rats. We used this rat line because our transgenic NephAT1R rat was generated on this background. Although the rats developed clinical diabetes early, indicated by increased glucose levels in the plasma and urine, polyuria, and polydipsia, the urinary albumin excretion increased only slightly (7mg/14hr in diabetic rats vs. 0.5 mg/24hr in controls) 7 months after onset of diabetes and no pathohistological alterations in the kidney developed. Besides hyperfiltration, increased albumin excretion is one of the first clinical sign for DN and points to the weakness of the filtration barrier. Next, we studied the ZSF1 ob/ob rat which spontaneously develops diabetes, including a metabolic syndrome[117]. In contrast to the STZ-diabetic rats, seven months after the onset of hyperglycemia, hypertension and obesity the ZSF1 rats exhibited severe renal injury, including prominent glomerulosclerosis, tubular atrophy and tubulo-interstitial fibrosis and severe albuminuria. Thus, DN in rats requires further factors interacting with hyperglycemia.

4.2 Hypertension and AT1R overexpression in podocytes accelerate rapid progression of renal failure in STZ-diabetic rats

In order to dissect the synergistic actions of hyperglycemia with hypertension from those of hypertension alone, we used the TGRCyp1a1Ren2 rat[97]. This rat carries a transgenic renin gene driven by the P4501a1 promoter, such that dietary I3C supplementation dose-dependently induces transgene expression resulting in controlled hypertension within 24 h. In order to specify the role of AT1R signaling in podocytes under these pathological conditions, we crossed the TGRCyp1a1Ren2 rat with heterozygous Neph-hAT1R rats (TGR)[39] to generate CRTL, HBP and D-HBP groups with TGR and Wild as subgroups in each. We induced diabetes by STZ-injections followed by I3C induced HBP two weeks later. This approach enabled us to

study the effects of HBP and synergistic D-HBP on the kidney in the presence (TGR) and absence (Wild) of AT1R overexpression under identical conditions and on the same genetic background.

The TGRNeph-hAT1R rat model was previously developed in our lab[39]. The AT1R overexpression in podocytes causes FSGS and renal failure in old rats. That's why it is important to know that throughout the experimental period the TGR-CTRL did not differ from the Wild-CTRL and exhibited normal values in all the parameters we tested including blood glucose, blood pressure, renal function, GFR, albumin excretion, clinical parameters in the plasma, kidney weight and glomerular tuft size. In addition, kidney morphology was normal in both groups. Moreover, HBP and D-HBP groups of both genotypes had comparable blood pressure and blood glucose levels. Thus, the AT1R in TGRs did not influence these parameters and the observed differences between diseased TGR and Wild groups directly result from the interaction of AT1R overexpression in podocytes and the disease conditions.

While STZ-diabetes by itself required 7 months of diabetes to induce only the earliest signs of DN - a mild micro-albuminuria of 8 mg/day without structural changes in the kidney, within 8 weeks hyperglycemia and hypertension synergistically caused renal damages including severe albuminuria (~200 mg/24hr), a significant drop in GFR, significant glomerular hypertrophy and glomerular lesions. In contrast, hypertension alone only had minor effects on the kidney. These data correlate well with the findings of the Mullins group who found a human DN like phenotype in rats 7 months after combined induction of diabetes and hypertension[98].

AT1R overexpression in podocytes remarkably aggravated the disease progression in the D-HBP and to a less extend also in the HBP group. Within 8 weeks of diabetes, only the D-HBP-TGRs showed the advanced stages of DN with widespread glomerular sclerosis and a remarkable drop in GFR. They developed all the typical features of DN, including GBM thickening, mesangial expansion and FSGS. 70% of the glomeruli were damaged and 26.1% of glomeruli were classified into the 2 most severe categories of the damage index. In comparison, in D-HBP WT, only 26% of the glomeruli were damaged, and only 3.3% of glomeruli were classified into the 2

most severe categories. This points to a crucial role of the AT1R signaling in podocytes in DN but also indicates that the beneficial effects of RAS blocker in DN not only results from improved hemodynamic actions but also from interference with the AT1R signaling in podocytes.

The mechanisms of AT1R signaling were intensively studied in this model and *in vitro*. The Gq coupled AT1R increase Rac1 expression[41, 43], which leads to increased production of ROS[43] and to vesicular insertion of the transient receptor canonical-5 TRPC5 ion channel into the podocyte plasma membrane, making them available for activation by the AT1R. Consequently, transient Ca2+ influx into podocytes increases and further activates rac1, feeding a circuit that promotes podocytes cytoskeletal remodeling[42]. Excessive ROS production is accompanied by an AT1R induced down-regulation of the anti-oxidative protein Prdx2 to maintain an oxidative environment in podocytes[122]. The Prdx family of peroxidases protects cells against oxidative damage. This AT1R-rac1-ROS pathway causes, via ERM proteins the phosphorylation of F-actin, cytoskeletal reorganization with stress fiber attenuation and a switch to a migratory phenotype[43] including α-actinin-4 down-regulation. Cross-linking of actin filaments bundles by α-actinin-4 is necessary for normal podocyte adhesion[123]. Notably, □-actinin-4 interacts with integrin and enhances podocyte-matrix interactions, preventing podocyte detachment. Thus, mutations in α-actinin-4 cause albuminuria[124]. The actin cytoskeleton network in podocyte FPs is linked to the GBM and slit membrane via different adapter molecules. Consequently, sustained AT1R signaling in the podocytes of TGRNeph-hAT1R rats may cause major changes to the F-actin cytoskeleton in FPs, impairs podocyte stability and podocyte adhesion and make them prone to detaching more easily from the GBM.

This scenario might be amplified due to the direct deleterious effects of high glucose levels on podocytes. Glucose activates intracellular Ang II production in podocytes, increases ROS formation[37] and the expression of another Ca^{2+} channel, TRPC6, via AT1R signaling[125]. Furthermore, both high glucose and Ang II weaken the density of the GFB by decreasing the expression of proteins involved in the SD signaling complex, including nephrin, CD2AP and podocin, as well as synaptopodin, an actin-associated protein that plays a role in podocyte shape and motility.

In both, HBP and D-HBP rats, the glomeruli and podocytes were challenged by comparable tension stress due to HBP and by an activated RAS due to transgenic renin production. Additionally, in the D-HBP model, the podocytes are also stressed by increased glucose levels, increased ROS[126] and increased shear stress due to the hyperfiltration which occurs in early diabetes. Increased glucose, ROS and shear stress alone is not sufficient to induce any pathohistological alteration as we have demonstrated. Kriz's group studied the effects of increased perfusion pressure on glomeruli[127]. He found that the GBM is the dominant structure generating wall tension to counteract expansion when pressure rises. He concluded that podocytes seem to be protected against the tensile stress by the limited distensibility of the GBM and their firm attachment to it. The mechanistically stability of the capillary network is largely maintained by the mesangial cells[1]. According to the findings of Kriz et al., increased perfusion pressure locally leads to a breakdown of the mesangial cell-GBM connection causing a displacement of the capillaries toward and into the urinary orifice, exposing the podocytes to the shear stress of the filtrate. In other situations, the capillaries and associated podocytes shifted radially, coming into contact with the parietal epithelium and starting to form tuft adhesions[14]. The second challenge is the activated RAS in the HBP and D-HBP group. Mesangial cells carry a high density of AT1Rs[128]. Overstimulation of these AT1Rs leads to proliferation and hypertrophy of mesangial cells and increased production of matrix components that might contribute to mesangial expansion[42, 129]. We observed in both the HBP and the D-HBP group, mesangial expansion and large, irregular capillaries as consequence of mesangial failure. Under these conditions, increased shear stress, due to hyperperfusion in the D-HBP group, seems to promote the detachment of podocytes from the GBM. Kriz et al. describes such podocytes as bottle shaped. A further challenge in the D-HBP rats is the thickened GBM as consequence of overproduction or reduced degradation of GBM material. Accumulation of worn-out GBM material substantially contributes to mesangial expansion in patients with DN[14] and aggravates the above-described scenario. Electron microscopy revealed in the D-HBP-TGR rats bottle-shaped and detached podocytes and worn out GBM material in the mesangium, supporting the findings of Kriz in human DN patients[130] and demonstrating the similarities between our rat model and human DN.

Thus, the aggravation of the disease progression in the D-HBP-TGR might result from the reduced resistance of the AT1R overexpressing podocytes to detaching from the GBM.

In conclusion, the concerted action of an activated RAS with hemodynamic and hyperglycemic effects on the glomerulus is required to induce rapid glomerular injuries in diabetic rats. AT1R signaling in podocyte accelerates and amplifies glomerular injuries in this context, pointing to a crucial role of podocytes in the progression of DN.

4.3 ExM enables to image and quantify nanoscale pathological changes in podocyte foot process morphology in diabetic nephropathy and hypertension

Podocytes react with FPE to cellular stressors challenging their adhesion to the GBM. Thus, podocyte FPE is an important diagnostic marker for DN. FPE is a result of retraction, widening and shortening of the FPs and seems to be a protective response to prevent podocyte detachment. In the complete stage of FPE, podocytes broadly attach to the GBM by their cell bodies, having lost all of their processes. While the early stages of FPE might be reversible, podocytes detach if FPE reaches a point of no return. Adjacent FPs are bridged by the SD, with nephrin as a major constituent. The intracellular domain of nephrin binds to podocin in the SD insertion site. The fine structure of the GFB is in the nanoscale range and was previously only resolvable by using electron microscopy or the recently developed super-resolution microscopy. The SD functions as a molecular size filter and has a size of 30 nm. The normal width of individual FPs is roughly 250 nm[127].

In the present work, we used the recently developed method ExM[111] which physically expands the kidney in a swellable gel to image the podocyte FPs. We labeled the secondary podocyte FPs and the SD by staining for podocin and nephrin, respectively. The advantage of ExM over EM is that it allows the study of thick tissue samples (500 nm) for a full volumetric 3D perspective of the whole glomeruli down to the podocyte FPs using confocal microscopy. A comparison between confocal

microscopy in expanded tissue and SIM from paraffin sections of the same kidney show similar results for both methods which highly correlated. A major concern was whether samples expanded uniformly. This was proven by calculating the ratio between the longitudinal and transverse glomerular diameter in non-expanded frozen sections and expanded kidney slices. This ratio was similar in all rats, independent of whether non-expanded or expanded tissue was used and whether the glomerular tuft was hypertrophied or not, as in the D-HBP and CTRL groups respectively, showing that the expansion was isotropic. Moreover, we verified the hypertrophic growth of the glomerular tuft size in HBP and D-HBP in both non-expanded and expanded tissue. The expansion factor for the maximal transverse and maximal longitudinal glomerular diameter was similar in all groups (r=0.97).

Interestingly, HBP rats of both genotypes exhibited shortened and widened FPs that fully covered the glomerular tuft in a regular and well-organized manner, although these rats exhibited albuminuria, with 20-50-fold increased albumin excretion compared to controls. D-HBP-TGR rats, however, showed large glomerular areas with disorganized and flattened FPs indicating FPE, which was confirmed by EM in the group of Prof. Kriz, Neuroanatomy, Medical Faculty Mannheim. Moreover, many glomeruli contained regions in the glomeruli that have lost podocin staining indicating the presence of naked or sclerotic glomerular tuft areas. The FP widths in CTRL (250 nm) were in good agreement with previously published data[111]. The FP width determined by EM was somewhat lower (150 nm), which is comprehensible since the pretreatment of the tissue for EM shrinks the tissue. FP widths moderately increased in the HBP group but strongly increased in the D-HBP group by more than two-fold in the D-HBP-TGR group specifically. The average FP widths correlated well with the functional and morphological alterations in the kidney of the different groups. The D-HBP-TGR group exhibited the highest FP widths and most severe renal damage as evaluated by AZAN staining, semithin sections and by electron microscopy. In addition, the group of Prof. Nicole Endlich in Greifswald (University Greifswald, NIKOPA) evaluated the FPs in our rat kidneys using SIM microscopy. We determined the FP widths as the distance between two podocin stains. In contrast to us, NIKOPA used a program PEMP to calculate the nephrin stained density per area to evaluate the filtration slit density[131]. Of note, these results highly inverse correlated with our data (r=0.975), proving the capacity of ExM to reliably quantify the altered

morphology of FPs. Widening and shortening of the FPs in conditions of HBP seem to be an adaptive response of podocytes, which might be reversible and probably does not result in podocyte loss. An additional shear stressed caused by hyperfiltration due to diabetes might cause massive detachment of podocytes, promoted by increased AT1R signaling. In summary, this work demonstrates that renal damage in diabetic rats requires the synergistic action of HBP with hyperglycemia and that AT1R signaling in podocytes strongly aggravates the disease progression. Moreover, we demonstrate that ExM is a suitable method to quantify nanoscale alterations in the podocyte FP structure during different glomerular diseases.

5   SUMMARY (ABSTRACT)

DN is a leading cause of end-stage renal disease and affects 30% of diabetic patients[116, 120]. Thus, 70% of diabetic patients are protected from DN, indicating that, besides hyperglycemia, DN requires additional factors to develop. Despite major advances in our understanding of the disease, the molecular pathogenesis of DN remains far from clear. A major barrier to further progress is the lack of a suitable diabetic animal model that mimics human DN. Existing diabetic models mostly exhibit only the earliest features of human DN[121]. A hallmark of DN is glomerulosclerosis. Leakage of the filtration barrier is one of the first clinical signs in DN and is associated with FPE and podocyte detachment. To diagnose these alterations required electron microscopy, since the fine structure of the GFB is in the nanoscale range. The currently first-line therapy is blocking Ang II.

The following study target the hypothesis that excess AT1R signaling in podocytes aggravates DN, which might be induced by combined induction of STZ-diabetes and hypertension in rats. Thus, the present study had two major aims. First, to develop suitable rat models allowing to assess the role of hypertension for the development of DN and to specify the role of Ang II signaling in podocytes in this context. Second, to establish and to verify an ExM method, which enable the visualization and quantification of alterations in podocyte FP structure in the disease models. To this end we crossed the TGRCyp1a1Ren2 developing hypertension after food supplementation with I3C with the TGRNeph-hAT1R rats overexpressing the AT1R specifically in podocytes. In part of rats, STZ-diabetes and high blood pressure were induced alone (HBP) or in combination (D-HBP). Renal function (GFR, albuminuria), blood pressure, clinical parameter in urine and blood were monitored. Pathohistological changes in glomeruli were determined by light microscopy, super-resolution light microscopy and electron microscopy. Further we developed and validated a method to visualize nanoscale alterations in podocyte FPs and FPE by confocal microscopy using tissue expansion. The obtained results were verified by SIM technology on paraffin embedded tissue.

Our data demonstrate that the synergistic action of diabetes and HBP is required to induce rapid renal damage in diabetic rats since neither HBP alone nor STZ-diabetes alone was able to induce a comparable deterioration in renal function and morphology. AT1R overexpression in podocytes strongly accelerates the disease progression, specifically in D-HBP conditions.

Further, this thesis revealed that Expansion microscopy is a useful tool to diagnose FPE in DN and provides similar results concerning the FP architecture as SIM technology. The podocyte FP widths strongly correlate with increases in albuminuria and the damage index and decreases in GFR. Although HBP induced a certain albuminuria, the FP architecture is preserved, however, FP widths are increased, and the FP lengths are shortened. AT1R signaling in podocytes strongly accelerated FPE in DN probably by increasing their sensitivity to be detached in stress conditions.

In summary, this work demonstrates that renal damage in diabetic rats requires the synergistic action of HBP with hyperglycemia and that AT1R signaling in podocytes strongly aggravates the disease progression. Moreover, we demonstrate that ExM is a suitable method to quantify nanoscale alterations in the podocyte FP structure during different glomerular diseases.

6   REFERENCES

1. Kriz, W: Maintenance and Breakdown of Glomerular Tuft Architecture. *J Am Soc Nephrol,* 29**:** 1075-1077, 2018.
2. Reiser, J, Gupta, V, Kistler, AD: Toward the development of podocyte-specific drugs. *Kidney International,* 77**:** 662-668, 2010.
3. Kriz, W, Lemley, KV: Potential relevance of shear stress for slit diaphragm and podocyte function. *Kidney Int,* 91**:** 1283-1286, 2017.
4. Peti-Peterdi, J, Kidokoro, K, Riquier-Brison, A: Novel in vivo techniques to visualize kidney anatomy and function. *Kidney International,* 88**:** 44-51, 2015.
5. Ilatovskaya, DV, Palygin, O, Levchenko, V, Endres, BT, Staruschenko, A: The Role of Angiotensin II in Glomerular Volume Dynamics and Podocyte Calcium Handling. *Sci Rep,* 7**:** 299, 2017.
6. Parr, SK, Matheny, ME, Abdel-Kader, K, Greevy, RA, Jr., Bian, A, Fly, J, Chen, G, Speroff, T, Hung, AM, Ikizler, TA, Siew, ED: Acute kidney injury is a risk factor for subsequent proteinuria. *Kidney International,* 93**:** 460-469, 2018.
7. Fioretto, P, Mauer, M: Histopathology of diabetic nephropathy. *Semin Nephrol,* 27**:** 195-207, 2007.
8. Frank, LL: Diabetes mellitus in the texts of old Hindu medicine (Charaka, Susruta, Vagbhata). *The American journal of gastroenterology,* 27**:** 76-95, 1957.
9. Mujais, SK: Nephrologic beginnings: the kidney in the age of Ibn Sina (980-1037 AD). *Am J Nephrol,* 7**:** 133-136, 1987.
10. Wetmore, JB, Liu, J, Li, S, Hu, Y, Peng, Y, Gilbertson, DT, Collins, AJ: The Healthy People 2020 Objectives for Kidney Disease: How Far Have We Come, and Where Do We Need to Go? *Clinical journal of the American Society of Nephrology : CJASN,* 12**:** 200-209, 2017.
11. Schwarz, U, Ritz, E: Glomerulonephritis and progression--Friedrich Theodor von Frerichs, a forgotten pioneer. *Nephrology, dialysis, transplantation : official publication of the European Dialysis and Transplant Association - European Renal Association,* 12**:** 2776-2778, 1997.
12. Woodyatt, RT: Bernhard Naunyn. *Diabetes,* 1**:** 240-241, 1952.
13. Ritz, E: Limitations and future treatment options in type 2 diabetes with renal impairment. *Diabetes Care,* 34 Suppl 2**:** S330-S334, 2011.
14. Kriz, W, Lowen, J, Federico, G, van den Born, J, Grone, E, Grone, HJ: Accumulation of worn-out GBM material substantially contributes to mesangial matrix expansion in diabetic nephropathy. *Am J Physiol Renal Physiol,* 312**:** F1101-f1111, 2017.
15. Kriz, W, Lemley, KV: Mechanical challenges to the glomerular filtration barrier: adaptations and pathway to sclerosis. *Pediatric nephrology (Berlin, Germany),* 32**:** 405-417, 2017.
16. Petermann, AT, Pippin, J, Krofft, R, Blonski, M, Griffin, S, Durvasula, R, Shankland, SJ: Viable podocytes detach in experimental diabetic nephropathy: potential mechanism underlying glomerulosclerosis. *Nephron Exp Nephrol,* 98**:** e114-123, 2004.
17. Kimmelstiel, P, Wilson, C: Intercapillary Lesions in the Glomeruli of the Kidney. *The American journal of pathology,* 12**:** 83-98.87, 1936.
18. Kimmelstiel, P, Wilson, C: Intercapillary Lesions in the Glomeruli of the Kidney. *Am J Pathol,* 12**:** 83-98.87, 1936.
19. Bjorck, S, Mulec, H, Johnsen, SA, Nyberg, G, Aurell, M: Contrasting effects of enalapril and metoprolol on proteinuria in diabetic nephropathy. *BMJ (Clinical research ed),* 300**:** 904-907, 1990.
20. Mogensen, CE: Progression of nephropathy in long-term diabetics with proteinuria and effect of initial anti-hypertensive treatment. *Scandinavian journal of clinical and laboratory investigation,* 36**:** 383-388, 1976.
21. Mogensen, CE: Renal function changes in diabetes. *Diabetes,* 25**:** 872-879, 1976.

22. Parving, HH, Andersen, AR, Smidt, UM, Svendsen, PA: Early aggressive antihypertensive treatment reduces rate of decline in kidney function in diabetic nephropathy. *Lancet (London, England),* 1**:** 1175-1179, 1983.

23. Bjorck, S, Herlitz, H, Nyberg, G, Granerus, G, Aurell, M: Effect of captopril on renal hemodynamics in the treatment of resistant renal hypertension. *Hypertension (Dallas, Tex : 1979),* 5**:** Iii152-153, 1983.

24. Schmieder, RE: End organ damage in hypertension. *Dtsch Arztebl Int,* 107**:** 866-873, 2010.

25. Mensah, GA: Hypertension and Target Organ Damage: Don't Believe Everything You Think! *Ethn Dis,* 26**:** 275-278, 2016.

26. Re, RN: Obesity-related hypertension. *Ochsner J,* 9**:** 133-136, 2009.

27. Cheung, BMY, Li, C: Diabetes and hypertension: is there a common metabolic pathway? *Curr Atheroscler Rep,* 14**:** 160-166, 2012.

28. Ohishi, M: Hypertension with diabetes mellitus: physiology and pathology. *Hypertension Research,* 41**:** 389-393, 2018.

29. Pourghasem, M, Shafi, H, Babazadeh, Z: Histological changes of kidney in diabetic nephropathy. *Caspian J Intern Med,* 6**:** 120-127, 2015.

30. Tervaert, TWC, Mooyaart, AL, Amann, K, Cohen, AH, Cook, HT, Drachenberg, CB, Ferrario, F, Fogo, AB, Haas, M, de Heer, E, Joh, K, Noël, LH, Radhakrishnan, J, Seshan, SV, Bajema, IM, Bruijn, JA: Pathologic Classification of Diabetic Nephropathy. *Journal of the American Society of Nephrology,* 21**:** 556-563, 2010.

31. Mise, K, Ueno, T, Hoshino, J, Hazue, R, Sumida, K, Yamanouchi, M, Hayami, N, Suwabe, T, Hiramatsu, R, Hasegawa, E, Sawa, N, Fujii, T, Hara, S, Wada, J, Makino, H, Takaichi, K, Ohashi, K, Ubara, Y: Nodular lesions in diabetic nephropathy: Collagen staining and renal prognosis. *Diabetes Res Clin Pract,* 127**:** 187-197, 2017.

32. Karnik, SS, Unal, H, Kemp, JR, Tirupula, KC, Eguchi, S, Vanderheyden, PM, Thomas, WG: International Union of Basic and Clinical Pharmacology. XCIX. Angiotensin Receptors: Interpreters of Pathophysiological Angiotensinergic Stimuli [corrected]. *Pharmacol Rev,* 67**:** 754-819, 2015.

33. Forrester, SJ, Booz, GW, Sigmund, CD, Coffman, TM, Kawai, T, Rizzo, V, Scalia, R, Eguchi, S: Angiotensin II Signal Transduction: An Update on Mechanisms of Physiology and Pathophysiology. *Physiological reviews,* 98**:** 1627-1738, 2018.

34. Li, XC, Zhu, D, Zheng, X, Zhang, J, Zhuo, JL: Intratubular and intracellular renin-angiotensin system in the kidney: a unifying perspective in blood pressure control. *Clinical science (London, England : 1979),* 132**:** 1383-1401, 2018.

35. Micakovic, T, Papagiannarou, S, Clark, E, Kuzay, Y, Abramovic, K, Peters, J, Sticht, C, Volk, N, Fleming, T, Nawroth, P, Hammes, HP, Alenina, N, Grone, HJ, Hoffmann, SC: The angiotensin II type 2 receptors protect renal tubule mitochondria in early stages of diabetes mellitus. *Kidney Int,* 94**:** 937-950, 2018.

36. Vidotti, DB, Casarini, DE, Cristovam, PC, Leite, CA, Schor, N, Boim, MA: High glucose concentration stimulates intracellular renin activity and angiotensin II generation in rat mesangial cells. *Am J Physiol Renal Physiol,* 286**:** F1039-1045, 2004.

37. Durvasula, RV, Shankland, SJ: Activation of a local renin angiotensin system in podocytes by glucose. *Am J Physiol Renal Physiol,* 294**:** F830-839, 2008.

38. Seikaly, MG, Arant, BS, Jr., Seney, FD, Jr.: Endogenous angiotensin concentrations in specific intrarenal fluid compartments of the rat. *J Clin Invest,* 86**:** 1352-1357, 1990.

39. Hoffmann, S, Podlich, D, Hähnel, B, Kriz, W, Gretz, N: Angiotensin II Type 1 Receptor Overexpression in Podocytes Induces Glomerulosclerosis in Transgenic Rats. *Journal of the American Society of Nephrology,* 15**:** 1475-1487, 2004.

40. Zhou, Y, Castonguay, P, Sidhom, EH, Clark, AR, Dvela-Levitt, M, Kim, S, Sieber, J, Wieder, N, Jung, JY, Andreeva, S, Reichardt, J, Dubois, F, Hoffmann, SC, Basgen, JM, Montesinos, MS, Weins, A, Johnson, AC, Lander, ES, Garrett, MR, Hopkins, CR, Greka, A: A small-molecule inhibitor of

TRPC5 ion channels suppresses progressive kidney disease in animal models. *Science (New York, NY),* 358**:** 1332-1336, 2017.

41. Buvall, L, Wallentin, H, Sieber, J, Andreeva, S, Choi, HY, Mundel, P, Greka, A: Synaptopodin Is a Coincidence Detector of Tyrosine versus Serine/Threonine Phosphorylation for the Modulation of Rho Protein Crosstalk in Podocytes. *Journal of the American Society of Nephrology,* 28: 837, 2017.

42. Schaldecker, T, Kim, S, Tarabanis, C, Tian, D, Hakroush, S, Castonguay, P, Ahn, W, Wallentin, H, Heid, H, Hopkins, CR, Lindsley, CW, Riccio, A, Buvall, L, Weins, A, Greka, A: Inhibition of the TRPC5 ion channel protects the kidney filter. *J Clin Invest,* 123**:** 5298-5309, 2013.

43. Hsu, HH, Hoffmann, S, Endlich, N, Velic, A, Schwab, A, Weide, T, Schlatter, E, Pavenstadt, H: Mechanisms of angiotensin II signaling on cytoskeleton of podocytes. *Journal of molecular medicine (Berlin, Germany),* 86**:** 1379-1394, 2008.

44. Becker, GJ, Hewitson, TD: Animal models of chronic kidney disease: useful but not perfect. *Nephrology Dialysis Transplantation,* 28**:** 2432-2438, 2013.

45. Mordes, JP, Bortell, R, Blankenhorn, EP, Rossini, AA, Greiner, DL: Rat Models of Type 1 Diabetes: Genetics, Environment, and Autoimmunity. *ILAR Journal,* 45**:** 278-291, 2004.

46. Genetic variation within and between lines of diabetes-prone and non-diabetes-prone BB rats; allele distribution of 8 protein markers. *Laboratory Animals,* 25**:** 207-211, 1991.

47. Mathieu, C, Kuttler, B, Waer, M, Bouillon, R, Hahn, HJ: Spontaneous reestablishment of self-tolerance in BB/Pfd rats. *Transplantation,* 58**:** 349-354, 1994.

48. Lenzen, S, Tiedge, M, Elsner, M, Lortz, S, Weiss, H, Jorns, A, Kloppel, G, Wedekind, D, Prokop, CM, Hedrich, HJ: The LEW.1AR1/Ztm-iddm rat: a new model of spontaneous insulin-dependent diabetes mellitus. *Diabetologia,* 44**:** 1189-1196, 2001.

49. Jorns, A, Gunther, A, Hedrich, HJ, Wedekind, D, Tiedge, M, Lenzen, S: Immune cell infiltration, cytokine expression, and beta-cell apoptosis during the development of type 1 diabetes in the spontaneously diabetic LEW.1AR1/Ztm-iddm rat. *Diabetes,* 54**:** 2041-2052, 2005.

50. Hanafusa, T, Miyagawa, J-i, Nakajima, H, Tomita, K, Kuwajima, M, Matsuzawa, Y, Tarui, S: The NOD mouse. *Diabetes Research and Clinical Practice,* 24**:** S307-S311, 1994.

51. Drel, VR, Pacher, P, Stavniichuk, R, Xu, W, Zhang, J, Kuchmerovska, TM, Slusher, B, Obrosova, IG: Poly(ADP-ribose)polymerase inhibition counteracts renal hypertrophy and multiple manifestations of peripheral neuropathy in diabetic Akita mice. *Int J Mol Med,* 28**:** 629-635, 2011.

52. Mathews, CE, Langley, SH, Leiter, EH: New mouse model to study islet transplantation in insulin-dependent diabetes mellitus. *Transplantation,* 73**:** 1333-1336, 2002.

53. Phillips, MS, Liu, Q, Hammond, HA, Dugan, V, Hey, PJ, Caskey, CJ, Hess, JF: Leptin receptor missense mutation in the fatty Zucker rat. *Nature genetics,* 13**:** 18-19, 1996.

54. Goto, Y, Kakizaki, M, Masaki, N: Spontaneous Diabetes Produced by Selective Breeding of Normal Wistar Rats. *Proceedings of the Japan Academy,* 51**:** 80-85, 1975.

55. Ostenson, CG, Efendic, S: Islet gene expression and function in type 2 diabetes; studies in the Goto-Kakizaki rat and humans. *Diabetes, obesity & metabolism,* 9 Suppl 2**:** 180-186, 2007.

56. Xu, ZG, Lanting, L, Vaziri, ND, Li, Z, Sepassi, L, Rodriguez-Iturbe, B, Natarajan, R: Upregulation of angiotensin II type 1 receptor, inflammatory mediators, and enzymes of arachidonate metabolism in obese Zucker rat kidney: reversal by angiotensin II type 1 receptor blockade. *Circulation,* 111**:** 1962-1969, 2005.

57. Kim, S, Soltani-Bejnood, M, Quignard-Boulange, A, Massiera, F, Teboul, M, Ailhaud, G, Kim, JH, Moustaid-Moussa, N, Voy, BH: The adipose renin-angiotensin system modulates systemic markers of insulin sensitivity and activates the intrarenal renin-angiotensin system. *Journal of biomedicine & biotechnology,* 2006**:** 27012, 2006.

58. Rossini, AA, Like, AA, Chick, WL, Appel, MC, Cahill, GF, Jr.: Studies of streptozotocin-induced insulitis and diabetes. *Proceedings of the National Academy of Sciences of the United States of America,* 74**:** 2485-2489, 1977.

59. Lee, TN, Alborn, WE, Knierman, MD, Konrad, RJ: The diabetogenic antibiotic streptozotocin modifies the tryptic digest pattern for peptides of the enzyme O-GlcNAc-selective N-acetyl-beta-d-glucosaminidase that contain amino acid residues essential for enzymatic activity. *Biochemical pharmacology,* 72**:** 710-718, 2006.

60. Vavra, JJ, Deboer, C, Dietz, A, Hanka, LJ, Sokolski, WT: Streptozotocin, a new antibacterial antibiotic. *Antibiotics annual,* 7**:** 230-235, 1959.

61. Murray-Lyon, IM, Eddleston, AL, Williams, R, Brown, M, Hogbin, BM, Bennett, A, Edwards, JC, Taylor, KW: Treatment of multiple-hormone-producing malignant islet-cell tumour with streptozotocin. *Lancet (London, England),* 2**:** 895-898, 1968.

62. RERUP, CC: DRUGS PRODUCING DIABETES THROUGH DAMAGE OF THE INSULIN SECRETING CELLS. *Pharmacological Reviews,* 22**:** 485-518, 1970.

63. Graham, ML, Janecek, JL, Kittredge, JA, Hering, BJ, Schuurman, H-J: The streptozotocin-induced diabetic nude mouse model: differences between animals from different sources. *Comp Med,* 61**:** 356-360, 2011.

64. El-Wakil, HS, Aboushousha, TS, El Haddad, O, Gamil, NB, Mansour, T, El-Said, H: Effect of schistosoma mansoni egg deposition on multiple low doses streptozotocin induced insulin dependent diabetes. *Journal of the Egyptian Society of Parasitology,* 32**:** 987-1002, 2002.

65. Tekula, S, Khurana, A, Anchi, P, Godugu, C: Withaferin-A attenuates multiple low doses of Streptozotocin (MLD-STZ) induced type 1 diabetes. *Biomedicine & pharmacotherapy = Biomedecine & pharmacotherapie,* 106**:** 1428-1440, 2018.

66. Yuan, X, Ni, H, Chen, X, Feng, X, Wu, Q, Chen, J: Identification of therapeutic effect of glucagon-like peptide 1 in the treatment of STZ-induced diabetes mellitus in rats by restoring the balance of intestinal flora. *Journal of cellular biochemistry,* 119**:** 10067-10074, 2018.

67. Hao, L, Li, Q, Zhao, X, Li, Y, Zhang, C: A long noncoding RNA LOC103690121 promotes hippocampus neuronal apoptosis in streptozotocin-induced type 1 diabetes. *Neuroscience letters,* 703**:** 11-18, 2019.

68. Bohuslavova, R, Cerychova, R, Nepomucka, K, Pavlinkova, G: Renal injury is accelerated by global hypoxia-inducible factor 1 alpha deficiency in a mouse model of STZ-induced diabetes. *BMC endocrine disorders,* 17**:** 48, 2017.

69. Chander, PN, Gealekman, O, Brodsky, SV, Elitok, S, Tojo, A, Crabtree, M, Gross, SS, Goligorsky, MS: Nephropathy in Zucker diabetic fat rat is associated with oxidative and nitrosative stress: prevention by chronic therapy with a peroxynitrite scavenger ebselen. *J Am Soc Nephrol,* 15**:** 2391-2403, 2004.

70. Pung, YF, Chilian, WM, Bennett, MR, Figg, N, Kamarulzaman, MH: The JCR:LA-cp rat: a novel rodent model of cystic medial necrosis. *American journal of physiology Heart and circulatory physiology,* 312**:** H541-H545, 2017.

71. van Dijk, CG, Oosterhuis, NR, Xu, YJ, Brandt, M, Paulus, WJ, van Heerebeek, L, Duncker, DJ, Verhaar, MC, Fontoura, D, Lourenco, AP, Leite-Moreira, AF, Falcao-Pires, I, Joles, JA, Cheng, C: Distinct Endothelial Cell Responses in the Heart and Kidney Microvasculature Characterize the Progression of Heart Failure With Preserved Ejection Fraction in the Obese ZSF1 Rat With Cardiorenal Metabolic Syndrome. *Circulation Heart failure,* 9**:** e002760, 2016.

72. Tsuboi, N, Utsunomiya, Y, Koike, K, Kanzaki, G, Hirano, K, Okonogi, H, Miyazaki, Y, Ogura, M, Joh, K, Kawamura, T, Hosoya, T: Factors related to the glomerular size in renal biopsies of chronic kidney disease patients. *Clinical nephrology,* 79**:** 277-284, 2013.

73. Henegar, JR, Bigler, SA, Henegar, LK, Tyagi, SC, Hall, JE: Functional and structural changes in the kidney in the early stages of obesity. *J Am Soc Nephrol,* 12**:** 1211-1217, 2001.

74. Reisin, E, Messerli, FG, Ventura, HO, Frohlich, ED: Renal haemodynamic studies in obesity hypertension. *J Hypertens,* 5**:** 397-400, 1987.

75. Chagnac, A, Weinstein, T, Korzets, A, Ramadan, E, Hirsch, J, Gafter, U: Glomerular hemodynamics in severe obesity. *Am J Physiol Renal Physiol,* 278**:** F817-822, 2000.

76. Tsuboi, N, Okabayashi, Y, Shimizu, A, Yokoo, T: The Renal Pathology of Obesity. *Kidney International Reports,* 2**:** 251-260, 2017.

77. Okamoto, K, Aoki, K: Development of a strain of spontaneously hypertensive rats. *Japanese circulation journal,* 27**:** 282-293, 1963.

78. Kurtz, TW, Morris, RC: Biological variability in Wistar-Kyoto rats. Implications for research with the spontaneously hypertensive rat. *Hypertension (Dallas, Tex : 1979),* 10**:** 127-131, 1987.

79. Nabika, T, Ohara, H, Kato, N, Isomura, M: The stroke-prone spontaneously hypertensive rat: still a useful model for post-GWAS genetic studies? *Hypertension Research,* 35**:** 477-484, 2012.

80. Inoue, BH, Arruda-Junior, DF, Campos, LC, Barreto, AL, Rodrigues, MV, Krieger, JE, Girardi, AC: Progression of microalbuminuria in SHR is associated with lower expression of critical components of the apical endocytic machinery in the renal proximal tubule. *Am J Physiol Renal Physiol,* 305**:** F216-226, 2013.

81. Schulz, A, Schutten-Faber, S, van Es, N, Unland, J, Schulte, L, Kossmehl, P, de Heer, E, Kreutz, R: Induction of albuminuria and kidney damage in SHR by transfer of chromosome 8 from Munich Wistar Fromter rats. *Physiological genomics,* 44**:** 110-116, 2012.

82. Bank, N, Klose, R, Aynedjian, HS, Nguyen, D, Sablay, LB: Evidence against increased glomerular pressure initiating diabetic nephropathy. *Kidney Int,* 31**:** 898-905, 1987.

83. Cooper, ME, Allen, TJ, Jerums, G, Doyle, AE: Accelerated progression of diabetic nephropathy in the spontaneously hypertensive streptozotocin diabetic rat. *Clin Exp Pharmacol Physiol,* 13**:** 655-662, 1986.

84. Ben-Ishay, D, Zamir, N, Feurstein, G, Kobrin, I, Le Quan-Bui, KH, Devynck, MA: Distinguishing Traits in the Sabra Hypertension-prone (SBH) and Hypertension-resistant (SBN) Rats. *Clinical and Experimental Hypertension,* 3**:** 737-747, 1981.

85. Yagil, C, Katni, G, Rubattu, S, Stolpe, C, Kreutz, R, Lindpaintner, K, Ganten, D, Ben-Ishay, D, Yagil, Y: Development, genotype and phenotype of a new colony of the Sabra hypertension prone (SBH/y) and resistant (SBN/y) rat model of slat sensitivity and resistance. *J Hypertens,* 14**:** 1175-1182, 1996.

86. Joe, B: Dr Lewis Kitchener Dahl, the Dahl rats, and the "inconvenient truth" about the genetics of hypertension. *Hypertension (Dallas, Tex : 1979),* 65**:** 963-969, 2015.

87. Tschopp, TB, Baumgartner, HR: Defective platelet adhesion and aggregation on subendothelium exposed in vivo or in vitro to flowing blood of fawn-hooded rats and storage pool disease. *Thrombosis and haemostasis,* 38**:** 620-629, 1977.

88. Dupont, J, Dupont, JC, Froment, A, Milon, H, Vincent, M: Selection of three strains of rats with spontaneously different levels of blood pressure. *Biomedicine / [publiee pour l'AAICIG],* 19**:** 36-41, 1973.

89. Vincent, M, Dupont, J, Sassard, J: Plasma renin activity as a function of age in two new strains of spontaneously hypertensive and normotensive rats. *Clinical science and molecular medicine,* 50**:** 103-107, 1976.

90. Bianchi, G, Fox, U, Imbasciati, E: The development of a new strain of spontaneously hypertensive rats. *Life Sciences,* 14**:** 339-347, 1974.

91. Lu, H, Howatt, DA, Balakrishnan, A, Moorleghen, JJ, Rateri, DL, Cassis, LA, Daugherty, A: Subcutaneous Angiotensin II Infusion using Osmotic Pumps Induces Aortic Aneurysms in Mice. *J Vis Exp***:** 53191, 2015.

92. Cassis, LA, Gupte, M, Thayer, S, Zhang, X, Charnigo, R, Howatt, DA, Rateri, DL, Daugherty, A: ANG II infusion promotes abdominal aortic aneurysms independent of increased blood pressure in hypercholesterolemic mice. *American journal of physiology Heart and circulatory physiology,* 296**:** H1660-1665, 2009.

93. Kuroki, MT, Fink, GD, Osborn, JW: Comparison of arterial pressure and plasma ANG II responses to three methods of subcutaneous ANG II administration. *American journal of physiology Heart and circulatory physiology,* 307**:** H670-H679, 2014.

94. Mullins, JJ, Peters, J, Ganten, D: Fulminant hypertension in transgenic rats harbouring the mouse Ren-2 gene. *Nature,* 344**:** 541-544, 1990.

95. Kelly, DJ, Wilkinson-Berka, JL, Allen, TJ, Cooper, ME, Skinner, SL: A new model of diabetic nephropathy with progressive renal impairment in the transgenic (mRen-2)27 rat (TGR). *Kidney Int,* 54**:** 343-352, 1998.

96. Bachmann, S, Peters, J, Engler, E, Ganten, D, Mullins, J: Transgenic rats carrying the mouse renin gene--morphological characterization of a low-renin hypertension model. *Kidney Int,* 41**:** 24-36, 1992.

97. Kantachuvesiri, S, Fleming, S, Peters, J, Peters, B, Brooker, G, Lammie, AG, McGrath, I, Kotelevtsev, Y, Mullins, JJ: Controlled hypertension, a transgenic toggle switch reveals differential mechanisms underlying vascular disease. *The Journal of biological chemistry,* 276**:** 36727-36733, 2001.

98. Conway, BR, Rennie, J, Bailey, MA, Dunbar, DR, Manning, JR, Bellamy, CO, Hughes, J, Mullins, JJ: Hyperglycemia and renin-dependent hypertension synergize to model diabetic nephropathy. *J Am Soc Nephrol,* 23**:** 405-411, 2012.

99. Alsaad, KO, Herzenberg, AM: Distinguishing diabetic nephropathy from other causes of glomerulosclerosis: an update. *J Clin Pathol,* 60**:** 18-26, 2007.

100. Maeda, K, Kikuchi, S, Miura, N, Suzuki, K, Kitagawa, W, Morita, H, Banno, S, Imai, H: Glomerular tip adhesions predict the progression of IgA nephropathy. *BMC nephrology,* 14**:** 272, 2013.

101. Stokes, MB, Valeri, AM, Herlitz, L, Khan, AM, Siegel, DS, Markowitz, GS, D'Agati, VD: Light Chain Proximal Tubulopathy: Clinical and Pathologic Characteristics in the Modern Treatment Era. *Journal of the American Society of Nephrology : JASN,* 27**:** 1555-1565, 2016.

102. Randles, MJ, Collinson, S, Starborg, T, Mironov, A, Krendel, M, Königshausen, E, Sellin, L, Roberts, ISD, Kadler, KE, Miner, JH, Lennon, R: Three-dimensional electron microscopy reveals the evolution of glomerular barrier injury. *Scientific reports,* 6**:** 35068-35068, 2016.

103. Conti, S, Perico, N, Novelli, R, Carrara, C, Benigni, A, Remuzzi, G: Early and late scanning electron microscopy findings in diabetic kidney disease. *Scientific Reports,* 8**:** 4909, 2018.

104. Pullman, JM: New Views of the Glomerulus: Advanced Microscopy for Advanced Diagnosis. *Frontiers in medicine,* 6**:** 37-37, 2019.

105. Artelt, N, Siegerist, F, Ritter, AM, Grisk, O, Schlüter, R, Endlich, K, Endlich, N: Comparative Analysis of Podocyte Foot Process Morphology in Three Species by 3D Super-Resolution Microscopy. *Frontiers in Medicine,* 5, 2018.

106. Siegerist, F, Endlich, K, Endlich, N: Novel Microscopic Techniques for Podocyte Research. *Frontiers in endocrinology,* 9**:** 379, 2018.

107. Chen, F, Tillberg, PW, Boyden, ES: Optical imaging. Expansion microscopy. *Science (New York, NY),* 347**:** 543-548, 2015.

108. Asano, SM, Gao, R, Wassie, AT, Tillberg, PW, Chen, F, Boyden, ES: Expansion Microscopy: Protocols for Imaging Proteins and RNA in Cells and Tissues. *Curr Protoc Cell Biol,* 80**:** e56, 2018.

109. Gao, R, Asano, SM, Boyden, ES: Q&A: Expansion microscopy. *BMC biology,* 15**:** 50, 2017.

110. Chozinski, TJ, Halpern, AR, Okawa, H, Kim, H-J, Tremel, GJ, Wong, ROL, Vaughan, JC: Expansion microscopy with conventional antibodies and fluorescent proteins. *Nature Methods,* 13**:** 485-488, 2016.

111. Unnersjo-Jess, D, Scott, L, Sevilla, SZ, Patrakka, J, Blom, H, Brismar, H: Confocal super-resolution imaging of the glomerular filtration barrier enabled by tissue expansion. *Kidney Int,* 93**:** 1008-1013, 2018.

112. Zhang, YS, Chang, J-B, Alvarez, MM, Trujillo-de Santiago, G, Aleman, J, Batzaya, B, Krishnadoss, V, Ramanujam, AA, Kazemzadeh-Narbat, M, Chen, F, Tillberg, PW, Dokmeci, MR, Boyden, ES, Khademhosseini, A: Hybrid Microscopy: Enabling Inexpensive High-Performance Imaging through Combined Physical and Optical Magnifications. *Scientific Reports,* 6**:** 22691, 2016.

113. Chozinski, TJ, Mao, C, Halpern, AR, Pippin, JW, Shankland, SJ, Alpers, CE, Najafian, B, Vaughan, JC: Volumetric, Nanoscale Optical Imaging of Mouse and Human Kidney via Expansion Microscopy. *Scientific Reports,* 8**:** 10396, 2018.

114. Chung, K, Wallace, J, Kim, SY, Kalyanasundaram, S, Andalman, AS, Davidson, TJ, Mirzabekov, JJ, Zalocusky, KA, Mattis, J, Denisin, AK, Pak, S, Bernstein, H, Ramakrishnan, C, Grosenick, L, Gradinaru, V, Deisseroth, K: Structural and molecular interrogation of intact biological systems. *Nature,* 497**:** 332-337, 2013.

115. Alicic, RZ, Rooney, MT, Tuttle, KR: Diabetic Kidney Disease. *Challenges, Progress, and Possibilities,* 12**:** 2032-2045, 2017.

116. Shahbazian, H, Rezaii, I: Diabetic kidney disease; review of the current knowledge. *J Renal Inj Prev,* 2**:** 73-80, 2013.

117. Pung, YF, Chilian, WM, Bennett, MR, Figg, N, Kamarulzaman, MH: The JCR:LA-cp rat: a novel rodent model of cystic medial necrosis. *American journal of physiology Heart and circulatory physiology,* 312**:** H541-545, 2017.

118. Sotocinal, SG, Sorge, RE, Zaloum, A, Tuttle, AH, Martin, LJ, Wieskopf, JS, Mapplebeck, JC, Wei, P, Zhan, S, Zhang, S, McDougall, JJ, King, OD, Mogil, JS: The Rat Grimace Scale: a partially automated method for quantifying pain in the laboratory rat via facial expressions. *Molecular pain,* 7**:** 55, 2011.

119. Micakovic, T, Banczyk, WZ, Clark, E, Kränzlin, B, Peters, J, Hoffmann, SC: Isolation of Pure Mitochondria from Rat Kidneys and Western Blot of Mitochondrial Respiratory Chain Complexes. *Bio-protocol,* 9**:** e3379, 2019.

120. Alicic, RZ, Rooney, MT, Tuttle, KR: Diabetic Kidney Disease: Challenges, Progress, and Possibilities. *Clinical journal of the American Society of Nephrology : CJASN,* 12**:** 2032-2045, 2017.

121. Betz, B, Conway, BR: An Update on the Use of Animal Models in Diabetic Nephropathy Research. *Current diabetes reports,* 16**:** 18, 2016.

122. Hsu, HH, Hoffmann, S, Di Marco, GS, Endlich, N, Peter-Katalinic, J, Weide, T, Pavenstadt, H: Downregulation of the antioxidant protein peroxiredoxin 2 contributes to angiotensin II-mediated podocyte apoptosis. *Kidney Int,* 80**:** 959-969, 2011.

123. Feng, D, Notbohm, J, Benjamin, A, He, S, Wang, M, Ang, LH, Bantawa, M, Bouzid, M, Del Gado, E, Krishnan, R, Pollak, MR: Disease-causing mutation in α-actinin-4 promotes podocyte detachment through maladaptation to periodic stretch. *Proceedings of the National Academy of Sciences of the United States of America,* 115**:** 1517-1522, 2018.

124. Henderson, JM, al-Waheeb, S, Weins, A, Dandapani, SV, Pollak, MR: Mice with altered α-actinin-4 expression have distinct morphologic patterns of glomerular disease. *Kidney Int,* 73**:** 741-750, 2008.

125. Sonneveld, R, van der Vlag, J, Baltissen, MP, Verkaart, SA, Wetzels, JF, Berden, JH, Hoenderop, JG, Nijenhuis, T: Glucose specifically regulates TRPC6 expression in the podocyte in an AngII-dependent manner. *Am J Pathol,* 184**:** 1715-1726, 2014.

126. Arora, MK, Singh, UK: Oxidative stress: meeting multiple targets in pathogenesis of diabetic nephropathy. *Current drug targets,* 15**:** 531-538, 2014.

127. Kriz, W, Lemley, KV: A Potential Role for Mechanical Forces in the Detachment of Podocytes and the Progression of CKD. *J Am Soc Nephrol,* 26**:** 258-269, 2015.

128. AbdAlla, S, Abdel-Baset, A, Lother, H, el Massiery, A, Quitterer, U: Mesangial AT1/B2 receptor heterodimers contribute to angiotensin II hyperresponsiveness in experimental hypertension. *Journal of molecular neuroscience : MN,* 26**:** 185-192, 2005.

129. Akaishi, T, Abe, M, Okuda, H, Ishizawa, K, Abe, T, Ishii, T, Ito, S: High glucose level and angiotensin II type 1 receptor stimulation synergistically amplify oxidative stress in renal mesangial cells. *Sci Rep,* 9**:** 5214, 2019.

130. Lowen, J, Grone, E, Grone, HJ, Kriz, W: Herniation of the tuft with outgrowth of vessels through the glomerular entrance in diabetic nephropathy damages the juxtaglomerular apparatus. *Am J Physiol Renal Physiol,* 317**:** F399-f410, 2019.

131. Artelt, N, Siegerist, F, Ritter, AM, Grisk, O, Schluter, R, Endlich, K, Endlich, N: Comparative Analysis of Podocyte Foot Process Morphology in Three Species by 3D Super-Resolution Microscopy. *Front Med (Lausanne),* 5**:** 292, 2018.

7 APPENDIX

Appendix-A: *Blood glucose concentration over the time.* Wild=Wild Type, TGR=Transgenic, CTRL= Control rats, HBP= Rats fed by the pellet food with I3C, D-HBP=Diabetic rats fed by the pellet food with I3C, N =number of rats in the group.

Sex	Age (weeks)	Group	Genotype	N	Blood Glucose Concentration [mg/dL]	Sex	Agen (weeks)	Group	Genotype	N	Blood Glucose Concentration [mg/dL]
Male	Week-0	CTRL	Wild	10	121.001 ± 5.457	Male	Week-4	CTRL	Wild	10	115.900 ± 8.949
			TGR	9	121.060 ± 7.228				TGR	9	112.11 ± 6.660
		HBP	Wild	10	122.100 ± 5.896			HBP	Wild	10	111.200 ± 5.411
			TGR	6	120.167 ± 5.913				TGR	6	121.833 ± 7.521
		D-HBP	Wild	12	121.250 ± 7.375			D-HBP	Wild	12	501.250 ± 19.749
			TGR	9	115.556 ± 9.342				TGR	9	479.889 ± 33.573
	Week-1	CTRL	Wild	10	119.100 ± 5.820		Week-5	CTRL	Wild	10	120.700 ± 9.381
			TGR	9	122.111 ± 6.333				TGR	9	117.889 ± 9.771
		HBP	Wild	10	119.000 ± 4.216			HBP	Wild	10	114.900 ± 6.806
			TGR	6	119.500 ± 4.929				TGR	6	118.833 ± 8.998
		D-HBP	Wild	12	480.500 ± 50.581			D-HBP	Wild	12	500.583 ± 32.704
			TGR	9	463.778 ± 41.686				TGR	9	483.000 ± 35.889
	Week-2	CTRL	Wild	10	120.100 ± 9.386		Week-6	CTRL	Wild	10	117.700 ± 8.858
			TGR	9	124.889 ± 7.991				TGR	9	113.889 ± 10.142
		HBP	Wild	10	120.500 ± 9.641			HBP	Wild	10	117.000 ± 6.960
			TGR	6	120.500 ± 11.327				TGR	6	125.167 ± 9.948
		D-HBP	Wild	12	474.667 ± 33.285			D-HBP	Wild	12	519.500 ± 41.478
			TGR	9	452.444 ± 24.259				TGR	9	479.667 ± 17.263
	Week-3	CTRL	Wild	10	117.800 ± 7.685		Week-7	CTRL	Wild	10	119.600 ± 2.252
			TGR	9	117.667 ± 9.219				TGR	9	119.000 ± 9.734
		HBP	Wild	10	122.300 ± 6.533			HBP	Wild	10	115.400 ± 9.047
			TGR	6	125.933 ± 6.210				TGR	6	118.167 ± 9.261
		D-HBP	Wild	12	520.750 ± 52.678			D-HBP	Wild	12	521.167 ± 38.076
			TGR	9	492.889 ± 39.072				TGR	9	483.111 ± 19.971

Appendix-B: *Urine production at the beginnig of the experiment and at the end of the experiment.* Wild=Wild Type, TGR=Transgenic, CTRL= Control rats, HBP= Rats fed by the pellet food with I3C, D-HBP=Diabetic rats fed by the pellet food with I3C, N =number of rats in the group.

Sex	Age (weeks)	Group	Genotype	N	Urine Produced [mL/24]
Male	Week-0	CTRL	Wild	10	13.5480 ± 5.56
			TGR	9	13.9522 ± 2.01
		HBP	Wild	10	10.7890 ± 3.31
			TGR	6	12.9140 ± 1.14
		D-HBP	Wild	12	10.8533 ± 1.01
			TGR	9	9.7400 ± 3.70
	Week-7	CTRL	Wild	10	13.046 ± 5.25
			TGR	9	14.462 ± 2.81
		HBP	Wild	10	11.223 ± 3.04
			TGR	6	16.59 ± 2.87
		D-HBP	Wild	12	233.81 ± 40.70
			TGR	9	192.151 ± 37.57

Appendix-C: *Water Consumption.* Wild=Wild Type, TGR=Transgenic, CTRL= Control rats, HBP= Rats fed by the pellet food with I3C, D-HBP=Diabetic rats fed by the pellet food with I3C, N =number of rats in the group.

Sex	Age (weeks)	Group	Genotype	N	Water Consumption [mL]
Male	Week-0	CTRL	Wild	10	24.68 ± 5.93
			TGR	9	26.26 ± 4.16
		HBP	Wild	10	23.37 ± 8.83
			TGR	6	25.69 ± 2.17
		D-HBP	Wild	12	26.36 ± 2.72
			TGR	9	24.94 ± 2.62
	Week-2	CTRL	Wild	10	23.71 ± 4.90
			TGR	9	26.62 ± 3.72
		HBP	Wild	10	28.83 ± 4.83
			TGR	6	32.22 ± 1.61
		D-HBP	Wild	12	239.34 ± 27.45
			TGR	9	249.93 ± 41.35
	Week-7	CTRL	Wild	10	23.54 ± 8.48
			TGR	9	24.28 ± 4.46
		HBP	Wild	10	27.71 ± 4.83
			TGR	6	30.53 ± 4.47
		D-HBP	Wild	12	201.34 ± 71.52
			TGR	9	199.05 ± 31.05

Appendix-D: *Blood Pressure.* Wild=Wild Type, TGR=Transgenic, CTRL= Control rats, HBP= Rats fed by the pellet food with I3C, D-HBP=Diabetic rats fed by the pellet food with I3C, N =number of rats in the group.

Sex	Age	Group	Genotype	N	Blood Pressure
					[mmHg]
Male	Week-0	CTRL	Wild	10	122.100 ± 4.306
			TGR	9	123.444 ± 7.367
		HBP	Wild	10	130.300 ± 9.441
			TGR	6	123.167 ± 6.795
		D-HBP	Wild	12	131.667 ± 6.513
			TGR	9	126.889 ± 8.300
	Week-2	CTRL	Wild	10	122.600 ± 5.038
			TGR	9	124.000 ± 9.093
		HBP	Wild	10	168.700 ± 6.816
			TGR	6	165.167 ± 6.178
		D-HBP	Wild	12	175.417 ± 6.973
			TGR	9	170.222 ± 10.244
	Week-4	CTRL	Wild	10	125.200 ± 5.594
			TGR	9	129.556 ± 6.691
		HBP	Wild	10	184.500 ± 4.301
			TGR	6	163.500 ± 6.221
		D-HBP	Wild	12	177.000 ± 11.086
			TGR	9	172.001 ± 11.023
	Week-6	CTRL	Wild	10	129.100 ± 4.383
			TGR	9	128.333 ± 9.179
		HBP	Wild	10	179.100 ± 6.522
			TGR	6	167.000 ± 7.616
		D-HBP	Wild	12	171.583 ± 5.616
			TGR	9	170.778 ± 6.553

Appendix-E: *FITC-sinistrin half-life (Transcutaneous GFR measurement).* Wild=Wild Type, TGR=Transgenic, CTRL= Control rats, HBP= Rats fed by the pellet food with I3C, D-HBP=Diabetic rats fed by the pellet food with I3C, N =number of rats in the group.

Sex	Age (weeks)	Group	Genotype	N	FITC-Sinistrin halflife [minutes]
Male	Week-2	CTRL	Wild	3	23.07 ± 1.93
			TGR	3	29.38 ± 5.18
		HBP	Wild	NA	NA
			TGR	4	22.65 ± 8.07
		D-HBP	Wild	4	46.32 ± 13.32
			TGR	4	24.24 ± 15.74
	Week-6	CTRL	Wild	3	26.51 ± 5.46
			TGR	3	25.35 ± 10.56
		HBP	Wild	NA	NA
			TGR	4	56.83 ± 6.91
		D-HBP	Wild	4	112.17 ± 28.78
			TGR	4	187.96 ± 55.46

Appendix-F: *Urinary Protein and Albumin (mg/24).* Wild=Wild Type, TGR=Transgenic, CTRL= Control rats, HBP= Rats fed by the pellet food with I3C, D-HBP=Diabetic rats fed by the pellet food with I3C, N =number of rats in the group.

Sex	Age (weeks)	Group	Genotype	N	Protein [mg/24]	Albumin [mg/24]
Male	Week-7	CTRL	Wild	10	3.20 ± 2.78	0.33 ± 0.178
			TGR	9	8.66 ± 1.11	4.33 ± 1.67
		HBP	Wild	10	10.80 ± 1.55	4.08 ± 2.33
			TGR	6	84.33 ± 12.55	51.92 ± 10.96
		D-HBP	Wild	12	262.58 ± 8.38	178.26 ± 32.67
			TGR	9	536.50 ± 33.41	354.92 ± 49.40

Appendix-G: Plasma Urea, Creatinine, Triglyceride and Cholesterol Concentration. Wild=Wild Type, TGR=Transgenic, CTRL= Control rats, HBP= Rats fed by the pellet food with I3C, D-HBP=Diabetic rats fed by the pellet food with I3C, N =number of rats in the group.

Sex	Age (weeks)	Group	Genotype	N	Plasma Urea Concentration [mg/dL]	Plasma Creatinine Concentration [mg/dL]	Plasma Triglyceride Concentration [mg/dL]	Plasma Cholesterol Concentration [mg/dL]
Male	Week-7	CTRL	Wild	10	34.84 ± 2.25	0.27 ± 0.030	149 ± 24.02	85.33 ± 6.58
			TGR	9	33.26 ± 2.28	0.29 ± 0.027	191.33 ± 34.77	79.22 ± 15.22
		HBP	Wild	10	33.63 ± 4.38	0.29 ± 0.024	91.80 ± 28.14	86.20 ± 27.17
			TGR	6	32.83 ± 1.70	0.24 ± 0.013	278.67 ± 67.59	160.33 ±21.29
		D-HBP	Wild	12	50.26 ± 8.78	0.15 ± 0.016	488.78 ± 167.5	263.44 ±83.81
			TGR	9	49.85 ± 5.84	0.16 ± 0.009	404.38 ± 145.6	422.5 ±110.83

Appendix-H: *Body Weight, Kidney weight, Kidney/Body Weight and Glomerular Area.* Wild=Wild Type, TGR=Transgenic, CTRL= Control rats, HBP= Rats fed by the pellet food with I3C, D-HBP=Diabetic rats fed by the pellet food with I3C, N =number of rats in the group.

Sex	Age (weeks)	Group	Genotype	N	Body Weight	Kidney Weight	Glomerular area
					[g]	[g]	[µm^2]
Male	Week-7	CTRL	Wild	10	381.67 ± 36.09	1.41 ± 0.20	10464.8 ± 1791.62
			TGR	9	381.67 ± 17.76	1.55 ± 0.38	10279.0 ± 3244.50
		HBP	Wild	10	345.70 ± 18.15	1.64 ± 0.19	12303.1 ± 2527.27
			TGR	6	402.58 ± 20.55	1.52 ± 0.16	14623.5 ± 3335.08
		D-HBP	Wild	12	228.35 ± 50.22	1.54 ± 0.24	13412.4 ± 2611.84
			TGR	9	259.38 ± 84.78	1.43 ± 0.23	14869.7 ± 3109.28

8 CURRICULUM VITAE AND PUBLICATIONS

PERSONALIEN

Name und Vorname: KUZAY YALÇIN

Geburtsdatum: 7 FEBRUAR 1990

Geburtsort: ISTANBUL

Familienstand: VERHEIRATET (mit HATICE KUZAY)

Vater: RAMAZAN

Mutter: YETER

SCHULISCHER WERDEGANG

2005 – 2009   **HabireYahşi Lisesi** (**Gymnasium**, Istanbul, Turkey)

12.06.2009   Graduation score: 67.75 /100

UNIVERSITÄRER WERDEGANG

09/2009 – 06/2014	**Bachelor of Science** Biology (English) Abant Izzet Baysal University, Bolu, Turkey Graduation score: 3.33/4.00
09/2012 – 02/2013	**Erasmus Exchange** Jagiellonian University, Krakow
09/2014 – 09/2016	**Master of Science, MSc.** EUCOMOR (Erasmus mundus joint degree) Universiteit Antwerpen, Antwerp Graduation score: Greatest Distinction (85/100)

09/2014 – 02/2015   **1st Semester:** Poznań University of Life Sciences, Poland
03/2015 – 08/2015   **2nd Semester:** Justus-Liebig-Universität Gießen, Germany
09/2015 – 02/2016   **3rd Semester:** University of Antwerp, Belgium
03/2016 – 07/2016   **4th Semester:** University of Naples Federico II, Italy
Thesis: Effect of HMGA1 to the expression of cell fate determinant Numb and asymmetric cell division in brain

tumor stem cell
Advisor: Prof. Dr. Alfredo Fusco and Dr. Sabrina Battista

Promotion, Dr.Sc.hum (scientiarum humanarum)
Titel:" The Role of Podocytes in Diabetic Nephropathy and Hypertension, and their Nanoscale Evaluation by Expansion Microscopy"

10/2016 – Now
Zentrum für Medizinische Forschung (ZMF) Medizinische Fakultät Mannheim Ruprecht-Karls-Universität Heidelberg, Deutschland
Doktormutter: Prof. Sigrid Christa Hoffmann

Note:

PUBLICATIONS

Micakovic, Tamara & Papagiannarou, Stamatia & Clark, Euan & **Kuzay, Yalcin** & Abramovic, Katarina & Peters, Jörg & Sticht, Carsten & Volk, Nadine & Fleming, Thomas & Nawroth, Peter & Hammes, Hans-Peter & Alenina, Natalia & Gröne, Hermann-Josef & Hoffmann, Sigrid. (2018). Angiotensin II type 2 receptors protect renal tubule mitochondria in early stages of diabetes mellitus. **Kidney International**. 94. 10.1016/j.kint.2018.06.006.

Colamaio, Marianna & Tosti, Nadia & Puca, Francesca & Mari, Alessia & Gattordo, Rosaria & **Kuzay, Yalcin** & Federico, Antonella & Pepe, Anna & Sarnataro, Daniela & Ragozzino, Elvira & Raia, Maddalena & Hirata, Hidenari & Gemei, Marica & Mimori, Koshi & del Vecchio, Luigi & Battista, Sabrina & Fusco, Alfredo. (2016). HMGA1 silencing reduces stemness and temozolomide resistance in glioblastoma stem cells. **Expert Opinion on Therapeutic Targets**. 20. 10.1080/14728222.2016.1220543.

Francesca Puca, Nadia Tosti, Antonella Federico, **Yalçın Kuzay**, Anna Pepe, Sonia Morlando, Teresa Savarese, Federica D'Alessio, Marianna Colamaio, Daniela Sarnataro, Sihana Ziberi, Marco De Martino, Alfredo Fusco & Sabrina Battista (2019) HMGA1 negatively regulates NUMB expression at transcriptional and post transcriptional level in glioblastoma stem cells, **Cell Cycle**, 18:13, 1446-1457, DOI: 10.1080/15384101.2019.1618541

9 ACKNOWLEDGEMENTS